Titre: Title:	Electrical properties of double layer dielectric structures for space technology
Auteur: Author:	Anqing Lian
Date:	1993
Type:	Mémoire ou thèse / Dissertation or Thesis
Référence: Citation:	Lian, A. (1993). Electrical properties of double layer dielectric structures for space technology [Ph.D. thesis, Polytechnique Montréal]. PolyPublie. https://publications.polymtl.ca/57983/

UNIVERSITE DE MONTREAL

ELECTRICAL PROPERTIES OF DOUBLE LAYER DIELECTRIC STRUCTURES FOR SPACE TECHNOLOGY

PAR

Anqing LIAN

DEPARTEMENT DE GENIE PHYSIQUE

ECOLE POLYTECHNIQUE

THESE PRESENTEE EN VUE DE L'OBTENTION

DU GRADE DE PHILOSOPHIAE DOCTOR (Ph. D.)

AVRIL 1993

ISBN 0-315-86547-4

UNIVERSITE DE MONTREAL

ECOLE POLYTECHNIQUE

Cette thèse intitulée:

ELECTRICAL PROPERTIES OF DOUBLE LAYER DIELECTRIC STRUCTURES FOR SPACE TECHNOLOGY

présentée par: Anqing LIAN

en vue de l'obtention du grade de Philosophiae Doctor (Ph. D.)

a été dûment acceptée par le jury d'examen constitué de:

M. Meunier, Michel	Ph. D., président-rapporteur
M. Wertheimer, Michel R.	D.Sc. A., directeur de recherche
M. Martinu, Ludvik	Ph. D., codirecteur
M. Lépine, Yves	Ph. D., membre du jury
M. Balmain, Keith G.	Ph. D., membre du jury

Abstract

Polymeric films such as Kapton® (polyimide, PI) and Mylar® [poly(ethylene terephthalate), PET] are extensively used in space technology as thermal blankets. In the hostile environment of space, they are subjected to various effects. The typical factors are: bombardment of particles such as atomic oxygen, causing surface erosion; and surface flashover due to charge accumulation, resulting in surface damage and interference with the operation of electronic instruments on board. Thin coatings (about 1 μm thick) of P-SiO_2 and P-SiN (silicon oxide and nitride, respectively), plasma-deposited onto the surfaces of PI and PET, have been proposed to protect the thermal blanket materials against the above-named effects. The investigation of electrical properties of this kind of double layer dielectric structures is of great importance for understanding mechanisms for suppressing charge accumulation and flashover, and consequently for their applications to space technology.

In this work, the d.c. bulk and surface electrical conductivities of thin single layer PI and PET samples, and of the double layer P-SiO_2/PI, P-SiN/PI, P-SiO_2/PET and P-SiN/PET structures are investigated within the range of applied electric field from 2×10^2 to 2×10^5 V/cm, from room temperature to 170°C, in vacuum. The C-V (capacitance-voltage) technique has been employed for the

analysis of charge transport and distribution near the $insulator_1/insulator_2$ ($P\text{-}SiO_2/PI$ or $P\text{-}SiN/PI$) interface in MI_1I_2S structures ($metal-insulator_1-insulator_2-semiconductor$).

We have found that the electrical current in the bulk of the $P\text{-}SiO_2/PI$ and $P\text{-}SiN/PI$ samples depends on the polarity of the applied electric field at $T \geq 60°C$, for electric field values $E \geq 2\times10^3$ V/cm. This is very different from the case of the PI, $P\text{-}SiO_2$ and $P-SiN$ samples, for which no polarity dependence was found. On the other hand, the $P\text{-}SiO_2/PET$ and $P\text{-}SiN/PET$ samples, like the PET sample, were not found to exhibit any such polarity effect in the investigated ranges of temperature and electric field. We attribute the polarity dependence, described above, to trapping of charges such as protons at the PI/plasma deposit interface. These protons derive from thermal dissociation and ionization of residual acid groups in PI; in PET their concentration is too low to give rise to this observation.

The C-V characteristics of the Al-PI-$(P\text{-}SiO_2)$-Si structure confirm that charges, such as protons, can be accumulated or trapped near the $P-SiO_2/PI$ interface at an applied voltage. These accumulated charges can cause an interfacial potential barrier and modify the local electric field.

We have proposed a model, based on the potential barrier at the $P-SiO_2/PI$

or P-SiN/PI interface, to interpret the properties of the transient and steady state currents in double layer structures. This model can semi-quantitatively explain all the observed results.

Sommaire

Les films de polymères, tels que le Kapton® (polyimide, PI) et le Mylar® (polyéthylène téréphtalate, PET), ont plusieurs applications. L'une d'entre elles est l'utilisation prolongée, en technologie spatiale, de couvertures thermiques afin de maintenir les équipements électroniques à bord d'un véhicule spatial à une température en dedans des limites d'opération. Dans l'environnement hostile qu'est l'espace, les couvertures thermiques sont sujettes à différents effets: le vide (10^4 à 10^{-8} Pa) et les cycles thermiques (-190°C à 150°C et plus), la radiation électromagnétique, l'irradiation par des particules chargées telles que les électrons et les protons (énergie = 0,1 keV à 4 MeV, flux > 10^8 cm^{-2} s^{-1}), et le bombardement par des particules neutres (ex: l'oxygène atomique). L'effet de chacun de ces facteurs sur les couvertures thermiques dépend cependant de l'altitude orbitale. Dans une orbite basse (150 à 700 km), ces conséquences du vide, de la radiation x et des effets de charges sont faibles, l'effet majeur étant causé par l'oxygène atomique: En orbite basse, la densité atmosphérique est encore relativement élevée, et l'oxygène atomique provient de la dissociation de l'oxygène moléculaire par la radiation ultraviolette. Les vols de navettes ont montré que même une exposition de courte durée à l'environnement spatial affecte de façon marquée la surface des couvertures thermiques. D'un autre côté, en orbite géosynchrone (altitude de 6 à 7 rayons terrestres), l'effet de l'oxygène atomique

est négligeable, alors que les effets du vide, de la radiation et de l'accumulation de charges dominent. Parmi ces facteurs, l'irradiation par les électrons est le facteur le plus important car il peut provoquer des décharges à la surface pouvant endommager les systèmes électroniques et ainsi interférer avec l'opération normale du véhicule.

Afin d'augmenter la durée de vie des couvertures thermiques, leur surface exposée au milieu spatial doit être protégée, mais les matériaux protecteurs ajoutés ne doivent pas changer l'efficacité des couvertures thermiques. Nous avons prouvé que de minces revêtements (~1 μm) de P-SiO_2 et de P-SiN (oxyde et nitrure de silicium) déposés par procédés plasma sur les surfaces de PI et PET peuvent protéger ces polymères contre les effets néfastes de l'espace. L'étude des propriétés électriques de ce type de couches doubles P-SiO_2/PI, P-SiN/PI, P-SiO_2/PET et P-SiN/PI est primordiale afin de comprendre la modification des mécanismes d'accumulation des charges et des décharges, et conséquemment leurs applications à la technologie spatiale.

Dans ce travail, les propriétés conductrices d.c. en volume et à la surface de couches minces de PI (51 μm) et de PET (12 et 25 μm), et de doubles couches de P-SiO_2/PI, P-SiN/PI, P-SiO_2/PET et P-SiN/PET sont étudiées pour des champs électriques allant de 2×10^2 à 2×10^5 V/cm, pour des températures allant de 19°C

à 170°C, dans le vide. Les mesures incluent l'étude du comportement transitoire des courants de charge et de décharge, du courant d'équilibre en fonction du voltage appliqué, et de la variation des conductivités de surface et de volume avec la température. Les techniques de mesures ASTM ("American Society for Testing and Materials") ont été adoptées pour notre cas. La technique "capacitance-voltage" (C-V) pour les structures MIS ("metal-insulator-semiconductor") et MI_1I_2S ("metal-insulator$_1$-insulator$_2$-semiconductor") fut utilisée pour l'analyse du transport et de la distribution de charges près de l'interface entre les deux isolants (P-SiO_2/PI, P−SiN/PI) lorsqu'un potentiel d.c. est appliqué à la structure en double couches.

Nous avons trouvé que les courants électriques transitoires et d'équilibre dans le volume des doubles couches P-SiO_2/PI et P-SiN/PI dépendent de la polarité du champ $E \geq 2\times10^3$ V/cm pour $T \geq 60°C$; par exemple, la différence entre les courants positif et négatif pour le P-SiO_2/PI est de plus d'un facteur 2 à 170°C (pour $E = 2\times10^4$ V/cm). Par contre, pour $T \leq 60°C$, ou $E \leq 2\times10^3$ V/cm, nous n'avons trouvé aucun effet de polarité. Ces observations diffèrent sensiblement des cas de mono-couches de PI, P-SiO_2 et P-SiN, pour lesquelles aucun effet de polarité ne fut trouvé pour toute la gamme de températures et champs électriques étudiées. Les structures P-SiO_2/PET et P-SiN/PET n'ont, elles non plus, manifesté aucun effet de polarité.

Nous avons trouvé que la conductivité volumique du PI ($E \leq 2\times10^4$ V/cm, région de conduction ohmique) augmente avec une succession de cinq cycles, et qu'elle obéit à la loi d'Arrhenius avec une énergie d'activation $E_a \approx 1$ eV jusqu'au cinquième cycle; cependant, lors d'un sixième cycle, E_a est divisée en deux parties, avec E_a=1,26 eV de 25 à 90°C, et E_a=0,86 eV pour 90°C < T < 170°C. La conductivité volumique du PET (sec) est très stable, E_a=1,85eV pour 70°C ≤ T ≤ 130°C, et E_a=0,33 eV de 25 à 70°C, la transition vitreuse étant 70°C, en accord avec la littérature publiée.

Les mesures de conductivité surfacique pour le PI et le PET montrent que l'énergie d'activation pour ce processus est le même que pour celui de volume. L'effet que la valeur de conductivité de surface pour un échantillon vierge est plus haute que pour l'échantillon recuit indique que l'eau adsorbée peut grandement augmenter la conductivité de la surface.

Un mécanisme de conduction ionique a été proposé pour le processus de conduction volumique dans les cas du PI et du PET, basé sur sauts activés thermiquement de protons. Ces protons sont thermiquement ionisés à partir de groupes -COOH dans le PI et le PET. En comparant les valeurs expérimentales et théoriques, des distances de sauts de 110 Å à 24°C et 158 Å à 120°C furent obtenues pour le PI, et 95 Å à 90°C pour le PET.

Les caractéristiques C-V de la structure Al-PI-(P-SiO_2)-Si ont confirmé que des charges peuvent être piégées près de l'interface P-SiO_2/PI lors d'un voltage appliqué. Ces charges peuvent causer la création d'une barrière de potentiel à l'interface P-SiO_2/PI et modifier le champ électrique local.

Afin d'expliquer le comportement transitoire et d'équilibre des doubles couches de P-SiO_2/PI ou de P-SiN/PI, on a proposé un modèle, dans lequel une barrière de potentiel est supposée à l'interface P-SiO_2/PI ou P-SiN/PI. Cette barrière a été confirmée par les mesures C-V et elle est responsable de la dépendance de la polarité des courants.

En appliquant ce modèle aux comportements transitoires d'équilibre, nous avons pu tirer les conclusions suivantes:

(1) Pour un champ électrique suffisamment fort, la théorie prévoit la dépendance du courant de décharge I_d et du courant équilibre $I_{c\infty}$ sur la polarité du champ électrique appliqué.

(2) Dans le cas d'un faible champ électrique, la dépendance du I_d et $I_{c\infty}$ sur la polarité disparaît. I_d et $I_{c\infty}$ sont alors proportionnels au champ électrique. Nous avons observé ce phénomène à $E < 2x10^3$ V/cm ($V < 10$ V).

(3) La courbe $\ln(I_d)$ en fonction de temps t est linéaire. Cela est différent de

la loi de puissance ($I_d \propto t^{-n}$) observée dans l'échantillon d'une seule couche de PI. L'expérience l'a confirmé.

(4) Une barrière de potentiel à l'interface P-SiO_2/PI d'environ 0.16 eV a été obtenue à 120°C en comparant les résultats mesurés avec les résultats théoriques.

Ce modèle proposé peut bien expliquer, au moins semi-quantitativement, les comportements observées.

L'accord entre la théorie et l'expérience confirme la présence de la barrière de potentiel à l'interface. Deux paramètres sont introduits, W_o et U_o, qui représentent les hauteurs des barrières de potentiel dans les processus de polarisation et de la conduction à l'équilibre. Si elles sont nulles, la dépendance du courant volumique sur la polarité disparaît. Donc, W_o et U_o peuvent jouer les rôles clés dans la détermination des propriétés de conduction d.c. dans le volume. La conductivité volumique du P-SiO_2/PET et du P-SiN/PET ne démontre aucune dépendance sur la polarité puisque les valeurs de W_o and U_o sont très faibles à basses et hautes températures. En effet, nous avons trouvé que la valeur de W_o est très proche de celle de U_o à l'interface P-SiO_2/PI.

Acknowledgements

I would like to express my sincere gratitude to my supervisors, Professor M. R. Wertheimer, and Dr. L. Martinu in the Department of Engineering Physics, Ecole Polytechnique, for their wise instruction and financial support during the period of four years. They have given me great encouragement and invaluable help in many ways.

Thanks are also due to Mrs J. E. Klemberg-Sapieha for her cooperation in this project and for preparation of the plasma deposited samples, and to Mr. G. Jalbert for his technical help in modifying the measuring system. Without their cooperation and help, it would have been difficult to carry out this project.

I wish to thank the other colleagues in the Department of Engineering Physics and my friends in Montreal for their help and encouragement during the period of my study.

Finally, I am thankful to my wife, Liyun Ma, for her understanding, support, and help. We once suffered from long separation, and I feel I owe her a great deal. Without her love, it would be impossible for me to carry out my Ph.D. study.

Table of Contents

List of Tables

List of Figures

List of Principal Symbols

T:	temperature
T_g:	glass transition temperature of a polymer
t:	time
k:	Boltzmann constant
e:	electron charge
E, E_L:	average and local electric fields
V:	voltage
E_a, E_{as}:	activation energies for bulk and surface conductivities
A:	electrode area of sample
L, d_o, d_1, d_2:	sample thicknesses
I_c, I_{cs}:	bulk and surface charging electrical currents
I_d, I_{ds}:	bulk and surface discharging electrical currents
$I_{c\infty}$, $I_{cs\infty}$:	steady state bulk and surface electrical currents
I_p:	polarization electrical current
σ_v, σ_s:	bulk and surface electrical conductivities
ρ_v, ρ_s:	bulk and surface electrical resistivities
R:	bulk electrical resistance
μ:	mobility of charge carriers
v:	velocity of a charge carrier

v_+, v_-: velocities of a charge carrier for two polarities of applied electric field in double layer dielectric structure

j: current densities

j_+, j_-: current densities for two polarities of applied electric field in double layer dielectric structure

j_p: polarization current density

P(t): polarization

ν: phonon frequency

ε_o: vacuum permittivity

ε_r', ε_{rs}': relative permittivities of dielectric and semiconductor

E_c, E_v: energies of conduction band bottom and valence band top

E_F: Fermi level

n_o: volume density of -COOH groups in PI or PET

n: volume density of charge carriers (protons) in PI or PET

N: volume density of pair elements at the P-SiO_2/PI interface for polarization process

N_D, N_A: impurity concentrations of n-type and p-type semiconductors

r, a_o, a: mean hopping distances of carriers

V_G: gate voltage applied to a MIS structure

V_{GF}: flat band voltage for a MIS structure

C, C_o: capacitance and capacitance per unit area

f:	frequency
p, p', p":	transition rates of a carrier across a potential barrier
f_i:	probability of an electron to occupy a localized state i
W, Δg:	heights of potential barriers between two potential wells
W_o, U_o:	heights of potential barriers at the interface between two insulators
Q_s:	surface charge density at the insulator/semiconductor interface
Q_o:	surface charge density in a thin layer at a distance x_o from the metal electrode in a MIS structure
ρ:	volume charge density
Q_i:	surface charge density at the $insulator_1$/$insulator_2$ interface.
N_{ss}:	surface state density at the insulator/semiconductor interface
K:	equilibrium constant for ionization process of an electrolyte
g:	ionization energy
φ:	extent of ionization
γ:	activity coefficient
T_s:	substrate temperature
h, S:	enthalpy and entropy
Δh, ΔS:	changes of enthalpy and entropy
α:	rate at which wavefunction of an electron at a particular site falls off with distance

Chapter 1

Introduction

Organic materials such as polymers and polymer matrix composites are extensively used in space technology. In addition to their traditional use as structural components or as electrical insulation, they are also used as thermal blankets, required to maintain the electronics payload within required operation temperature limits. The infrared part of solar radiation can be absorbed or emitted by the spacecraft surface. Thermal blankets are designed to prevent the heat from entering into the system and to reduce the loss of heat from the inside of the system. Therefore, the requirement for a thermal blanket material is high thermal emmitance, low solar absorptance and the ability to withstand the hostile environment of space. Kapton® (polyimide, PI) and Mylar® [poly(ethylene terephthalate), PET] are good candidates as thermal blankets due to their low mass density, and good mechanical, electrical and thermal properties[1-6].

1.1 Effects of space environment

All materials on the spacecraft's surface are exposed to the hostile environment of space in which there are a lot of factors affecting the properties of thermal blanket materials[7]. For instance, vacuum (10^4 to 10^{-8} Pa) and thermal

cycling (-190°C to 150°C or higher), which can cause mass loss and change of electrical and mechanical properties; electromagnetic radiation, ranging from x-ray and γ-ray to infrared, resulting in variation of photoconductivity and solar-absorption coefficients. However, the most serious problem is the irradiation from charged particles such as electrons and protons in geosynchronous orbit, and the neutral particle bombardment, for example, atomic oxygen in low Earth orbit (LEO).

In LEO, at altitudes ranging from 150 to 700 km, the atomic oxygen, dissociated from molecular oxygen by ultraviolet radiation, can attack the exposed surface of thermal blanket, causing surface erosion. The experience on shuttle flights has shown that even a short-term exposure to the space environment can have harmful effects on thermal blankets[5]. On the other hand, in geosynchronous orbit, at altitudes of 6 to 7 Earth radii, there are electrons and protons with different energy levels (0.1 keV - 4 MeV, flux > 10^8 $cm^{-2}s^{-1}$) arising from the Van Allen Radiation Belts and solar wind, and among them the most important ones are the electrons with a typical energy of 20 keV. Energetic electrons can charge the thermal blanket in spacecraft, causing charge build-up at its surface or subsurface. If the surface potential reaches a threshold value, discharge, accompanied by surface flashover, can occur. This process is believed to be responsible for arc breakdown, strong electromagnetic interference, and consequent "operational anomalies" or irreversible component (e.g. thermal blanket) failures on spacecraft.

1.2 Protection of thermal blankets

In order to increase lifetime of thermal blankets, their exposed surfaces must be protected, but the corresponding protective materials must not change the key physical properties of the thermal blanket. Many researchers have been working to resolve this problem[1-10].

One way is to change the structure of thermal blanket, for example, using a multilayer design[2,8-10], composed of Polyimide-Al-Adhesive-Polyimide-Al. The principle for effectively suppressing surface flashover when irradiated by electrons is that the conductive layer, buried a few micrometers below the surface, can enhance the leakage current to cancel the incident electronic current, so that the surface potential cannot reach a threshold value for discharging. However, this design is unable to suppress surface erosion by atomic oxygen.

Another possible way to protect a thermal blanket is to apply a protective coating on its surface. Banks et al. reported that Al_2O_3 and SiO_2 thin layers sputtered onto a PI surface can protect it against atomic oxygen[5]. In recent years, the research in our laboratory has also shown that thin protective coatings such as plasma-deposited silicon-oxide and -nitride (P-SiO_2, P-SiN) onto the surfaces of polymers not only suppress erosion by atomic oxygen, but they can also reduce

surface charge accumulation and flashover[6,11]. For example, when exposed to a simulated LEO environment (O_2 flow is 200 sccm), the weight loss rate of bare polyimide is 4.6 mg cm^{-2} h^{-1}; however, the loss rate of the P-SiO_2 and P-SiN (0.5 μm thick) coated polyimide is only 0.1 and 0 mg cm^{-2} h^{-1}, respectively[6]. All of the investigated coatings are proven to reduce the weight loss very substantially, in some cases to an immeasurably small value. The coated samples also exhibit faster decay rate of negative surface potential[6], and this greatly decreases the probability of flashover at the charged surfaces. For instance, when exposed to corona discharge using a charging voltage of - 4000 V, the final surface potential of bare polyimide sample (51 μm thick) was high up to - 2560 V, and after 4 days it decayed to -820 V; while the surface potential of the P-SiO_2 coated polyimide was only - 400 V, and it decayed to 0 in only 2 hours. This is, a priori, rather unexpected and surprising: SiO_2, an excellent electrical insulator, is hardly expected to possess good antistatic properties. It has been shown that these protective coatings on the surfaces of various polymers do not significantly change the emmitance and the absorptance[6] necessary for thermal blankets.

1.3 Objectives of this thesis

We have mentioned that the coatings of P-SiO_2 and P-SiN are suitable for protection of thermal blanket materials, because they suppress the effect of atomic

oxygen, while at the same time they appear to hinder charge accumulation. This latter aspect has motivated in-depth studies of the electrical properties of such double layer structures.

The samples to be used are single layer PI and PET samples, double layer P-SiO_2/PI, P-SiN/PI, P-SiO_2/PET, and P-SiN/PET samples. The experiments include measurements of the transient and steady state d.c. bulk and surface electrical currents as a function of time and applied voltage, and of the bulk and surface electrical conductivities as a function of temperature in single and double layer structures. Corresponding model will be proposed for interpreting properties of these currents and conductivities. The capacitance-voltage (C-V) technique for the metal-insulator-semiconductor (MIS) and metal-$insulator_1$-$insulator_2$ (MI_1I_2S) structures are used to understand the charge distribution and transport near the insulator/semiconductor or $insulator_1$/$insulator_2$ interface.

Chapter 2

Electrical Conduction Mechanisms in Dielectrics

In this chapter, we first briefly describe the molecular structure of polymers and the d.c. electrical conduction mechanisms in dielectrics. Then, we review the electrical properties of PI and PET, and also of P-SiO_2 and P-SiN. Finally, research on electron-beam charging of polymers, which is related to the surface charging of thermal blanket material in space environment, is discussed.

2.1 Molecular structure of polymers

Polymers are covalently bonded molecules with very large molecular weights and sizes, having a repeat unit or "mer". If we classify polymers according to their structures, then three principal kinds of molecules can be distinguished: linear, branched, and network systems. However, if we classify polymers according to chemical fabrication process, they can be divided into two large groups: (1) The polymers resulting from step polymerization, in which a polymer chain grows only by reactions that can occur between two molecular species. (2) The polymers resulting from chain polymerizations, in which a polymer chain grows only by reaction of monomer with a reactive end-group on the growing chain[12]. Step polymerization that involves reaction in which small molecules are eliminated is

termed polycondensation, and the polymers produced by this reaction are called condensation polymers. PI and PET are typical examples. Step polymerization in which the monomers react together without the elimination of other molecules is termed polyaddition, and the polymers produced by this reaction type are called addition polymers, typical examples being polyvinyl chloride (PVC) and polyethylene (PE).

Because of their special molecular structure, the electrical properties of polymers are quite different from those of low molecular weight organic and inorganic materials. A solid polymer can be a mixture of a crystalline and an amorphous phase, depending on the molecular nature and the preparation conditions. In later subsections of this chapter, we will describe in detail the characteristics of the two main polymers we have selected, namely PI and PET.

The modified energy band concept for inorganic crystalline insulators can also be used to explain the electrical properties of polymers. Typically, the localized states in the band gap between the conduction and the valence bands may be distributed continuously, forming traps for charge carriers, which contribute to d.c. electrical conduction by hopping even if at a relatively low d.c. electric field. The contribution of thermally-excited electrons in the conduction band and of the holes in valence band to the electrical current can generally be neglected in low electric

fields because of their very low densities.

2.2 Electrical conduction mechanisms in polymers

The principal electrical conduction mechanisms in bulk of polymers are reviewed as follows[13-15].

a) Ohmic conduction

For insulating polymers, the d.c. electrical conduction is often observed to be ohmic in a low applied electric field (typically below 10^5 V/cm), that is, the bulk current density is proportional to the applied electric field E:

$$j(T,E) = \sigma_v(T)\,E \tag{2.1}$$

where σ_v(T) is the bulk conductivity. For many polymers, one has experimentally found that σ_v(T) can be expressed as:

$$\sigma_v(T) = \sigma_{vo}(T)\exp\left(-\frac{E_a}{kT}\right) \tag{2.2}$$

T is the absolute temperature, k the Boltzmann constant, E_a the activation energy for bulk conduction. σ_{vo} is a pre-exponential factor, which is a weak function of temperature. For the Arrhenius type of behaviour expressed by equation (2.2), plotting of $ln\sigma(T)$ versus reciprocal temperature T^{-1} is linear, which allows one to determine E_a and σ_{vo}.

Charge carriers responsible for the ohmic conduction can be ions arising from either impurities or from thermal ionization. In some polymers there may be a rather special kind of conduction process called protonic conduction. Protons may be thermally ionized from some chemical groups to become charge carriers. The ionic conduction is by hopping from one site to another across a potential barrier in a polymer.

b) Schottky emission

At medium or high fields, other conduction mechanisms due to the effects of bulk and electrode material can dominate over the effects of the ionic hopping conduction. The Schottky emission is such a conduction mechanism having its origin at the electrode/insulator interface, and this process is field-assisted thermionic emission. A charged particle leaving the electrode metal is retarded by its own image force in the metal. The current density can be expressed as

$$j(T,E) = A^* T^2 \exp\left(-\frac{\phi - \beta_s \sqrt{E}}{kT}\right), \qquad (2.3)$$

where

$$\phi = E_C - E_F , \qquad (2.4)$$

$$\beta_s = \left(\frac{e^3}{4\pi\varepsilon_o \varepsilon_r'}\right)^{\frac{1}{2}} , \qquad (2.5)$$

and

$$A^* = \frac{4\pi emk^2}{h^3} \qquad (2.6)$$

A^* is the Richardson constant, ϕ is the energy level difference between the bottom of the conduction band of the polymer E_c and the Fermi level of the metal E_F; ε_o is the vacuum permittivity, ε_r' the relative permittivity of polymer, h is Planck's constant, and e is the electron charge. Evidently, the current is dependent on the electrode material when the Schottky mechanism is active. Movaghar has shown that this relationship between j and E can be applied to many cases.

c) Fowler-Nordheim emission

Another high field conduction mechanism involving the electrode is the

Fowler-Nordheim emission. In this case, electrons from the metallic electrode can tunnel by quantum effect through the potential barrier to the conduction band of the polymer. The current density at T = 0 K can be expressed as:

$$j(E) = \frac{e^3 E^2}{8\pi h\phi} \exp\left(-\frac{4\sqrt{2m\phi^3}}{3eEh} 2\pi\right) \tag{2.7}$$

d) Poole-Frenkel emission

A high field conduction mechanism involving only the bulk materials is known as the Poole-Frenkel emission: Trapped electrons can be emitted to the conduction band by tunnelling through a potential barrier modified by a Coulomb potential. The current density is given by

$$j(T,E) \propto E \exp\left(-\frac{\phi_o - \beta_{PF}\sqrt{E}}{kT}\right) \tag{2.8}$$

where

$$\beta_{PF} = \left(\frac{e^3}{\pi\varepsilon_0\varepsilon'_r}\right)^{\frac{1}{2}} = 2\beta_s \tag{2.9}$$

ϕ_o is the trap depth in the gap with respect to the bottom of the conduction band.

e) Space-charge limited current

When the carrier concentration in the insulator bulk is relatively high, the current becomes space-charge limited current (SCLC):

$$j(V) = \frac{9}{8}\varepsilon_0\varepsilon'\mu_e\frac{V^2}{L^3} \qquad (2.10)$$

where μ_e is the mobility of electrons, L is the sample thickness and V is the applied voltage. This mechanism combines the effects due to the bulk and the electrode processes.

Presence of the above conduction mechanisms in polymers depends on many factors, for instance, the type of material, electrode metal, applied electric field, temperature and other experimental conditions. In general, for most polymers, the upper limit of the "low field" regime is about 10^5 V/cm. Usually, uniform E is assumed as given simply by V/L (average field). In many cases, this is a good approximation. But in some cases, the local field E_L inside the sample may be different from this average field when charge injection and charge build-up occur. This can lead to difficulties in analyzing the conduction behaviour of polymers.

2.3 Properties of polyimide

2.3.1 Chemical structure

Polyimide (PI), or poly(pyromellitimide) (Kapton is the Du Pont trade name) is produced by condensation polymerization of a dianhydride acid and a diamino base[16-18]. First, a dianhydride acid reacts with a diamino base at room temperature in an acid environment to form polyamic acid, then polyamic acid has to be cured at 200 - 400°C for dewatering to finally form PI. The polycondensation reaction of PI is illustrated in Fig.2.1. Functional groups R' and R" can be selected. For Du Pont Kapton-H, R' and R" are shown in Fig.2.1, i.e. the anhydride is pyromellitic dianhydride (PMDA), and the base is 4,4'-diamino diphenylether (DADPE).

The properties of particular PI are dependent on R', R" and on the manufacturing process. This is one of the main reasons why different researchers have reported very different measured results of electrical properties. Du Pont Kapton-H has yellow colour, and possesses very good electrical and chemical stabilities at room temperature. Its density is about 1.4 g/cm^3, and the temperature range over which it is stable is -269°C to 400°C. The glass transition temperature T_g varies within a very large range. Generally, T_g is above 200°C, depending on R', R", and on thermal treatment etc..

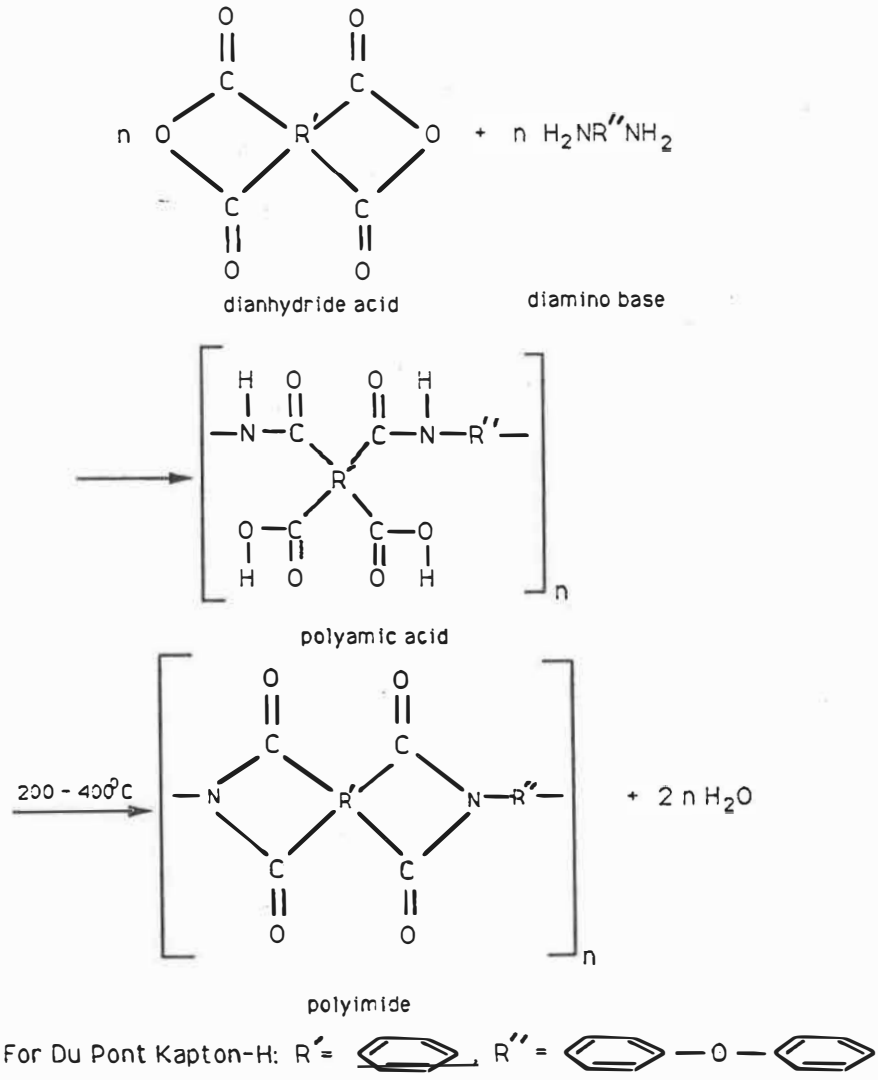

Fig. 2.1 Polycondensation reaction of polyimide

2.3.2 Electrical properties

Relative permittivity ε_r' of PI is reported to be between 3.0 and 4.1, loss tangent tanδ is in the order of 10^{-3}, depending on relative humidity (the higher the relative humidity, the larger the permittivity)[17]. Breakdown field E_b is about 3×10^6 V/cm or higher[16].

Numerous reports on the measurement of bulk conductivity of PI suffer from vast scatter in experimental data, mainly because of different R' and R", the manufacturing process and the experimental conditions. The low field ($<10^5$ V/cm) conduction is ohmic. The d.c. bulk conductivity at room temperature σ_v is lower than 10^{-18} $(\Omega\cdot cm)^{-1}$ [19-22]. However, Nevin reported bulk conductivity of 10^{-16} $(\Omega\cdot cm)^{-1}$ at room temperature[23]. Many researchers proposed that the charge carriers in PI are ions, most probably the protons originating from carboxyl groups (-COOH) in unimidized polyamic acid (see Fig.2.1). The dissociation of a carboxyl group is expressed as[21]

$$-COOH \rightleftharpoons -COO^- + H^+ \qquad (2.11)$$

Table 2.1 gives a summary of results on the bulk conductivity of polyimide. It is worth giving some detailed review on Sacher's results because his work was done early in 1979[21], and the report was typical. Two thicknesses, 127 μm and 25.4 μm, of samples were used. The measurements were done in two measuring environments: dry and wet (the relative humidity RH=75%). Ohmic conduction at low field was found. The bulk conductivity has been found to depend on both thickness and thermal cycling. For dry sample, the conductivities on cooling were invariably higher than on heating, however, the activation energies E_a for different samples' thicknesses and different thermal cycling directions (cooling and heating) were almost the same, i.e. E_a=1.4 eV. For wet sample, no dependence of σ_v on thermal cycling was found, but, the activation energies for different thicknesses varied: E_a=0.7 eV for 127 μm thick sample, and E_a=0.9 eV for 25.4 μm thick sample. The conductivity of dry samples has been shown to be due to protons ionized from carboxyl groups in non-reacted polyamic acid as shown in equation (2.11), while that of wet samples, 1-2 orders of magnitude higher, was found to be due to residual impurity ions.

Smith et al.[19] have reported the electrical conduction in PI between 20 and 350°C in the ohmic region in dry air environment. Ionic conduction was also proposed by them. They have investigated and discussed the behaviour of charging, discharging (polarization), and steady state currents both at low and high

Table 2.1 Summary of d.c. electrical conduction of polyimide

Authors	Material	Test condition	Temperature Range	Activation Energy(E_a, eV)	Carrier, Hopping Distance(Å)	Field Dependence	Notes
Smith[19]	PMDA-ODA	1 hr. in dry air at test temperature	20 - 350°C	0.5(T<175°C) 1.5(T>175°C)	ion	$I \propto E$	
Sessler[20]	DuPont Kapton-H		50 - 270°C	1.7(100-270°C)	positive carrier	$I \propto V$(low field) $I \propto V^2$ (high field)	
Sacher[21]	DuPont Kapton-H	dry in vacuum wet in 75% RH	45 - 90°C	1.4(dry sample) 0.7-0.9(wet sample)	proton	ohmic	σ_v dependent on thickness and thermal cycling
Nevin[23]	DuPont 2555		26 - 100°C	0.36(T<60°C) 1.04(T>60°C)	ion, 252 (T=80°C), 274 (T=100°C)	$\ln(I) \propto V^{0.5}$ $\ln(I) \propto V$	
Chang[24]	DuPont Kapton-H	at 150°C, short circuit for 24 hr. before meas.	80 - 240°C	1.0(80-150°C) 1.6(150-200°C) 0.8(200-240°C)	ion	ohmic	multiple transitions and relaxations
Sawa[25]	DuPont Kapton-H	at 250°C for 20 mins in vacuum before measurement.	120 - 180°C	1.1(extra-ploated)	ion, 80(180°C) 115(120°)	$I \propto E$($E<10^5$V/cm) $\ln(I) \propto E$($E>10^6$V/cm)	change of hopping distance may arise from heat treatment
Brown[26]	DuPont 2555	dry N_2	30 - 200°C	1.1(low field) 0.7(high field)	ion	$I \propto E$($E \leq 10^5$V/cm) $\ln(I) \propto V^{0.5}$ ($E>10^5$V/cm)	
Sharma[27]	Kapton-H	at 75°C short circuit for 6 hr. before meas.	100 - 200°C	1.04 (T<150°C)	ion, 52(100°C) 59(200°C)	$I \propto E^5$ ($E<10^5$V/cm)	
Nagao[29]	Polyimde				ion, 75 (T>200°C)		result obtained from breakdown research
Tanaka[30]	Polyimide				46(186°C)		result obtained from TDC method

temperatures. The polarization current is nearly independent of temperature and is well modeled by the molecular dipole theory of polarization. The 3 μm thick sample was used, and E_a was found to be divided into two regions: E_a = 0.5 eV for 23°C < T < 175°C, and E_a = 1.5 eV for 175°C < T < 350°C.

From Table 2.1, we can see that below 150°C, most of reported results E_a is around 1.0 eV[22-27], differing from those reported by Sacher and Smith et al.. In addition, E_a values less than 0.3 eV has also been reported[28], but not shown in Table 2.1. The values for hopping distance of ions, are very different from author to author, varying from 46 to 274 Å[23,25,27,29,30].

2.4 Properties of poly(ethylene terephthalate)

2.4.1 Chemical structure

Poly(ethylene terephthalate) (PET), commercially called Mylar, is made from terephthalic acid and ethylene glycol by dewatering reaction, which still belongs to polycondensation[12]. The chemical reaction scheme is shown in Fig.2.2. Mylar (typically 12.5 and 25 μm thick) is a transparent film. At room temperature, its mechanical and chemical stability is very good. The glass transition temperature T_g is between 70°C and 80°C. Its continuous working temperature range is narrow (-70°C to 157°C) compared with that of polyimide. The density is about 1.4 g/cm^3.

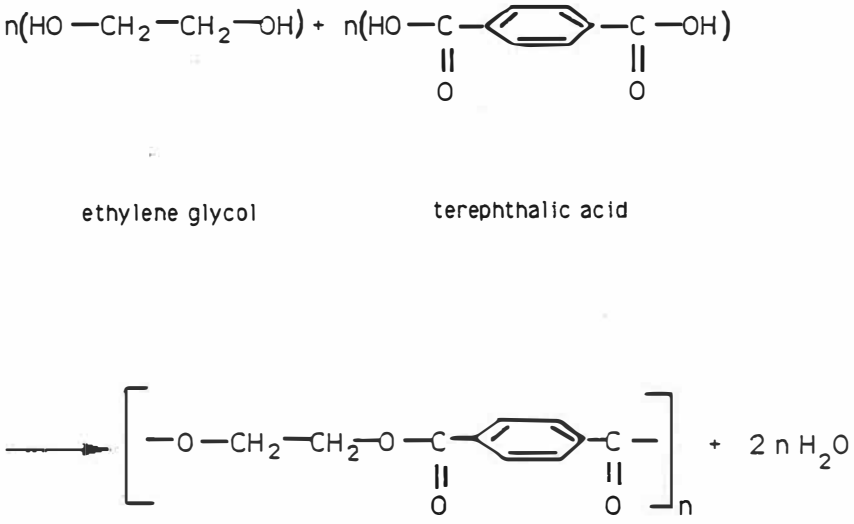

ethylene glycol terephthalic acid

poly(ethylene terephthalate) (Mylar)

Fig. 2.2 Polycondensation reaction of Mylar

2.4.2 Electrical properties

Mylar is a very good insulator in its whole working temperature range. Its permittivity varies from 2.9 to 3.2, the loss tangent is between 10^{-3} and 10^{-2} [16], the bulk conductivity at room temperature is lower than $10^{-18}(\Omega \cdot cm)^{-1}$. During the past three decades, many workers reported their investigations on bulk electrical conduction of PET. Table 2.2 gives a summary of d.c. bulk conducting behaviour of Mylar.

Like PI, the results for PET shown in Table 2.2 also exhibit a very big scatter from one author to another. The kind of charge carriers in Mylar has been a controversial issue in the past research. Sacher[38] once gave a brief review on this problem and mentioned the respective evidences for ionic carriers and electronic carriers from different authors. Although the data and reasoning may vary, there is general agreement as to the electronic nature of the phenomenon below 80°C. However, the evidences for both electronic and ionic conduction above 80°C have been reported. Similarly to Kapton, the reactant terephthalic acid (see Fig.2.2) may be residual in PET, and the carboxyl group -COOH in it can be thermally dissociated to give protons as shown in equation (2.11). Therefore, some researchers believed that the charge carriers in PET are protons[31,39]. The evidence to support this assumption is the independence of bulk current on electrode material, and the current-voltage characteristic of hopping type as

Table 2.2 Summary of d.c electrical conduction of Mylar

Authors	Material	Test Condition	Temperature Range	Activation Energy (E_a, eV)	Field Dependence	Carrier, Hopping Distance	Notes
Sacher[31]	DuPont Mylar T polyester	at 145°C in vacuum before meas.	70 - 140°C	1.7 (70-85°C), 2.2 (100 - 140°C)	ohmic($E<10^5$V/cm)	proton	σ_v depends on thermal cycling
Caserta[32]	commercial PET	in vacuum	293K		$I \propto V \exp(aV)$ (trap uniformly distributed-modified SCLC ($E>2\times10^5$V/cm)	injected holes	localized energy levels are due to the lack of order rather than impurities
Smith[33]	PET		180 - 290°C	0.62 (molten state) 0.90 (annealed solid)		ion	
Lilly[34]	DuPont Mylar		70 - 163°C	1.87 (25μm thick) 1.94 (250μm thick) ($E = 1.6\times10^5$V/cm)	$I \propto \exp(aV^{0.5})$ ($E>2\times10^5$V/cm)	electron	
Amborski[35]	PET		70 - 200°C	3.4 (amorphous) 1.6 (crystallized or oriented) ($E=5\times10^4$V/cm)	$I \propto \sinh(aV)$	ion, 69 Å (130°C) 78 Å (180°C)	crystalization and orientation result in a decrease in conductivity
Taylor[36]	ICI Meline grade PET	in vacuum	20 - 150°C	0.52-1.26(Al electrode), 0.8 - 1.9 (Au_4 electrode) ($E=4\times10^4$ - 1.2×10^6 V/cm)	$I \propto \exp(aE^{0.13})$ ($E>1.6\times10^5$V/cm, space charge-modified Schotty emission)	electron	$E_a = \phi - e\beta E^{0.13}$ ϕ: difference of energy between bottom of conduction band and Fermi level of metal
Hanscomb[39]	DuPont Mylar C	heat in vacuum before meas.	100 - 180°C	3.34	$I \propto E^{0.5}\exp(\beta E^{0.5})$ (high field) $I \propto \sinh(aE)$ (middle field)	positive ion, probably proton, 19-23 Å	two conduction mechanisms acting independently

mentioned in section 2.2. Some researchers have mentioned that the carriers are ions as shown in Table 2.2[33,35], however, they did not clearly identify the carriers due to the lack of evidence. Taylor et al.[36] found a conduction mechanism of space charge-modified Schottky emission at high field ($E > 1.6\times10^5$ V/cm), while Lilly et al.[34] found a Schottky current at $E > 2\times10^5$ V/cm. Electronic carriers were proposed in these two cases. Sacher[38] mentioned that different thermal treatment before measurements can probably change the conduction classification. In fact, both mechanisms can exist in PET at both low and high fields, however, the ionic conduction may dominate in low fields and the electronic conduction may dominate in high fields. Above T_g, the reported E_a of charge carriers suffers a very large scatter, varying from 0.52 to 3.40 eV. However, most of researchers, for example Sacher[31] and Lilly et al.[34], reported E_a of from 1.7 to 2.2 eV. The E_a value dependent on sample thickness and electrode material was also reported by Lilly et al.[34] and Taylor et al.[36]. In addition, the test conditions such as thermal cycling can also affect measured results. E_a also depends on crystallization and the degree of orientation, as reported by Amborski[35]. E_a is not continuous at T_g, however, due to the difficulties in accurately measuring very low current at low temperatures, only few reports exist, for example, $E_a = 0.3$ eV below 70°C by Hayashi et al.[37].

The density n of charge carriers (protons) in PI or in PET depends on the

ionization or dissociation equation (2.11), and is described by a model for polymers proposed by Barker and Sharbaugh[40,41]. This model applies the theory of weak electrolytes to "strong electrolytes" within solid polymeric systems. Sacher has also used this model to discuss the ionization process of -COOH groups in PI[21]. The −COOH groups are assumed to be an electrolyte which is dissolved in PI or PET. Let n_o represent the density of -COOH groups, and φ the extent of ionization, then

$$n = n_o \varphi$$

The equilibrium constant K is given as follows:

$$K = \frac{[H^+]\,[-COO^-]}{[-COOH]}\,\gamma^2 = n_o\,\varphi^2\,\gamma^2 = K_o \exp\left(-\frac{g}{kT}\right) \qquad (2.12)$$

Here, we have used the weak ionization condition $\varphi << 1$. Therefore, n can be expressed as

$$n = \frac{\sqrt{n_o K_o}}{\gamma} \exp\left(-\frac{g}{2kT}\right) \qquad (2.13)$$

where γ is the activity coefficient, K_o the equilibrium constant of the reference state, and g the Gibbs free energy of ionization.

2.5 Electron-beam charging of polymers

We have indicated previously that PI and PET, used as thermal blankets in

space systems, can be subjected to surface flashovers due to charge build-up, when they stay in outer space. Especially in geosynchronous orbit, the electrons with energy of 0.1 keV to 0.1 MeV dominate, and they charge the surface of thermal blankets, sometimes to levels as high as -10 kV[42]. The occurrence of surface flashover can interfere with electronic payloads on board and cause surface damage. In order to resolve this problem, it is important to first understand the behaviour of polymers films irradiated by an electron beam[42-47]. One usually simulates the space environment in the laboratory, and observes the electron-beam charging and discharging of polymers to obtain common rules for the process, finally determining the ways to resolve the above problems. Numerous researchers have worked on this field for several years. Among them, Balmain has done most about the surface charging and discharging of space materials.

The basic experimental arrangement used by Balmain for evaluation of charging and discharging phenomena in polymer surfaces is illustrated in Fig.2.3[45]. We may see that the tested sample is in fact a metal-backed sample, while its other surface (the top surface) is exposed to the irradiation of an electron beam. When the monoenergetic beam (with a typical energy of 20 keV) is incident upon polymer surface, the electrons penetrate to a stopping depth (about 7-8 μm for the energy of 20 keV). After some time, electrons will be distributed inside the sample in a complicated way. If the surface or bulk potential

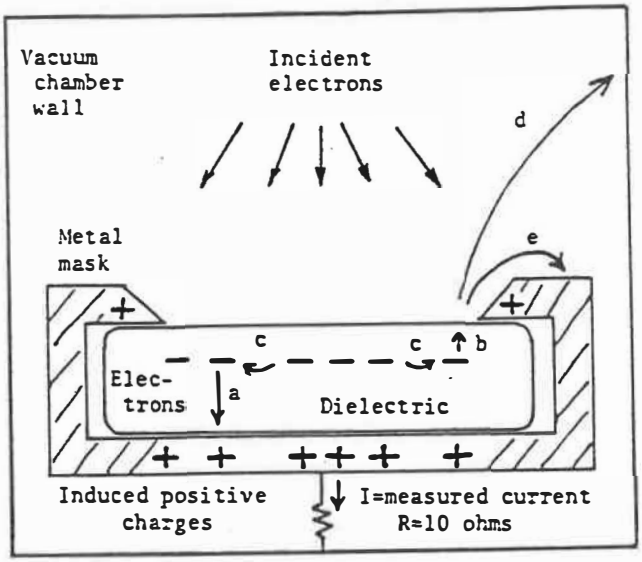

Fig.2.3 Possible charging and discharging phenomena: (a) punchthrough arc with top surface of dielectric blown off, (b) blowoff arc to surface, (c) flashover arc or propagating subsurface discharge, (d) ejected electrons going to chamber wall, (e) ejected electrons going to mask.

reaches a threshold value, discharges between the sample surface and the vacuum chamber wall will occur. Three possible discharging arcs may occur. The charged sample may discharge from the embedded electron layer through to the substrate via the punchthrough arc mentioned as "a" in Fig.2.3. A blowoff arc to surface indicated by "b" can also occur in cases where there is a high near-surface field and especially close to an edge. Due to the ejection of electrons by blowoff, a high-field region inside the sample is left, and consequently leading to flashover arc "c". The flashover may produce sporadic or continuous blowoff of material as it propagates, resulting in surface damage. The observation using a scanning electron microscope (SEM) confirmed this damage[45-47].

The discharge current flowing through a load resistor R can be obtained by measuring the voltage across R. It was directly recorded with an oscilloscope. The results for 125 μm thick PET sample revealed that the physical quantities such as peak current I_m, total charge Q passing through the resistor R during discharging, the dissipated energy E_d, and average pulse duration T_d can be correlated with the exposed sample area A in a power law[45]:

$$F \propto A^n \qquad (2.14)$$

where F represents any one of I_m, Q, E_d, and T_d. For I_m and T_d, n ~ 0.5, for Q, n ~ 1, and for E_d, n ~ 1.5 (A = 0.1 ~ 100 cm^2). It was also found that the surface discharges appear to propagate at a well-defined velocity of 3×10^5 m/s which was estimated with an aperture radius of 1 cm and a pulse duration of 33 ns. The experiments with PI gave the similar results.

Balmain et al. also made the observation on the 51 μm thick PI coated by P-SiO_2 and P-SiN (about 0.5 μm thick)[11]. The most prominent feature of the results is the complete absence of arc occurrence for the coated samples, compared with the presence of arc for the bare samples in the same test conditions. This proves that the protective layer P-SiO_2 and P-SiN can effectively suppress the build-up of surface charges, and consequently preventing discharge arcs.

Distribution of charges in the e-beam charged polymers is another important aspect, and it has been extensively studied in past several years[48-50]. The experimental description and theoretical treatments were given in many papers, for example, in a review paper by Frederickson[42].

2.6 Electrical properties of P-SiO_2 and P-SiN

There are several methods for the preparation of SiO_2 and SiN thin films: evaporation, ion beam deposition or thermal growth, and plasma-enhanced chemical vapour deposition (PECVD). Among those, plasma deposition has been extensively adopted because it has several advantages from the point of view of both fabrication process and properties of thin films. For example, high deposition rates, in the range of several hundred ångströms per second, can be mentioned. Another advantage is the ability to "tailor" (that is, to vary predictably and reproducibly) film structure and properties by controlled variation of substrate temperature T_s or power density in the plasma or both. Together with chemical composition, morphological and physicochemical properties are affected by the preparation parameters: films deposited at high T_s or power density are free of defects and adhere strongly to their substrate; they are dense, and have low permeability to gases or vapours.

In the plasma deposition process, electron-impact dissociation of the introduced precursor gases in the glow discharge is the primary step for chemical reaction. Neutral fragments (radicals), produced in the gas phase, diffuse toward the substrate and chamber wall, and ionic species move toward the electrodes under the influence of the applied electric field. Some of the neutral species are

electronically or vibrationally excited by electron impact and emit light whose wavelength ranges from vacuum UV to IR. Secondary processes such as ion-molecule and neutral-molecule reactions take place through collisions in the gas phase. Finally, heterogeneous chemical reactions among reactive atoms, molecules, and ions impinging onto the surface may proceed to form a deposit. Many variables must be controlled in plasma deposition. The most important parameters affecting the deposition rate and the properties of films are discharge frequency, power, pressure, and T_s. The frequencies used in the plasma deposition are generally microwave frequency (MW, 2.45 GHz), radio frequency (RF, 13.56 MHz) and dual mode microwave/radio frequency[51,52]. The typical pressure used is about 100 mTorr. The introduced gases are chosen in dependence on the thin film which is required.

There are numerous reports on the electrical properties of P-SiO_2 and P-SiN. However, because their electrical properties are strongly dependent on the preparation conditions, the reported results have suffered from large scatter[53,54]. In our laboratory, P-SiO_2 and P-SiN thin films were deposited using both MW frequency and dual mode MW/RF at both ambient and higher T_s[51,52,55,56]. P-SiO_2 films were deposited using a SiH_4 and N_2O feed gas mixture, while the SiH_4 and NH_3 feed gas mixture was used for the deposition of P-SiN films.

The electrical properties of P-SiO_2 and P-SiN deposited using MW frequency discharge in our laboratory can be summarised as follows. The preparation conditions are: MW power = 100 W, T_s = 280°C, Pressure = 100 mTorr (1 Torr = 133 Pa)[55,56]. The permittivities of P-SiN and of P-SiO_2 at low frequency (f = 10^2 ~ 10^5 Hz) and room temperature are 7 and 4, and the high frequency (or optical) permittivities of P-SiN and P-SiO_2 are 4 and 2, respectively. The loss tangent tanδ of P-SiO_2 varies from 10^{-3} to 10^{-4} between 10^2 and 10^5 Hz (RH = 30%), while tanδ of P-SiN ranges between 10^{-1} and 10^{-2}. The d.c. electrical conduction is ohmic for $E \leq 5\times10^5$ V/cm. At room temperature the bulk conductivity of P-SiN and P-SiO_2 is in the order of 10^{-14} and 10^{-16} $(\Omega\ cm)^{-1}$, respectively, i.e. P-SiN is more conductive than P-SiO_2. The variation of the bulk conductivity with temperature obeys the Arrhenius type from room temperature to 120°C. The activation energy E_a is 0.30 eV for P-SiN, and is 0.65 eV for P-SiO_2[53,54].

Martinu et al.[52] in our laboratory have recently reported the electrical properties of P-SiO_2 and P-SiN deposited using dual mode MW/RF (2.45 GHz and 13.56 MHz). The MW power was 100 W; the RF power was varied from 0 to 450 W, which induces a negative substrate voltage V_b ranging from 0 to - 800 V. The pressure was 80 mTorr, and T_s = 25°C. Compared with earlier reports described above, the difference here consists in the lower T_s and the addition of RF. The measured results have shown that V_b can influence the electrical properties

significantly. First, the film deposited at higher negative V_b has lower dielectric loss than at lower negative V_b. For instance, tanδ of P-SiN varies from about 1 to 10^{-3} for V_b values from 0 to -800 V, and tanδ of P-SiO_2 is close to 10^{-1} at V_b = 0 and to 10^{-3} at V_b = 200 V. The higher negative V_b also causes a decrease in the bulk conductivity. For example, the conductivity of P-SiN at V_b = 0 is 10^{-13} $(\Omega \cdot cm)^{-1}$, and it is 10^{-16} $(\Omega \cdot cm)^{-1}$ at V_b = - 800 V; the conductivity of P-SiO_2 changes from 3×10^{-13} $(\Omega \cdot cm)^{-1}$ to 2×10^{-15} $(\Omega \cdot cm)^{-1}$ when V_b is varied from 0 to - 300 V. Therefore, the dual-frequency deposition technique has proven to be a powerful approach for fabrication of high quality dielectric thin film materials at ambient substrate temperature if a high negative V_b is used. The sample preparation for this thesis is based on this MW/RF technique.

Chapter 3

Experimental Methodology

In this chapter, we will first describe the process of sample preparation, and then discuss the experimental methods for the measurements of bulk and surface conductivities, and of the C-V characteristics for MIS structure.

3.1 Sample preparation

3.1.1 The samples for conductivity measurements

PI and PET samples or substrates for the preparation of double layer dielectric structures are Du Pont Kapton-H and Du Pont Mylar films. The thickness of PI samples is 51 μm, and that of PET is 12 or 25 μm.

Thin films of P-SiO_x and P-SiN with thicknesses from 0.5 to 1.5 μm were deposited onto PI or PET in dual-frequency plasma using a large volume microwave (MW) plasma (LMP®) apparatus. The substrates were placed onto a RF (13.56 MHz) biased electrode and were simultaneously exposed to MW (2.45 GHz) discharge excited by a slow wave applicator. The application of the RF power induces a negative substrate bias voltage (-150 V). The pressure in the reaction chamber during deposition was 80 mTorr, and the applied MW power was 150 W.

The substrate temperature was ambient (about 25°C). P-SiO_x films were deposited using a SiH_4 (6 sccm) and N_2O (12 sccm) feed gas mixture, while the SiH_4 (8 sccm) and NH_3 (24 sccm) feed gas mixture was used for the deposition of P-SiN films.

The thicknesses of P-SiO_x and P-SiN were measured using both a Leitz MPVSP multiple-wavelength optical interferometer and a Sloan-Dektak profilometer. Film composition was determined by X-ray photoelectron spectroscopy in a VG-ESCALAB 3MkII system, using MgK_α radiation. Under the preparation conditions described above, we found that the compositions of P-SiN and of P-SiO_x are stoichiometric, namely Si_3N_4:H and SiO_2:H, respectively. The atomic content of hydrogen is about 20%. A more detailed description of plasma deposition in our laboratory has been reported in several papers[51,56,57].

For the electrical measurements, aluminum electrodes (about 2000 Å thick) were vacuum-evaporated on both sides, to form metal-insulator-metal (MIM) or metal-$insulator_1$-$insulator_2$-metal (MI_1I_2M) structures. Figure 3.1 shows sample configuration and the arrangements for the bulk and surface conductivity measurements of double layer structure sample. Electrodes 1 and 3 are used for bulk conductivity measurement with electrode 2 as a guard; electrodes 1 and 2 are used for surface conductivity measurements, with electrode 3 as a guard,

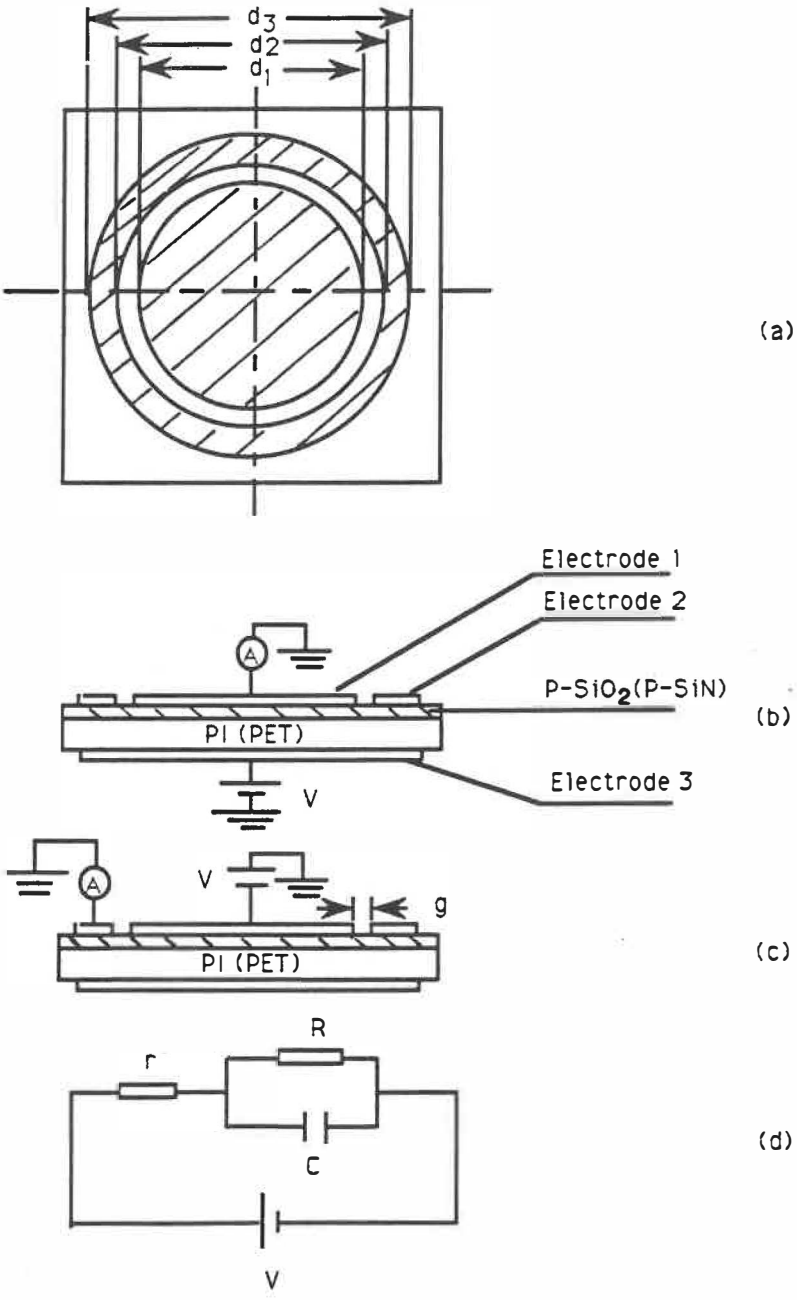

Fig. 3.1 Sample configuration for bulk (b) and surface (c) conductivity measurements, and the equivalent circuit (d) for bulk conductivity measurement. d_1 = 49 mm, d_2 = 50 mm, d_3 = 60 mm, g = 0.5 mm.

according to the standard test method for d-c resistance of insulating materials from the ASTM (American Society for Testing and Materials)[58].

3.1.2 The samples for C-V measurements

The samples used for the C-V measurements are MIS and MI_1I_2S structures, the metal being Al, with a work function of 4.25 eV[59]. The semiconductor is a n-type silicon wafer [phosphorus-doped, (100) oriented], with an impurity concentration of 4.5×10^{15} cm^{-3}, the work function is 4.29 eV[59].

First, the Si wafer was cleaned with 1,1,1-trichloroethane (TCE, CH_3CCl_3), acetone [$(CH_3)_2CO$] and 2-propanol ($CH_3CHOHCH_3$), then the naturally-oxidized thin layer of SiO_2 on the surfaces (about 40 Å thick) was removed using 10% hydrofluoric acid (HF). Following this, the Si wafer was carefully rinsed with deionized water, to remove possible residual ions on the surfaces. After having deposited a layer of Al on the back side (about 2000 Å), the sample was annealed at 500 °C to assure a good ohmic contact between Al and Si. We have found that at 500°C the Al electrode was not oxidized even in atmosphere.

Polyamic acid from Du Pont was spin-coated onto the other side of the Si wafer, and the sample was baked at 300 °C for 1.5 hours. Thus, polyamic acid is converted into polyimide as shown in Fig.2.1. The thickness of polyimide was

measured optically, a thickness of 0.9 - 1.0 μm being obtained at 10,000 RPM, and a spin time of 120 seconds. Aluminum was then evaporated onto the PI-coated sample to form an Al-PI-Si structure, or a thin layer of P-SiO_2 or P-SiN was plasma-deposited on top of the polyimide, followed by metallization to form Al-(P-SiO_2)-PI-Si or Al-(P-SiN)-PI-Si structure. The order of the films could be inverted to form Al-PI-(P-SiO_2)-Si or Al-PI-(P-SiN)-Si structure.

Thin layers of SiO_2 were also prepared by thermal oxidation. A layer of 2200 Å thick thermal SiO_2 was grown on the surfaces of a Si wafer in dry oxygen at 1200°C in about half an hour. The SiO_2 on the rear side was removed with 10% HF, photoresist being used for protection of the SiO_2 on the reverse sample side.

The electrode diameter of MIS or MI_1I_2S structure was about 5 mm. Thin copper wires were attached onto electrodes with silver paste, resulting in a very good contact, even at 170°C in vacuum.

3.2 Electrical measurements

3.2.1 Measurements of d.c. bulk and surface conductivities

The d.c.measurements were performed in vacuum (10^{-5} Torr). A Keithley 240 A voltage source and a Keithley 619 electrometer were employed for the

measurements of I-V characteristics. The voltage source provided a d.c. voltage from 1 to 1000 volts, and the electrometer was capable of measuring currents as low as 10^{-14} A. The sample was mounted on a heated support, and its temperature was measured with two K-type thermocouples in intimate contact with the sample surface. The temperature range investigated was from 19°C to 170°C.

The d.c. conductivity was measured as described below. If a d. c. voltage V is applied to the sample between electrodes 1 and 3 (see Fig.3.1b), a charging current I_c flowing through the sample is composed of three parts:

$$I_c(t) = I_g(t) + I_p(t) + I_{c\infty} \qquad (3.1a)$$

I_g is the component due to geometrical capacitance, $I_g \propto \exp(-t/\tau)$. The measuring circuit is equivalent to a series circuit composed of a resistance r with a parallel circuit of the sample capacitance C and its d.c. resistance R (see Fig.3.1d). Here, r is the summation of the internal resistance of the voltage source and of the wires, and r is $<<$ R. We can show that the relaxation time τ is $<<$ 1 s in our case. Therefore, I_g decreases very rapidly with time, and one can observe it only within a very short charging time. It can be neglected if we do not concentrate on the charging behaviour at very short time, which results in:

$$I_c(t) = I_p(t) + I_{c\infty} \qquad (3.1b)$$

$I_{c\infty}$ is the steady state current determining the d. c. conductivity. I_p, the polarization current, can be caused by many factors such as electron tunnelling, thermal activation in the localized electronic states in amorphous or partly-crystalline materials, and dipole orientation[19]. I_p decreases with time very fast, and it generally drops monotonously with time. After some time, I_c will be constant or will decrease with t very slowly. In this case, we can assign I_c at this time to $I_{c\infty}$. Let A be the area of the electrode, and L the sample thickness, then the bulk conductivity σ_v and the bulk resistivity ρ_v can be calculated as follows:

$$I_{c\infty} = \frac{V}{R} = V\frac{A}{\rho_v L} \tag{3.2a}$$

$$\sigma_v = \rho_v^{-1} = \frac{I_{c\infty}}{V}\frac{L}{A} \tag{3.2b}$$

If V is applied between electrodes 1 and 2 (see Fig.3.1c), the surface conductivity σ_s and the surface resistivity ρ_s (also termed sheet resistance) are calculated from the steady state surface current $I_{cs\infty}$:

$$\sigma_s = \rho_s^{-1} = \frac{g}{\pi(d_1+g)}\frac{I_{cs\infty}}{V} \tag{3.3}$$

where g is the gap between electrodes 1 and 2. ρ_s (unit: Ω/□) means that any square of the sample surface has the same resistance ρ_s.

In the ohmic conduction range, σ_v and σ_s are independent of applied voltage. If the electric field is high, conduction will deviate from the ohmic regime, and they depend on the applied electric field.

σ_v of a sample can in principle be correlated with its σ_s by a simple relation:

$$\sigma_s = L \sigma_v \tag{3.4}$$

However, this holds only in an ideal case. σ_s is strongly dependent on the degree of surface contamination, ambient atmosphere, relative humidity, and other factors. Values of σ_s measured at high humidity may be by several orders of magnitude higher than those measured in a dry environment or under vacuum.

The time duration (waiting time) required to reach a "steady state current" is an important aspect. In principle, this period should be infinite or very long. For every type of samples we chose the duration long enough that I_c does not vary too much any more. At low temperature (for example, at room temperature) we need long duration than at high temperature, because I_p dominates in I_c in short

charging time.

For many materials, I_p follows the Curie-von Schweidler power law[15]:

$$I_p \propto E\, t^{-n} \tag{3.5a}$$

where n is a positive number varying with T, generally $n \leq 1$. For intermediate times (typically $t \leq 600$ s) and at low temperatures ($T \leq 25^{\circ}C$), $I_{c\infty} << I_p$, and $I_c \equiv I_p$, consequently resulting in the following expression:

$$I_c(t) \propto E\, t^{-n} \tag{3.5b}$$

The discharging current I_d is the current when the sample's electrodes are short-circuited after some charging time. I_d is opposite to I_c as shown in Fig.3.2. According to the polarization theory of dielectrics[19], the magnitude of I_d is equal to the magnitude of I_p:

$$I_p = -I_d = |I_d| \tag{3.5c}$$

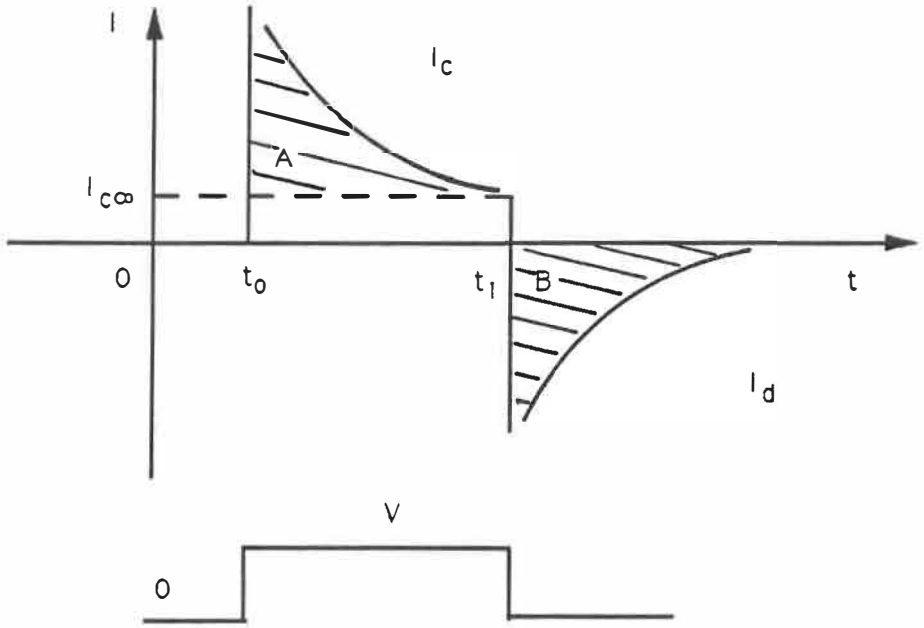

Fig. 3.2 Transient phenomena after the voltage application at time t_o and sample shortcircuiting at time t_1.

As expected in equations (3.5), I_p should drop monotonously with time until zero. Therefore, equations (3.1b) and (3.5c) result in the following expression:

$$I_\infty = I_c - I_p = I_c - |I_d| \qquad (3.6)$$

where I_c and I_p have be assumed > 0. Equation (3.6) can be illustrated in Fig.3.2, in which the shaded part A has the same area as the shaded part B. Therefore, as long as we apply a voltage to a sample and wait until the difference I_c - $|I_d|$ becomes constant, then I_c - $|I_d|$ represents $I_{c\infty}$. Usually, the waiting time is not very long, typically between 15 and 30 minutes[60].

In fact, the above description may not hold for some materials. Neuhaus et al.[61] reported the existence of maxima and minima in the $I_c(t)$ curve in Na-doped polyimide at a high temperature. In Chapters 4 and 5, we will see that $I_c(t)$ relation of P-SiO_2/PI does not obey the power law. In general, it is necessary to choose an appropriate method to determine the steady state current. The variation of I_c and I_d with time is in fact one of research subjects from which additional information about the material itself can be obtained.

The effect of discharging time on reliability of measurement should be considered when another measurement follows immediately on the same sample.

In our case we waited for a sufficiently long time for discharging in order to suppress the "history" of the first measurement.

3.2.2 Measurements of the C-V characteristics

The measurement of the C-V characteristics for a MIS or a MI_1I_2S structure is to measure the total capacitance C of the structure as a function of a applied gate voltage V_G and an a.c. signal frequency f. The charge distributed in the insulator(s) and at the insulator/semiconductor or $insulator_1$/$insulator_2$ interface can affect their capacitances. Therefore, the C-V measurement is a good tool for investigating charge distribution, charge transport, and interfacial behaviour.

Figure 3.3 shows the MIS and MI_1I_2S structures where V_G is applied. ε_r', ε_{r1}', ε_{r2}' and ε_{rs}' represent the relative permittivities of the insulators and of the semiconductor. The capacitances of the corresponding insulating layers and of the semiconductor are symbolized by C_I, C_1, C_2 and C_s, respectively. They can easily be calculated as parallel-plate capacitors. The impurity concentration of the semiconductor is expressed by either N_D (n-type) or N_A (p-type). V_G is said to be positive if the metal electrode is positively biased with respect to the ohmic contact. Another small a.c. signal is applied to the sample together with V_G in order to observe the dependence of sample capacitance on both V_G and f.

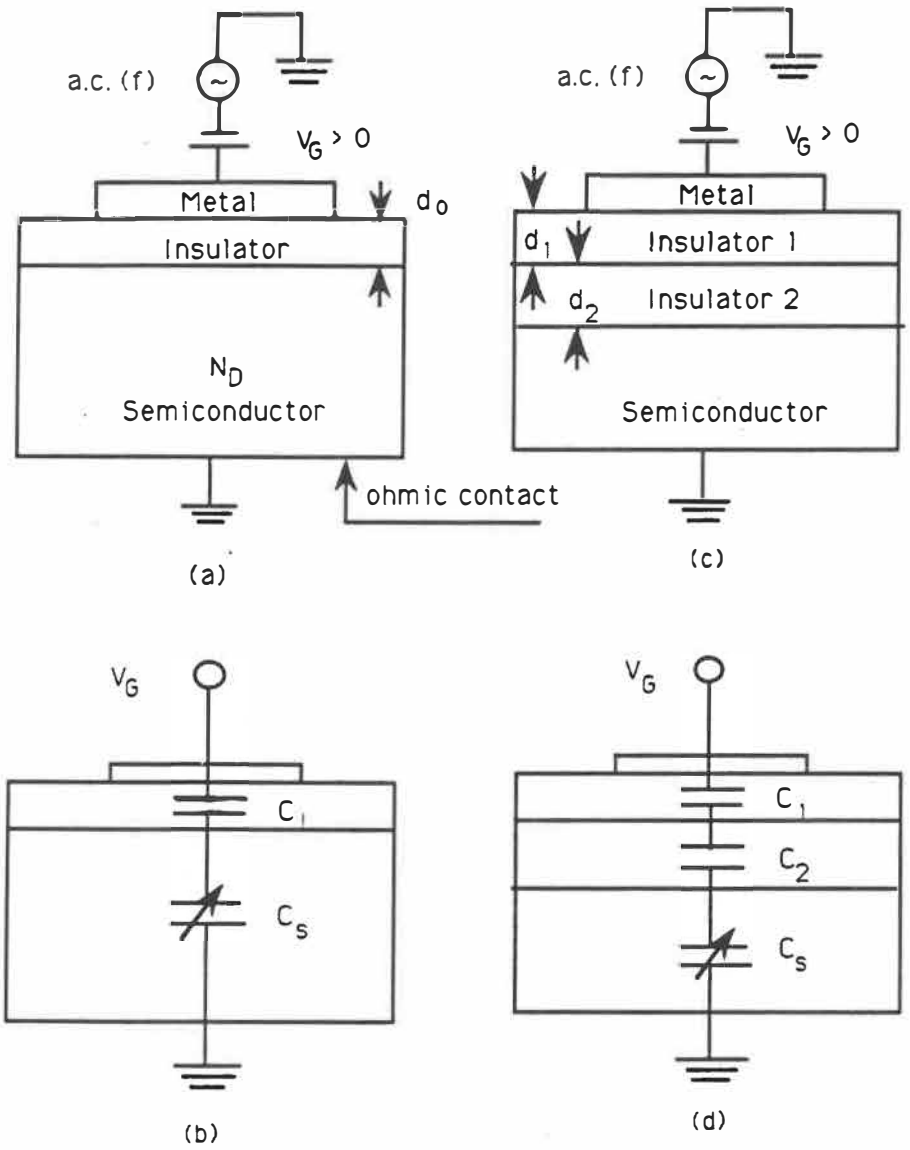

Fig. 3.3 A MIS structure (a) and its equivalent circuit (b), and a MI_1I_2S structure (c) and its equivalent circuit (d).

The MIS structure is equivalent to a capacitor represented by a serial combination of C_i, which neither depends on V_G nor on f, and C_s, which is a function of both V_G and f (see Fig.3.3). The theory of the MIS structure was established in the late 1950's[59,62]. The initial treatment uses an ideal MIS which is defined as follows: (1) the difference between the work function W_m of the metal and work function W_s of the semiconductor is zero, (2) there is no charge in the insulator, (3) there are no interfacial states at the insulator/semiconductor interface.

When V_G is applied to the ideal MIS, the charge in the metal electrode is distributed at its surface, while the charge distribution in the semiconductor depends on V_G. When $V_G = 0$, both conduction and valence bands of semiconductor do not bend because there are no net charges both in bulk and adjacent surface. The voltage that causes no bending of energy bands is called flat band voltage V_{GF}. Obviously, $V_{GF} = 0$ for an ideal MIS. Take n-type semiconductor as an example in the following discussion. If a large positive V_G is applied, the bands bend downward, the density of electrons near the surface is very high, the semiconductor in this case behaves similarly to a metal, and C_s is very large. The total capacitance C of the MIS is the same as C_i. This situation is called accumulation of majority carriers. When V_G is decreased, the density of electrons becomes lower, C_s decreases, and C drops. If $V_G < 0$, the energy bands bend upward, and electrons start to be depleted to form a depletion layer near the

semiconductor surface. The width of the layer becomes larger with increasing negative V_G, and C_s and C further decrease. If V_G reaches a negative value at which the density of holes (minority carriers) is larger than that of electrons, an inversion state is reached. When a strong inversion state occurs, the width of surface depletion layer reaches a maximum, and both C_s and C become minimum. If the negative V_G continues to increase, the density of holes keeps increasing, the semiconductor will again behave like a metal, and C will again reach C_I. However, this analysis holds only for very low frequencies (usually $f \leq 10^{-2}$ Hz). For high frequency, the minority carriers cannot follow the a.c. signal during inversion, they do not contribute to the capacitance, and C will not return to C_I, but it will remain constant at a minimum value in a strong inversion voltage range. The C-V characteristic at high frequency is more significant, and it is usually used to understand the charge distribution and transport in insulator. Figure 3.4 shows a typical MIS capacitance at both a low and a high frequency for n-type semiconductor. For p-type semiconductor, the shape of C-V curve must be exchanged between positive and negative voltage. If the parameters d_o, N_D, T, ε_r', and ε_{rs}' etc. are known, the C-V relationship can theoretically be calculated. Detailed analytical expressions for capacitance can be found in numerous publications[59,62].

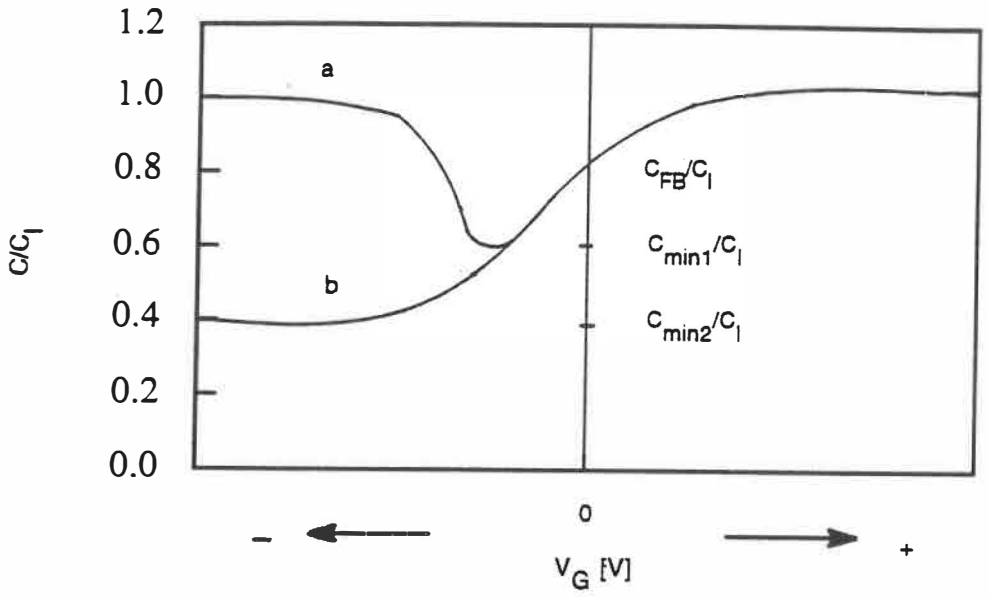

Fig.3.4 Capacitance-Voltage curves of an ideal MIS at low (a) and at high (b) frequency.

In fact, the ideal MIS is rarely encountered. The practical MIS is nonideal. Nonideal factors are the metal-semiconductor work function difference, the charges in the insulating layer and the semiconductor surface states which introduce charges into the insulator/semiconductor interface. The first two factors cause V_{GF} shift of the C-V curve along V_G axis, and the third factor results in the distortion of the C-V curve, because in this case the surface charge density introduced into the insulator/semiconductor interface varies with V_G.

The flat band voltage shift ΔV_{GF} caused by the metal-semiconductor work function difference is given by

$$\Delta V_{GF} = \frac{W_m - W_s}{e} \tag{3.7}$$

If $\Delta V_{GF} < 0$, the curve moves toward the left with respect to the ideal curve, and it moves toward the right for $\Delta V_{GF} > 0$. Usually, ΔV_{GF} caused by other factors is much larger than this, we can neglect the effect of work function difference.

Charges can be distributed spatially or in a thin layer at a distance x_o from the metal electrode in the insulating layer. For either of these two cases, ΔV_{GF} can be expressed using an equivalent surface charge density Q_s at the insulator/semiconductor interface:

$$\Delta V_{GF} = -\frac{Q_s}{C_o} \tag{3.8a}$$

where, $C_o = \varepsilon_o \varepsilon_r'/d_o$, being the capacitance per unit area of the insulating layer. For the surface charge distribution, Q_s is expressed as

$$Q_s = \frac{x_o}{d_o} Q_o \tag{3.8b}$$

and for the spatial charge distribution, Q_s is

$$Q_s = \frac{1}{d_o} \int_0^{d_o} x\,\rho(x)dx \qquad (3.8c)$$

Q_o is the surface charge density at x_o, and $\rho(x)$ is the spatial charge density.

In order to estimate the charge density in the MIS structure, bias–temperature (B.T.) experiment is usually done according to the following process. At low temperature (typically at room temperature), mobility of some charge carriers is so low that they can not move an obvious distance under a d.c. bias within experimental time; however, at higher temperature, their mobility is high enough to move an obvious distance. Therefore, one usually applies a bias V_B to the sample at high temperature (e.g. 120 or 150°C) for some time, then these carriers can be driven toward the metal/insulator or the semiconductor/insulator interface. This bias is maintained, and the sample is cooled to room temperature, so the charges accumulated either at the metal/insulator or the semiconductor/insulator interface are frozen, which cause ΔV_{GF}. Using equations (3.8), we can calculate the amount of transferred charges during this process.

In the MI_1I_2S structure (see Fig.3.3c), the charges are probably trapped at

the insulator$_1$/insulator$_2$ interface, ΔV_{GF} in this case is

$$\Delta V_{GF} = - \frac{Q_i}{C_{o1}} \tag{3.9}$$

Here, $C_{o1} = \varepsilon_o \varepsilon_{r1}'/d_1$, and Q_i is the surface charge density at the insulator$_1$/insulator$_2$ interface.

ΔV_{GF} can be obtained by comparing the experimental curve with the ideal curve, therefore, Q_s and Q_i can easily be calculated. However, we can not obtain the values of Q_o and x_o only with the C-V technique. The nonideal factors will be further discussed, in conjunction with our measured results in Chapter 5.

Chapter 4

D.C. Electrical Conduction Results

In this chapter, we will present the experimental results of the d.c. bulk and surface conductivity measurements on single layer PI and PET samples, and on double layer P-SiO_2/PI, P-SiN/PI, P-SiO_2/PET, and P-SiN/PET samples. These results include transient behaviour of the charging and discharging currents, the relationship between the steady state current and the applied voltage, and the variation of conductivity with temperature. Preliminary discussion and comparison will be given. Detailed analysis and proposed model will be presented in Chapter 6. All measurements were carried out in vacuum (10^{-5} Torr) except for those described in Section 4.3 where the measurement conditions are specified.

4.1 Bulk conduction in PI, P-SiO_2/PI and P-SiN/PI structures

The properties of polymers are generally affected by their "history". Therefore, we always performed the measurements for PI, P-SiO_2/PI and P – SiN/PI in several thermal cycles. The first thermal cycle was used to eliminate the effect of absorbed water on electrical conduction: the sample was baked at 150°C for 2 hours, then cooled down to room temperature. I_c was found to increase systematically with thermal cycling till the sixth thermal cycle (a more detailed

discussion will be presented in section 4.1.3). Usually, the reproducibility from sample to sample in the second cycle was not yet very good, however it was from the third cycle. In the following, the presented transient and steady state currents were always measured in the third thermal cycle, using an applied voltage of 100 V ($E = 2\times10^4$ V/cm).

4.1.1 Transient currents

a) Single layer PI films

Figure 4.1 gives I_c and I_d as a function of time t for PI at several temperatures. Both I_c and I_d decrease monotonicaly with time, and I_d has a direction opposite to that of I_c.

At a low temperature of 19°C, a Curie-von Schweidler power law[15], $I_c \propto t^{-n}$, $n \approx 0.80$, can be applied in the time interval between 3 and 300 seconds. After 300 seconds, I_c tends to be constant. At the higher temperatures of 90 and 120°C, I_c drops very slowly in the same period. It also obeys the power law, but the corresponding n values are much smaller than that at the low temperature.

I_d is lower than I_c, and it can also be expressed as $I_d \propto t^{-m}$ at both low and high temperatures. At 19°C, the value of m is the same as that of n, i.e., $m \approx 0.80$,

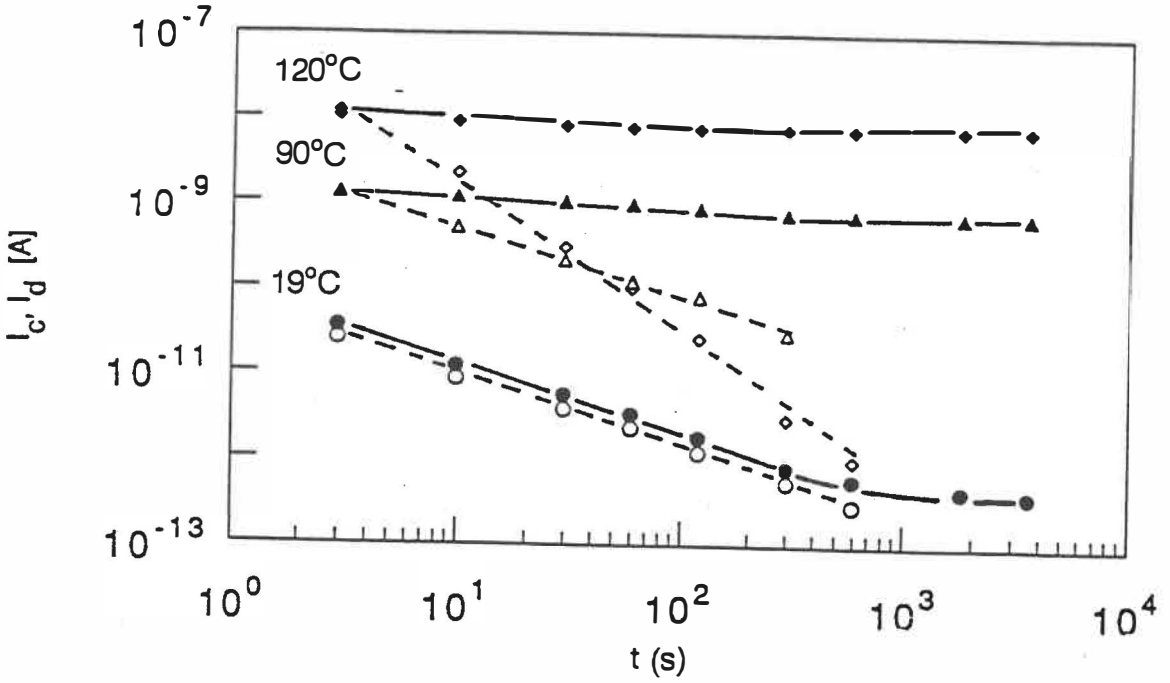

Fig.4.1 Charging I_c (●, ▲, ♦) and discharging I_d (o, ▵, ◇) currents as a function of time for PI at 19°C (●, o), 90°C (▲, ▵), and 120°C (♦, ◇).

and the difference I_c - $|I_d|$ is very small because of high resistivity. This indicates that at low temperature I_c and I_d are almost mirror image of each other in the short time. These are consistent with many reports, which were briefly reviewed by Smith et al.[19]. At high temperatures, I_d drops fast with time, while I_c decreases very slowly. They are not mirror images during this period of time. In fact, the period in which they are mirror images is probably less than 3 s at high temperature, short enough not to be observable. The stability of I_c at high temperature is consistent with reports from other authors[19,24,25]. The reason is that at high

temperature the transport current (i.e., the steady state current $I_{c\infty}$) dominates in I_c. The values of n and m for both I_c and I_d at several temperatures are summarized in Table 4.1.

Table 4.1 Values of n and m for I_c and I_d for polyimide

(3 s < t < 300 s, $I_c \propto t^{-n}$, $I_d \propto t^{-m}$)

T (°C)	19	90	120	150	170
n	0.80	0.12	0.05	0	0
m	0.80	0.80	1.70	1.50	1.10

The m and n values at 19°C are very close to those reported by Smith et al. ($0.6 < m < 0.8$)[19] and Kliem et al. ($m = 1$)[63]. There were only few reports on the I_d behaviour at high temperatures. According to Smith et al.[19], I_d exhibits a weak temperature dependence between the room temperature and 150°C. However, our results in Fig.4.1 and Table 4.1 indicate that I_d and m are very dependent on temperature. This difference most probably arises from different kinds of PI used in various experiments.

b). Double layer P-SiO_2/PI and P-SiN/PI structures

Figure 4.2 shows I_c for P-SiO_2/PI and P-SiN/PI at different temperatures. In

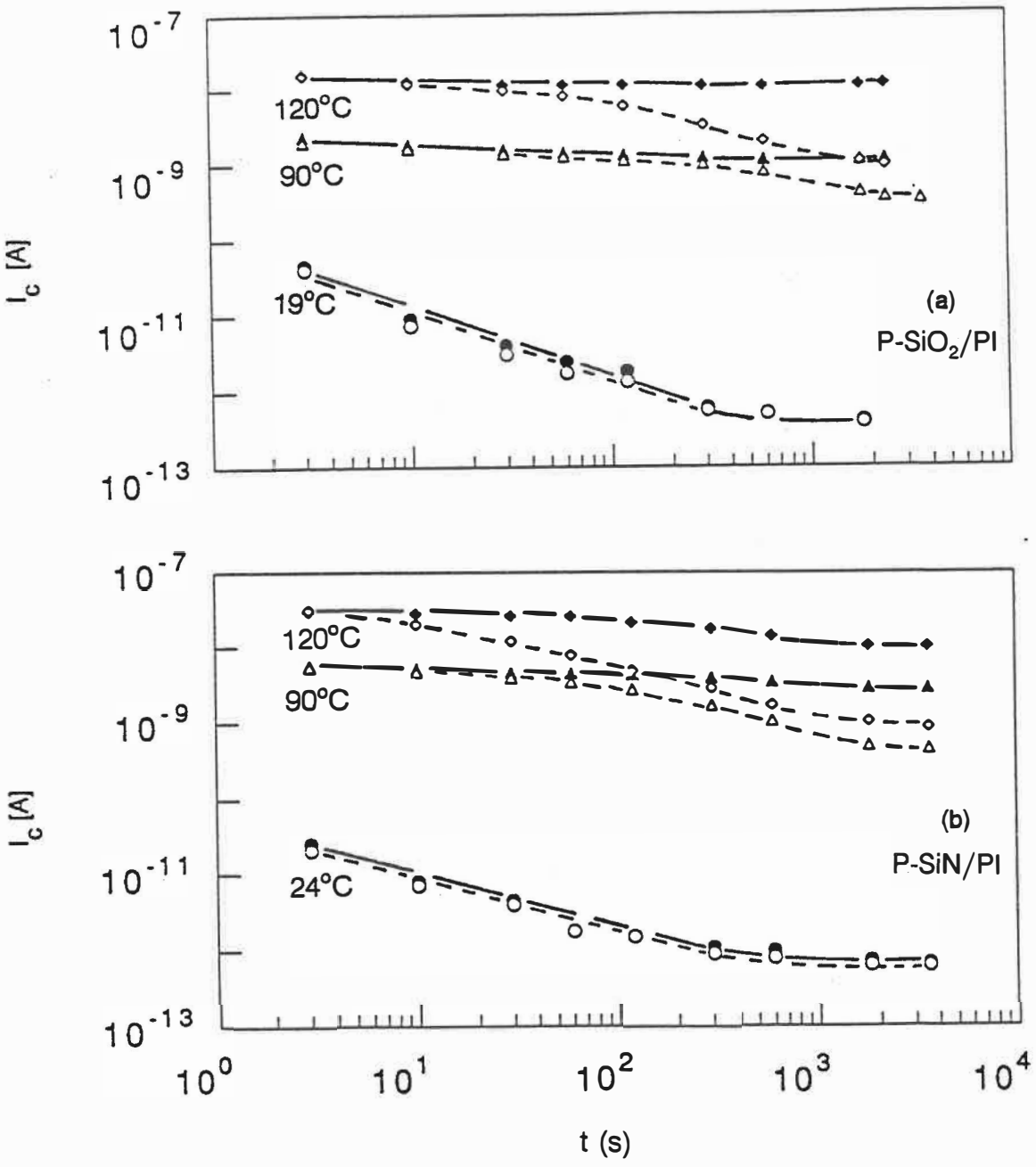

Fig.4.2 Charging current I_c as a function of time for P-SiO_2/PI (a) and for P-SiN/PI (b) at positive (I_{c+}: ●, ▲, ♦) and negative (I_{c-}: o, ▵, ◇) polarities at 19°C (a: ●, o), 24°C (b: ●, o), 90°C (▲, ▵), and 120°C (♦, ◇).

order to make comparison with PI, Fig.4.3 shows I_c and I_d for PI, and I_{c+}, I_{c-}, I_{d+}, and I_{d-} for P-SiO_2/PI at 120°C. Here, I_{c+} and I_{c-} (I_{d+} and I_{d-}) indicate the charging (discharging) currents at positive and negative polarities of the voltage applied to the electrode facing the P-SiO_2 (or P−SiN) layer, respectively. The corresponding cases are also represented by P−SiO_2(+)/PI and P−SiO_2(−)/PI [or P-SiN(+)/PI and P-SiN(-)/PI], respectively.

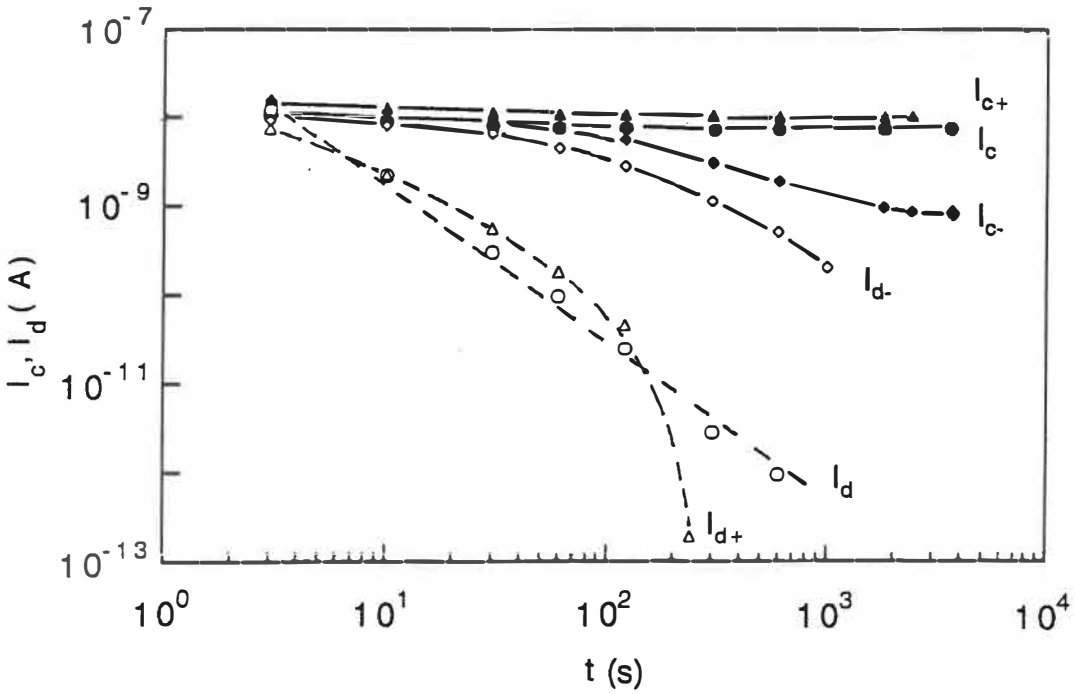

Fig.4.3 Charging I_c (●, ▲, ♦), and discharging I_d (o, ▵, ◇) currents as a function of time for PI and for P-SiO_2/PI at 120°C. PI (I_c: ●, I_d: o), P-SiO_2(+)/PI (I_{c+}: ▲, I_{d+}: ▵), P-SiO_2(-)/PI (I_{c-}: ♦, I_{d-}: ◇).

Like PI, at low temperatures of 19°C and 24°C, I_c of double layer samples does not exhibit any appreciable polarity dependence (see Fig.4.2). In contrast to PI, a difference between I_{c+} and I_{c-} is found in P$-SiO_2$/PI and in P-SiN/PI at high temperatures. The I_{c+} values are qualitatively similar to that of PI, but the I_{c-} values are quite different from that of PI (see Fig.4.3). At high temperatures I_{c+} and I_{c-} are basically the same for small t, but their difference increases with time. The longer the charging time, the larger the difference between I_{c+} and I_{c-}. The higher the temperature, the shorter the time when this difference occurs: for P-SiO_2/PI after 100 s at 90°C, and after 30 s at 120°C (see Fig.4.2a); for P-SiN/PI after 30 s at 90°C, and after 10 s at 120°C (see Fig.4.2b). After long waiting time, I_{c+} and I_{c-} tend to be constant, and the difference between them also becomes unchanged.

I_d of double layer samples is similar to that of PI at low temperature. However, a difference at high temperatures can be seen in Fig.4.3: I_{d+} of P-SiO_2/PI at 120°C is comparable to that of PI for $t \leq 100$ s, but I_{d-} is very different from I_{d+}, it drops much more slowly with time than I_{d+}. The power dependence on time ($I_d \propto t^{-m}$) cannot be applied to both I_{d+} and I_{d-}.

The dependence of I_c and of I_d on the polarity of applied voltage is qualitatively similar for both kinds of double layer samples. Since we did not

observe any effect of polarity for PI in the entire temperature range, this behaviour is judged to be typical for these double layer structures. As will be discussed later, the polarity-induced phenomena are believed to be related the P-SiO_2/PI and P-SiN/PI interfaces.

4.1.2 Steady state currents

The variation of the steady state charging current with the applied voltage V is studied in this section. Figure 4.4 shows the relationships between the steady state current and V for PI and P-SiO_2/PI at 24°C and 120°C. A waiting time of 1800 seconds was taken for obtaining the steady state current. The behaviour of P-SiN/PI is qualitatively the same as that of P-SiO_2/PI.

Before annealing, the electrical conduction of PI at 24°C is ohmic below 1000 V (E = 2×10^5 V/cm). However, the current becomes larger after annealing at 24°C, and the ohmic conduction regime applies only up to 100 V (E = 2×10^4 V/cm). This phenomena can probably be attributed to the transition of electrical conduction mechanism in PI. Presumably, the electronic conduction may dominate before annealing for virgin sample, while the ionic conduction, i.e. the protonic hopping conduction as discussed in Chapter 2, may dominate after annealing. This is very possible because many researchers, for example Nevin et al.[23] and

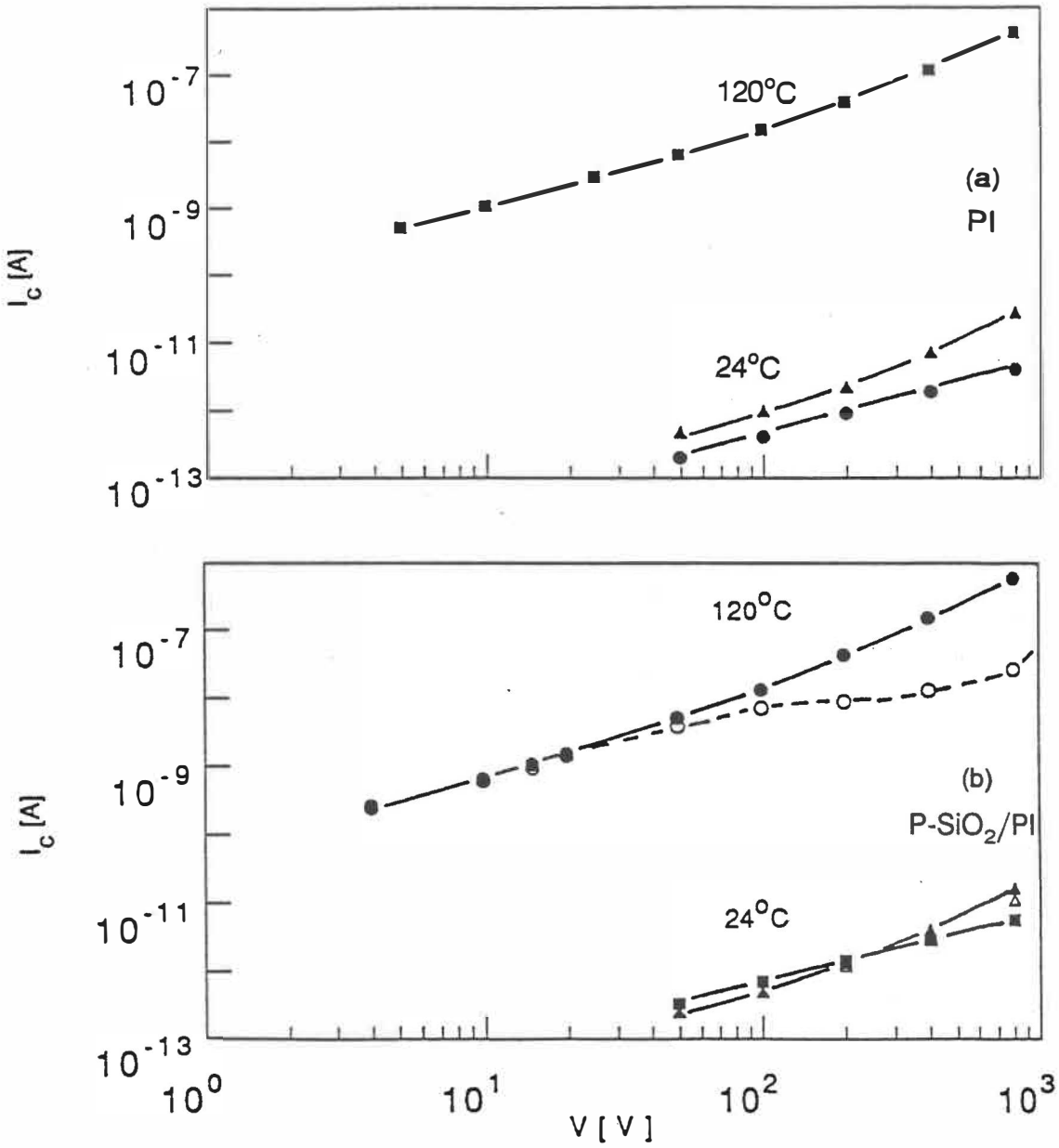

Fig.4.4 Steady state current as a function of applied voltage for PI (a) and for P−SiO_2/PI (b). (a): ●, ▲: T = 24°C before and after heating; ■: T = 120°C. (b): ●, o: I_{c+}, I_{c-}(120°C); ■: I_{c+}, I_{c-} (24°C, before heating); ▲, △: I_{c+}, I_{c-} (24°C, after heating).

Sacher[31] have mentioned that the pre-treatment can affect the conduction mechanism dramatically. The effect of electrode metal (Al) diffusion into polymer can be neglected because polymers usually have low diffusion coefficient toward Al and temperature is not very high.

The polarity dependence of I_c can be seen again in the double layer samples. At high temperatures, both I_{c+} and I_{c-} can be divided into two regions: (1) The ohmic conduction range at low electric field in which these two currents are close. (2) The non-ohmic conduction range at higher electric field in which I_{c+} is always greater than I_{c-}, and the difference between them increases with V.

4.1.3 Bulk conductivity of PI

Figure.4.5 shows the bulk conductivity for PI in successive thermal cycles, in the ohmic region, using V = 100 V (E = 2×10^4 V/cm). From the second to the fifth thermal cycle, the measurement at each temperature was carried out for about 2 hours (about 12 hours to complete all measurements for one thermal cycle). After finishing a thermal cycle, we immediately cooled the sample to room temperature, in order to start the next one. After the fifth thermal cycle, we did not immediately cool the sample, but it was kept at 170°C for 10 hours, after which the conductivity σ_v was no longer found to change after the sixth thermal cycle.

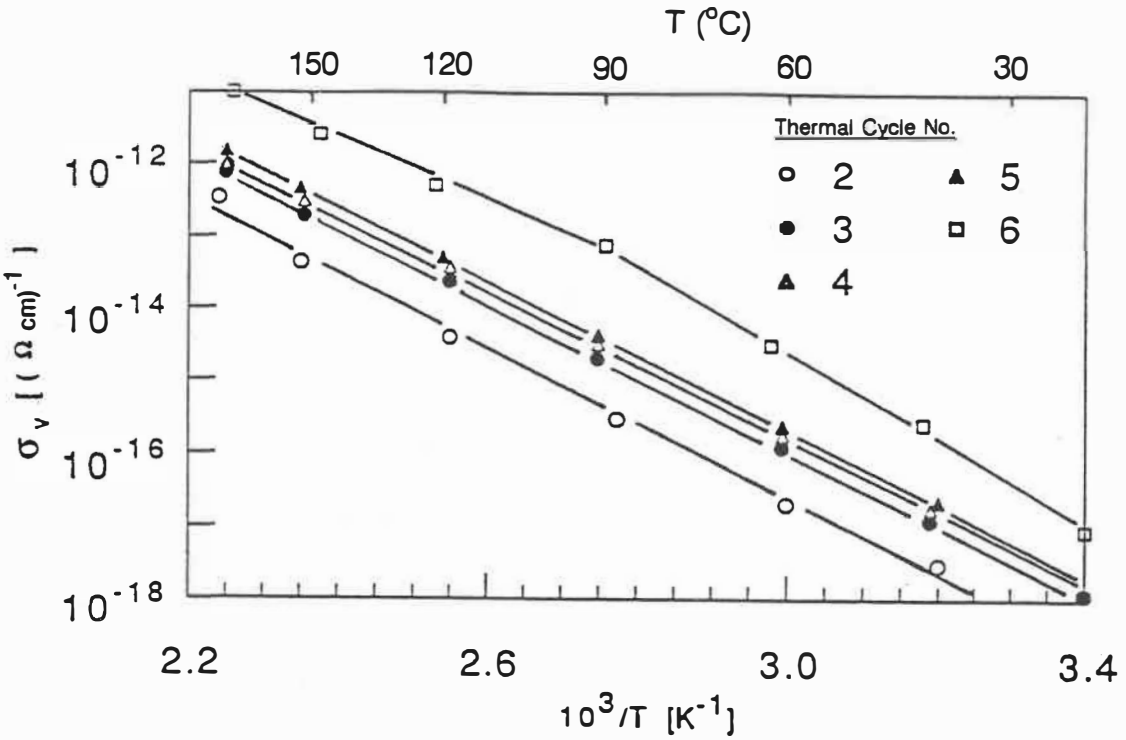

Fig. 4.5 Bulk conductivity as a function of reciprocal temperature for PI in subsequent thermal cycles using V=100 V (E=2x10⁴ V/cm).

Three main observations can be made from Fig.4.5: (a) σ_v is found to increase systematically during a series of thermal cycles; (b) σ_v obeys equation (2.2) from the second to the fifth thermal cycles; (c) the activation energy E_a is discontinuous at 90°C in the sixth thermal cycle.

The successive increase of σ_v during thermal cycles is an interesting phenomenon, it is worth discussing in more detail. Generally, annealing the sample at elevated temperature (e.g. at 150°C for PI) for a reasonably long time can

remove the absorbed water in the polymer, leading to a lower conductivity[19]. On the contrary, our observation shows that baking raises σ_v. The increase in σ_v suggests that more charge carriers are created in the sample by thermal ionization, as described by equation (2.11), during long-term heating. The reason is that the equilibrium in equation (2.11) is slow and cannot keep up with the temperature changes. The longer the annealing time is, the more the protons ionized from -COOH groups will be. In fact, Sacher[21,31] observed the different conductivities in the cooling and heating processes, and he also attributed this phenomenon to the non-equilibrium of equation (2.11) during these two processes.

It can be seen in Fig.4.5 that until the fifth thermal cycle the activation energy E_a remains constant, E_a = 1.0 eV, for 25°C ≤ T ≤ 170°C, consistent with other published data[22-26]. In the sixth thermal cycle, E_a varies within two temperature regions: E_a = 1.26 eV below 90°C, and E_a = 0.86 eV above 90°C. This may be a consequence of microstructural rearrangements after long thermal treatments. The pre-factors σ_{vo} in equation 2.2, readily obtained from Fig.4.5 for each thermal cycle, are summarized in Table 4.2.

Table 4.2 σ_{vo} values for PI for successive thermal cycles

thermal cycle	2	3	4	5	6
$\sigma_{vo}[(\Omega \cdot cm)^{-1}]$	0.058	0.24	0.39	0.49	3557($T<90^{o}C$) 0.034($T>90^{o}C$)

Another measurement process was also taken. After the first thermal cycle, two similar samples were kept at 170°C for 10 hours and 48 hours, respectively; after which, measurements were done in the same way. It was found that the $\sigma_v(T)$ relationship for the 48 hours' heating repeats that for the sixth thermal cycle discussed above, while the $\sigma_v(T)$ for the 10 hours' heating is between the σ_v in the second thermal cycle and the σ_v in the fifth thermal cycle. Therefore, we can conclude that the time of annealing is important.

4.1.4 Bulk conductivities of P-SiO_2/PI and P-SiN/PI structures

The conductivities of double layer P-SiO_2/PI and P-SiN/PI samples are presented in Fig.4.6. The thicknesses of P-SiO_2 and P-SiN deposited onto the PI film (51 μm) are 1.5 μm and 0.9 μm, respectively. We found that the measured results did not markedly depend on thickness d of P-SiO_2 or P-SiN for values 0.5 $\mu m \leq d \leq 2$ μm.

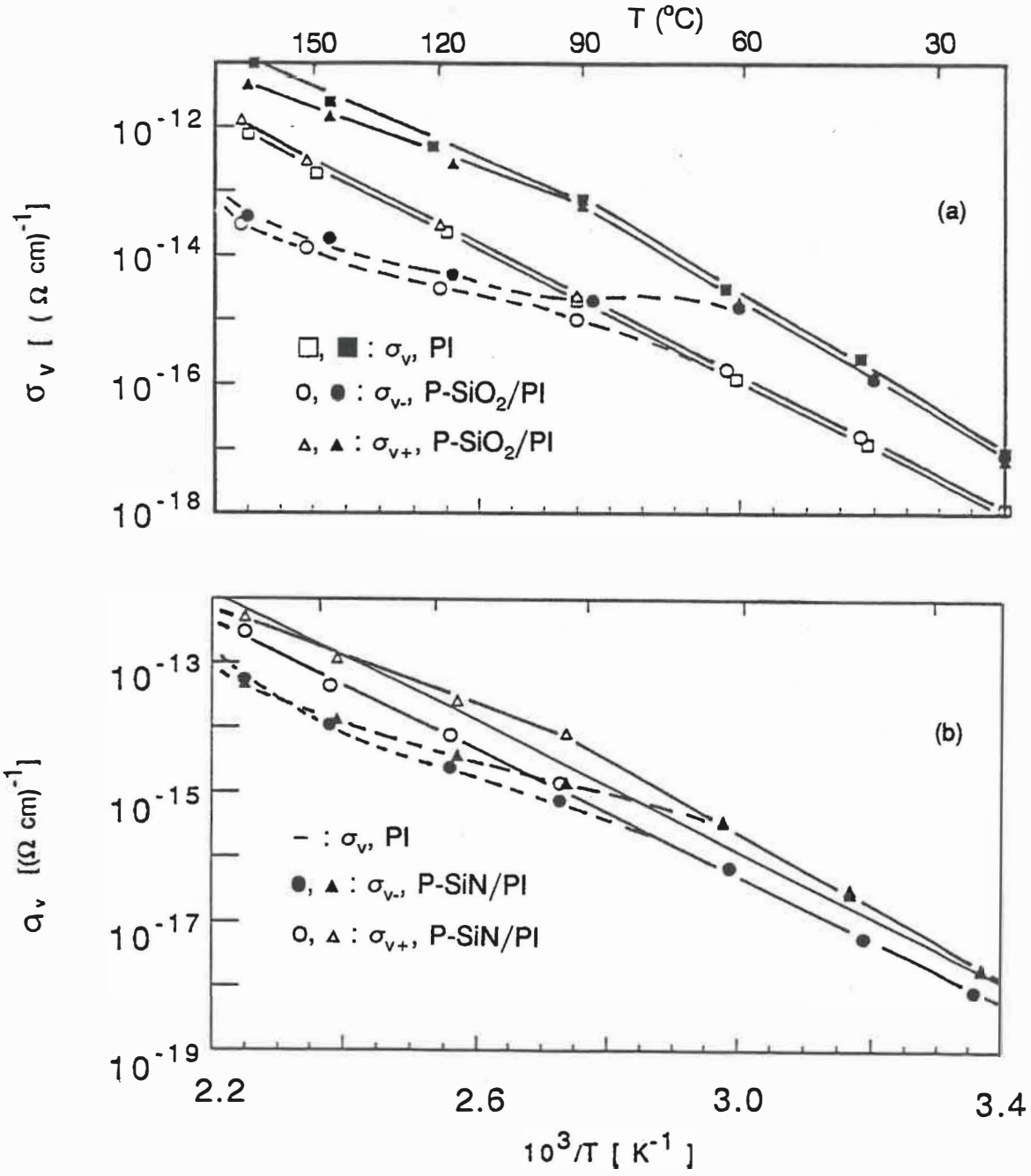

Fig.4.6 Bulk conductivity as a function of reciprocal temperature for PI and P-SiO_2/PI in (a), and for PI and P-SiN/PI in (b) using 100 V. (a): P-SiO_2(+)/PI (σ_{v+}: △, ▲), P-SiO_2(-)/PI (σ_{v-}: o, ●), and PI (□, ■); the third (□, △, o) and sixth (■, ▲, ●) thermal cycles. (b): P-SiN(+)/PI (σ_{v+}: o, △), P-SiN(-)/PI (σ_{v-}: ●, ▲), and PI (—); the second (o, ●) and third (—, △, ▲) thermal cycles.

Figure 4.6a shows σ_{v+} (calculated from I_{c+}) and σ_{v-} (from I_{c-}) of P-SiO_2/PI together with σ_v of PI in the third and sixth thermal cycles. From this figure we clearly note a critical temperature, $T \approx 60^{\circ}C$ ($1000/T = 3.00\ K^{-1}$), above which the polarity dependence of σ_v of P-SiO_2/PI occurs. This critical temperature does not change with successive thermal cycles. $\sigma_{v+}(T)$ (Fig.4.6a) of P-SiO_2/PI is similar to that of PI. However, σ_{v-} above 60°C is lower than σ_{v+} or σ_v in each thermal cycle. For the same thermal cycle, the higher the temperature, the larger is the difference between σ_{v+} and σ_{v-}. For the same temperature, the difference between σ_{v+} and σ_{v-} increases with the number of thermal cycles.

Up to the fifth thermal cycle, the E_a value of σ_{v+} for P-SiO_2/PI is exactly the same as for PI (E_a = 1.0 eV), but in the sixth cycle, E_a of σ_{v+} above 90°C (0.80 eV) is slightly smaller than that for PI (0.86 eV). The absolute values of the two conductivities in the same thermal cycle are close to each other.

Qualitatively similar behaviour has been observed for the P-SiN/PI system (see Fig.4.6b). Quantitative differences, however, may result from the difference of electrical properties between the two interfaces. The same critical temperature (60°C) can be noted in this figure.

4.2 Bulk conduction in PET, P-SiO_2/PET and P-SiN/PET

The behaviour of structures including PET has been observed to differ substantially from their PI counterparts in two aspects: The bulk conductivity of PET is independent of the thermal cycle, if the samples were baked at 130°C for 2 hours before the measurement. Secondly, the bulk conductivity of double layer P-SiO_2/PET and P-SiN/PET samples does not exhibit any dependence on polarity of the applied voltage, from 25 to 130°C. This means that addition of a thin layer (0.9 μm thick) of P-SiO_2 or P-SiN on PET (12 μm thick) does not appear to affect its electrical conduction significantly. Similarly to PI, I_c at low temperature is a power function of time, $I_c \propto t^{-n}$, for $t < 300$ s. Ohmic conduction was found for $E \leq 8\times10^4$ V/cm, consistent with the reported values[31].

σ_v, as a function of temperature for PET, and for P-SiO_2/PET and P-SiN/PET, is given in Fig.4.7. An apparent discontinuity in E_a is observed at 70°C ($10^3/T = 2.92\ K^{-1}$), the glass transition temperature. E_a is 1.85 eV for $T > 70$°C, and about 0.33 eV below 70°C, in agreement with reported values[31,34]. The lower activation energy at low temperature implies that the conduction mechanism is electronic, as discussed in Chapter 2. If we assume that the charge carriers above T_g are protons thermally-ionized from the -COOH groups, as some researchers have proposed, the independence of σ_v on thermal cycle implies that the

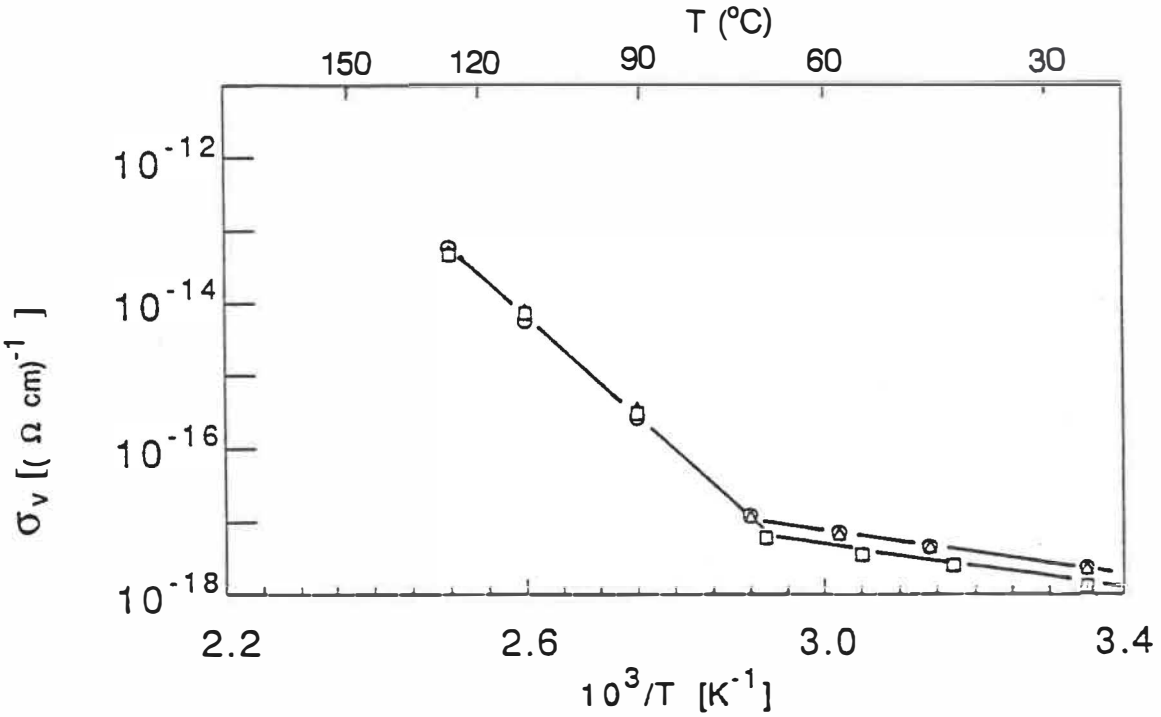

Fig.4.7 Bulk conductivity as a function of reciprocal temperature for PET (o), P-SiO_2/PET (Δ), and P-SiN/PET (□) using E=8.3x10⁴ V/cm.

equilibrium in equation (2.11) in PET can be established faster than in PI. This is not very surprising because the -COOH groups in PI are from the residual polyamic acid, while those in PET are from the residual terephthalic acid. The process of thermal ionization for these two acids in PI and PET may be different. The independence of σ_v on thermal cycle also suggests a fundamental difference of the bulk conduction process between PI and PET. We will further discuss the reasons causing the difference in bulk conduction for the P-SiO_2 or P-SiN coated PI and PET in Chapter 6.

4.3 Surface conductivity

According to the method described in Chapter 3, we carried out measurements of the surface conductivity of single and double layer samples, both in atmosphere and in vacuum. The behaviour of surface charging I_{cs} and discharging I_{ds} currents at room temperature is shown in Fig.4.8, both in atmosphere and in vacuum before annealing, for P-SiO_2/PET and P-SiN/PET.

We can see that I_{cs} is always greater in atmosphere than in vacuum. When the samples were kept in vacuum ($< 10^{-5}$ Torr) for more than 10 hours, the steady state I_{cs} of P-SiO_2/PET is about 2.5 times lower than in atmosphere. However, the steady state I_{cs} of P-SiN/PET in vacuum drops much faster than in atmosphere, and it becomes unmeasurable after a long charging time. The P-SiO_2/PET sample appears to adsorb water more readily, resulting in larger charging current in atmosphere. The vacuum appears to affect P-SiO_2/PET and P-SiN/PET in different ways. The surface conduction is ohmic below 400 V. I_{ds} of each case in Fig.4.8b is similar, namely opposite to I_{cs}, and it follows the Curie-von Schweidler power law[15]: $I_{cs} \propto t^{-n}$, $n = 0.9 \sim 1.0$.

It is generally accepted that in a "wet" environment the surface electrical conduction of a solid is caused by the adsorbed water if the solid surface is

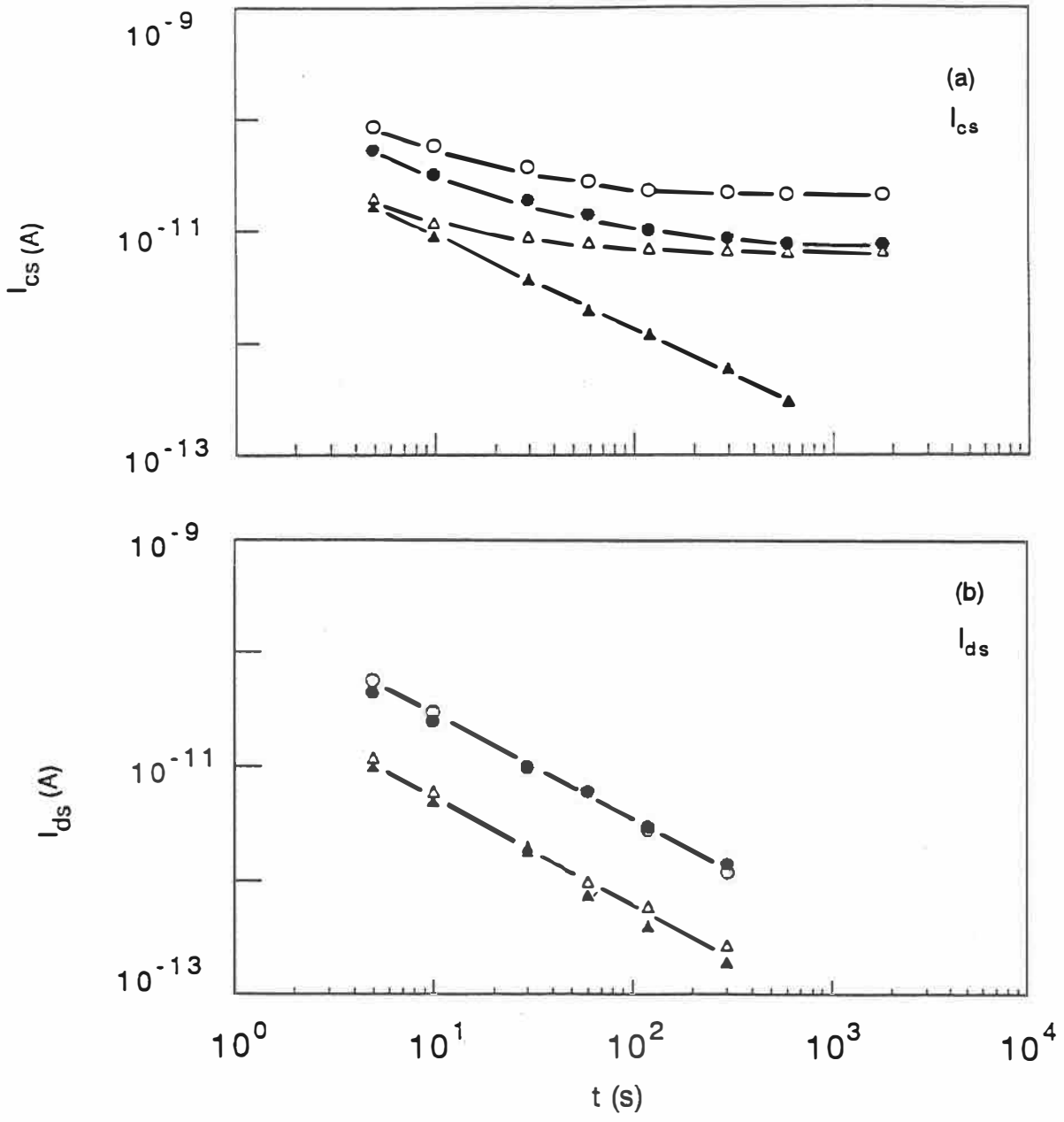

Fig.4.8 Surface charging I_{cs} (a) and discharging I_{ds} (b) currents as a function of time at 25°C before heating using 100 V. o: P-SiO_2/PET in atmosphere (RH = 50%), ●: P-SiO_2/PET in vacuum (10^{-5} Torr), ▵: P-SiN/PET in atmosphere (RH = 50%), ▲: P-SiN/PET in vacuum (10^{-5} Torr).

covered by more than a monolayer of water molecules, which are not strongly bound to the surface[64,65]. After annealing these samples at 90°C for two hours in vacuum, we found that their steady state currents are too low to be measured. This suggests that annealing removes the adsorbed water. Table 4.3 gives a summary of surface conductivities in the ohmic region, at 25°C.

Table 4.3 Surface conductivities of single layer and double layer samples at 25°C

Samples	σ_s (Ω^{-1})		
	in atmosphere RH=50%	in vacuum(10^{-5} Torr) before heating	in vacuum after heating
PET	$< 5 \times 10^{-18}$	$< 5 \times 10^{-18}$	$< 2 \times 10^{-18}$
P-SiO_2/PET	7.1×10^{-16}	2.6×10^{-16}	$< 2 \times 10^{-18}$
P-SiN/PET	2.3×10^{-16}	$< 7 \times 10^{-18}$	$< 2 \times 10^{-18}$
PI,P-SiO_2(SiN)/PI	$< 5 \times 10^{-18}$	$< 5 \times 10^{-18}$	$< 2 \times 10^{-18}$

Next, we studied the variation of σ_s with temperature. Similarly to σ_v, we also found that σ_s of PI and of P-SiO_2/PI increases with thermal cycling. Figure 4.9 shows the surface conductivities of PI and of P-SiO_2/PI, together with the bulk conductivity of PI in the third and sixth thermal cycles in vacuum for comparison. One finds that σ_s is also temperature-activated, and the activation energy for PI for

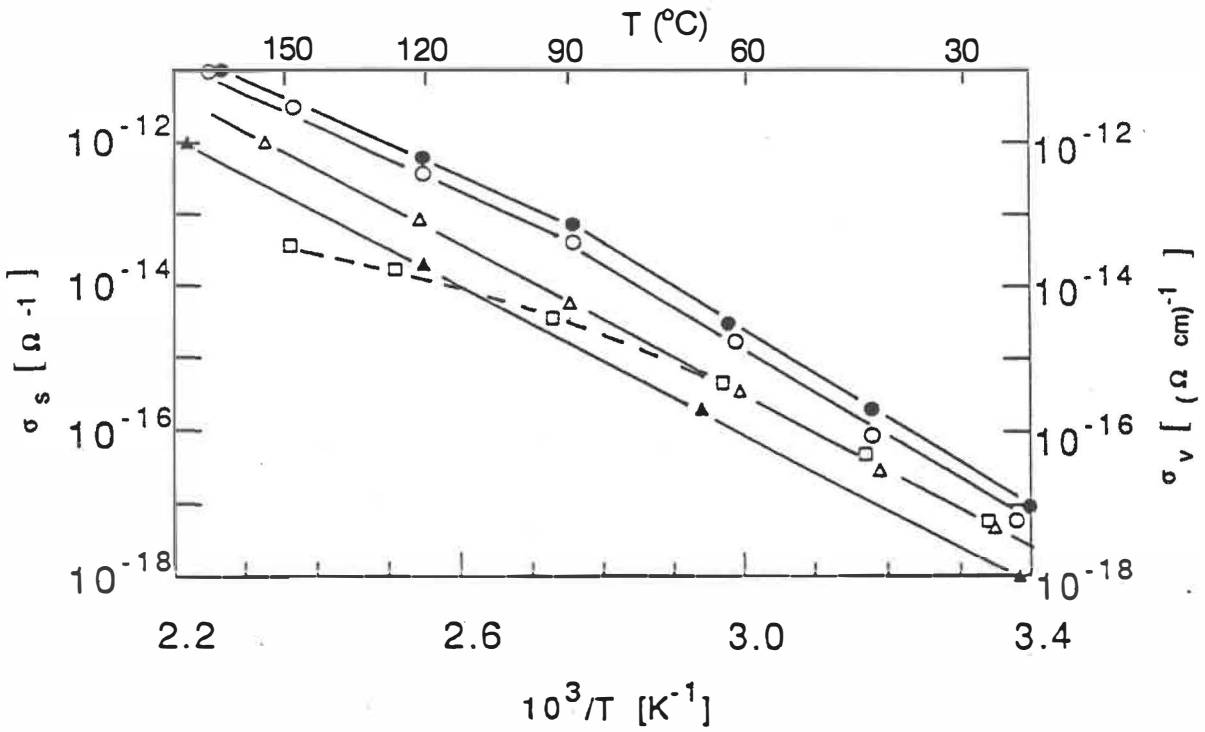

Fig.4.9 Surface and bulk conductivies as a function of reciprocal temperature in different thermal cycles. (▲) σ_v: the third cycle (PI), (●) σ_v: the sixth cycle (PI), (Δ) σ_s: the third cycle (PI), (o) σ_s: the sixth cycle (PI), (□) σ_s: the third cycle (P-SiO_2/PI).

the surface conduction process is E_{as} = 1.0 eV from the second to the fifth thermal cycles. E_{as} has two values for two temperature regions in the sixth cycle, namely $E_{as} \approx$ 1.26 eV below 90°C, and 0.86 eV above 90°C. Comparing with σ_v of PI shown in the same figure, we note that $E_{as} = E_a$, which means that the type of charge carriers for surface conduction are the same as that for the bulk conduction in PI.

The difference in σ_s between PI and P-SiO_2/PI can be clearly seen from Fig.4.9. At low temperatures, the two values are similar, but they deviate from each other above 60°C (1000/T = 3.0 K^{-1}). This critical temperature is the same as that for the bulk conductivity. Therefore, the P-SiO_2/PI interface can also play a role in the surface conduction process, similarly to bulk conduction (see section 4.1). This also means that the surface current in P-SiO_2/PI is distributed in the thin layer of several micrometers below the surface, because the thickness of P-SiO_2 on PI is 2 μm. In fact, the surface conduction in P-SiO_2/PI is a combination of conduction processes in the P-SiO_2 layer and in PI.

An Arrhenius plot for σ_s of PET, P-SiO_2/PET and P-SiN/PET in vacuum is given in Fig.4.10. The bulk conductivity of PET is also plotted in the same figure for comparison. Due to the difficulties in measuring the very low surface current at low temperatures, only the results above 70°C are given. From this figure we note that: $E_{as} = E_a = 1.85$ eV. We find that all three sample types exhibit a phase transition for the surface conduction process at about 70°C, at which E_{as} is discontinuous, similar to what was reported above for the case of bulk conduction.

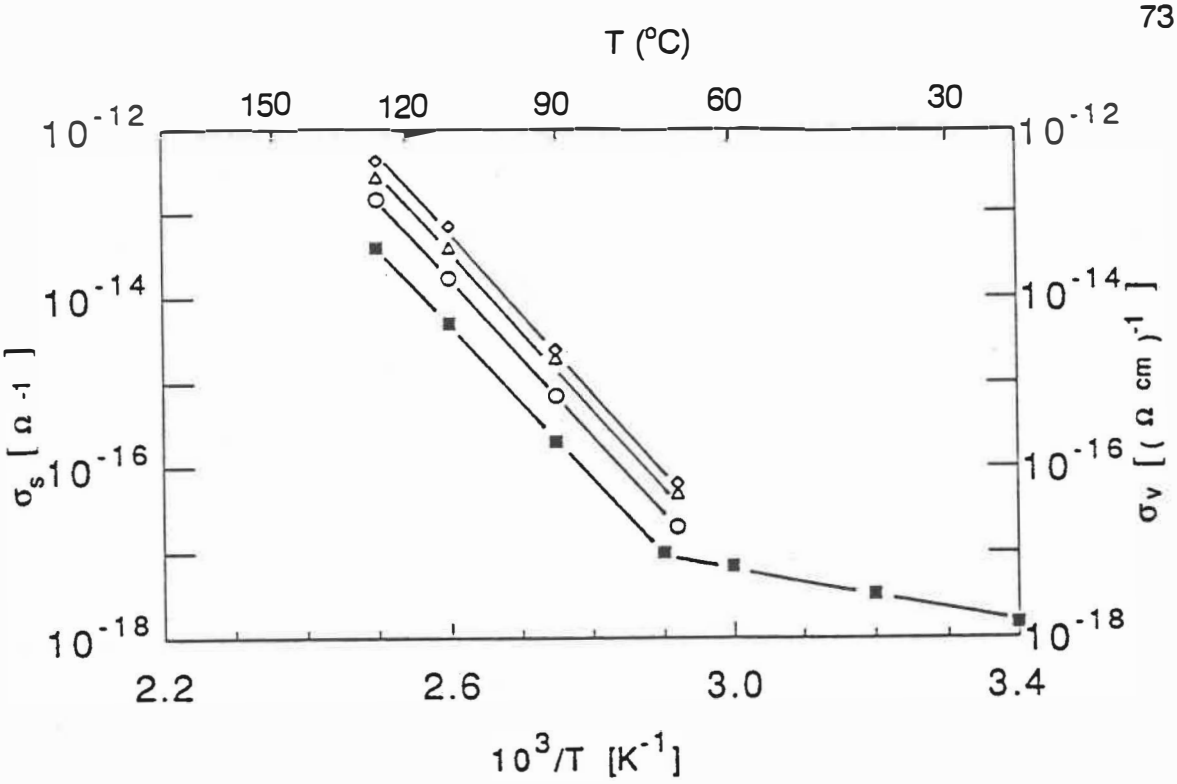

Fig. 4.10 Surface and bulk conductivities as a function of reciprocal temperature. (■) σ_v: PET, (o) σ_s: P-SiN/PET, (Δ) σ_s: PET, (◊) σ_s: P-SiO_2/PET.

Chapter 5

C-V Characteristic Measurements

In Chapter 4, we have presented the results of the d. c. measurements for single and double layer dielectric structures, and found the polarity dependence of currents in P-SiO_2/PI and P-SiN/PI. We preliminarily feel that this polarity dependence is originated from the potential barrier at the P-SiO_2/PI or P-SiN/PI interface. This barrier may be correlated to either of the contact potential difference and the charge accumulation at the interface or both. However, the d.c. measurements can not give further and enough information about the charge distribution and transport near the interface. As mentioned in Chapter 3, the C-V characteristic measurement of MIS and MI_1I_2S structures can overcome this shortcoming. It can help us to further clarify the interfacial properties: formation of the interfacial potential barrier, charge transport and distribution at the interface. Measured C-V characteristics of MIS and MI_1I_2S structures will be presented in this chapter. Further discussion of the interfacial properties in the double layer dielectric structures will be based on these characteristics. The process of sample preparation, basic measuring techniques and methods of analysis have been described in detail in Chapter 3.

The samples used are summarized in Table 5.1 below.

Table 5.1 Parameters for C-V measurements

N_D(n-type Si) = 4.5×10^{15} cm^{-3}, ε'_{rs}(Si) = 12, ε'_r(dry PI) = 3, ε'_r(T or P-SiO_2)=4				
Sample	Al-PI-Si	Al-(T-SiO_2)-Si	Al-PI-(T-SiO_2)-Si	Al-PI-(P-SiO_2)-Si
Thickness(PI)	d_o=0.90 μm		d_1=1.00 μm	d_1=0.90 μm
Thickness(T-SiO_2)		d_o=0.22 μm	d_2=0.22 μm	
Thickness(P-SiO_2)				d_2=0.15 μm
Electrode Radius	2.43 mm	2.50 mm	2.43 mm	2.60 mm
$C_o=C_i/A(F/m^2)$	2.95×10^{-5}	1.61×10^{-4}	2.30×10^{-5}	2.62×10^{-5}

In this table, T-SiO_2 and P-SiO_2 refer to thermal and plasma-deposited materials, respectively. Measurements were performed in vacuum, at room temperature and at a high frequency (f = 100 kHz) using the circuits shown in Fig.3.3. The normalized total capacitance C/C_i is always used for convenience of comparisons. Positive and negative gate voltage V_G and bias V_B are measured with respect to the metal electrode, as mentioned in Chapter 3.

5.1 Al-(T-SiO_2)-Si system

The C-V characteristics of the metal-(T-SiO_2)-semiconductor system have

been extensively investigated. For example, Grove et al.[66] described the properties of this system in detail, and a comprehensive book was written by Nicollian and Brews in 1982[62].

Figure 5.1 shows the C-V characteristics for the Al-(T-SiO_2)-Si sample at 23°C in our measurements. Curves 1 and T represent the measured results for the actual virgin sample and theoretical results for an ideal sample, respectively. Curve

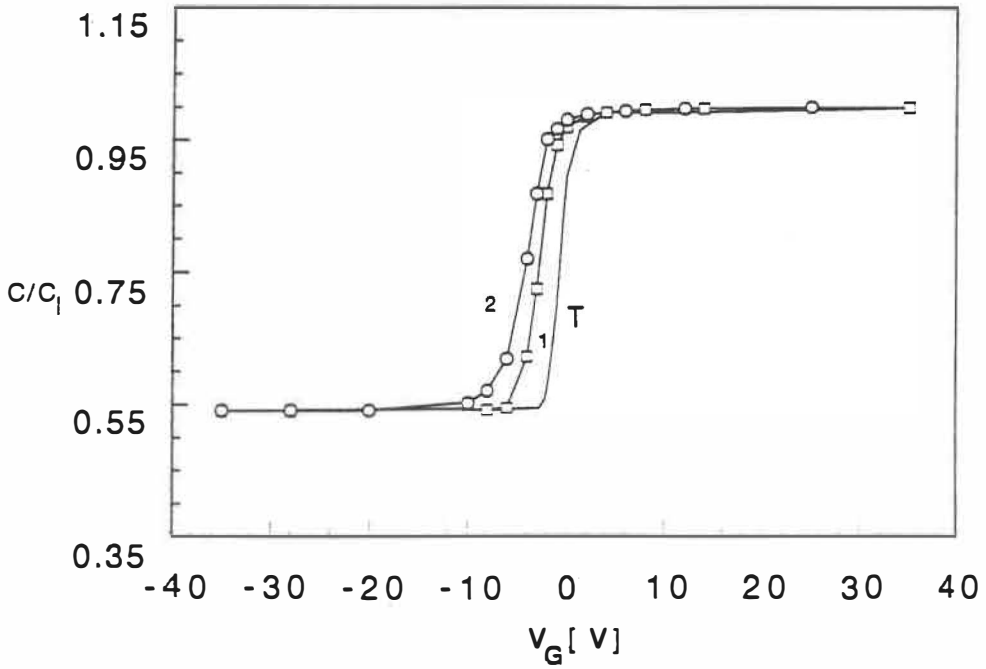

Fig.5.1 C-V curves for Al-(T-SiO_2)-Si measured at 23°C in vacuum at f = 100 kHz. 1 (□): virgin sample; 2 (o); sample applied a bias of + 20 V at 120°C for 20 min., then cooled down to 23°C; T: theoretical result for ideal sample.

2 represents the results after a B.T. experiment (the sample was subjected to a V_B of + 20 V at 120°C for 20 minutes). The observed left-shift suggests that positive charges, which are mobile at high temperature but not at low temperature, have migrated to the T-SiO_2/Si interface at 120°C. In fact, curve 2 is superimposed onto curve 1 when a V_B of -20 V is applied to the sample at 120°C for 20 minutes. This confirms that the positive charges are initially at the Al/T-SiO_2 interface. In addition, the left-shift and broadening of curve 1, compared with curve T, implies that there are fixed positive charges and surface states at the T-SiO_2/Si interface. The mobile charges are probably positive ions such as Na^+ introduced during sample preparation, and the fixed positive charges are due to excess ionic silicon, as discussed in the literature on this subject[59,62,66,67].

Using equations (3.7) and (3.8) and combining the theoretical formulas for MIS structure with measured results, we find a fixed charge density Q_{sf} at the T−SiO_2/Si interface: Q_{sf} = + 10^{11}e cm^{-2}, and a surface state density: N_{ss} = 2.6×10^{11} cm^{-2} eV^{-1}. In the same way, we find from curve 2 a mobile charge density Q_{sm} at the T-SiO_2/Si interface: Q_{sm} = + 5×10^{10}e cm^{-2} ($\neq Q_{sf}$). These Q_{sf}, N_{ss} and Q_{sm} values agree with those given by Sze[59], Nicollian[62], and Grove et al.[66]. Unlike Q_{sf}, which is immobile even at elevated temperatures, Q_{sm} is mobile at elevated temperatures.

5.2 Al-PI-Si system

C-V curves for the Al-PI-Si sample, both in the virgin state and after annealing, are shown in Fig.5.2. A large difference is noted between the virgin sample (curves 1 and 2) and following annealing at 120°C for 2 hours (curves 3 and 4), and also between these experimental curves and the theoretical counterpart (curve T). Curves 1 and 2 display hysteresis during the first V_G cycle

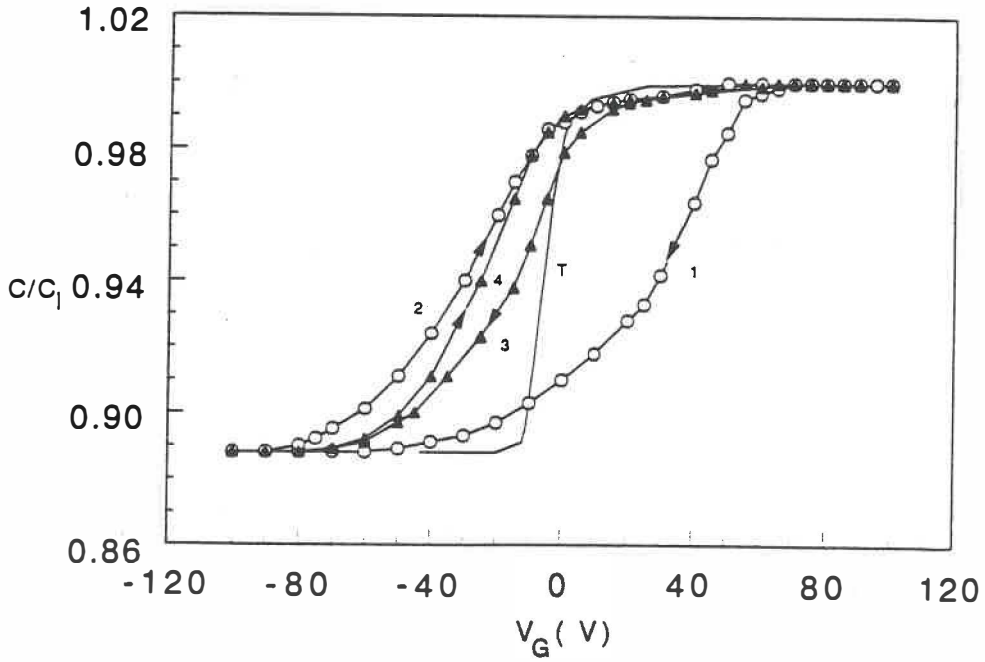

Fig.5.2 C-V curves for Al-PI-Si measured at 23°C in vacuum at f=100 kHz. 1, 2 (o): virgin sample; 3, 4 (▲): sample annealed at 120°C for 2 hours, then cooled down to 23°C; T: ideal sample.

in the range -100 V ≤ V_G ≤ +100 V, which reproduce during subsequent cycles, and the situation is the same for curves 3 and 4. This hysteresis is symptomatic of charge motion in the PI layer during the V_G cycle. The transferred charge density for curves 1 to 2 is $Q_{s1} = 1.1\times10^{12}$e cm^{-2}, being calculated from ΔV_{GF} = - 60 V. For curves 3 and 4, we find ΔV_{GF} = - 10 V, and $Q_{s2} = 1.8\times10^{11}$e cm^{-2}.

Similar hysteresis phenomena in metal-polymer-semiconductor structures have been reported by other researchers[68-72]. Maisonneuve et al.[68,69] have attributed it to mobile positive charges migrating toward or away from the polymer/Si interface, which possess high enough mobility, even at room temperature, to move an appreciable distance within the polymer layer during the period of one measurement cycle. The much less pronounced hysteresis of curves 3 and 4 shows that heating under short circuit condition can greatly reduce the density of mobile charges. Broadening of the experimental C-V curves with respect to the theoretical case again demonstrates the presence of surface states, this time at the PI/Si interface. We obtain: $N_{ss} = 10^{12}$ cm^{-2} eV^{-1}. This is a factor of 4 higher than the value ($N_{ss}=2.6\times10^{11}$ cm^{-2} eV^{-1}) found for the T-SiO_2/Si interface.

5.3 Al-PI-(T-SiO_2)-Si system

Figure 5.3 shows the measured C-V characteristics of the Al-PI-(T-SiO_2)-Si

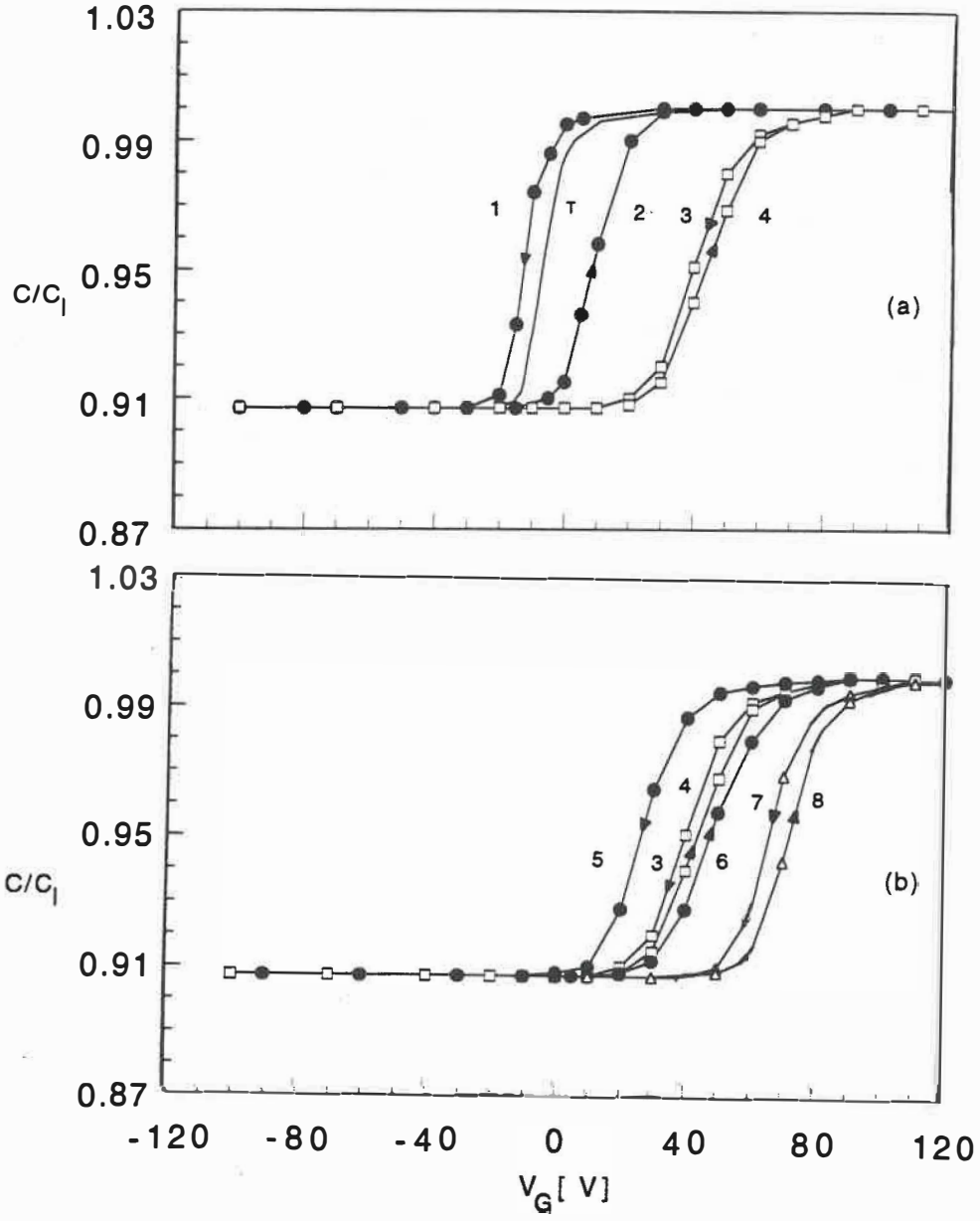

Fig.5.3 C-V curves for Al-PI-(T-SiO_2)-Si system measured at 23°C in vacuum at f=100 kHz. (a): 1, 2 (●): sample annealed at 120°C for 2 hours, then cooled down to 23°C, the first cycle ; 3, 4 (□): sample following 1 and 2, the fourth cycle; T: ideal sample. (b): 3, 4 (□): the same as 3 and 4 in (a); 5, 6 (●): sample applied a bias of +20 V at 120°C for 1 hour, then cooled down to 23°C; 7, 8 (Δ): sample applied a bias of -20 V at 120°C for 1 hour, then cooled down to 23°C.

sample at 23°C. Curve T again represents the theoretical result, while curves 1 and 2 demonstrate the hysteresis in the first V_G cycle (- 100 V ≤ V_G ≤ + 100 V), after the sample had been annealed for 2 hours at 120°C with short-circuited electrodes. For each subsequent cycle, we found similar hysteresis, but the C-V curve shifts systematically to the right; curves 3 and 4 represent the results for the fourth cycle. In each of these cycles, the time during which the sample was subjected to a negative V_G was about 15 minutes. We found that if V_G is varied between + 100V and 0 V, the hysteresis disappears, and the C-V curves are the same during different cycles. This suggests that the right-shift of the C-V curve is caused by negative charges (most probably electrons), injected from the Al electrode and trapped in the T-SiO_2/PI double layer structure, when a negative V_G is applied to the sample. However, no charges can been trapped when a positive V_G is applied.

We did not observe such trapped negative charges in Al-PI-Si and Al – (T – SiO_2) – Si, even though they may have been injected from the Al electrode. Therefore, the observed phenomenon may be related to the T – SiO_2/PI interface at which these negative charges are most probably trapped. Compared with the theoretical curve T, curve 1 displays a left-shift by ΔV_{GF} = -8 V, corresponding to a fixed positive charge density at the T-SiO_2/Si interface: Q_{sf} = + 1.1×10^{11}e cm^{-2}. This is very close to the value obtained for Al-(T-SiO_2)-Si.

B.T. experimental results are presented in Fig.5.3b, where curves 3 and 4 (the same as curves 3 and 4 in Fig.5.3a) represent the measurements before the B.T. experiment. Curves 5 and 6 show the results (V_G = 120 V → -100 V → 120 V) after a V_B of +20 V was applied at 120°C for 1 hour. Following 5 and 6, curves 7 and 8 represent the results (V_G = 120 V → -100 V → 120 V) after a V_B of -20 V has been applied. Curve 5 exhibits a left-shift with respect to curve 4 by $\Delta V_{GF} \approx$ -20 V, while curve 7 exhibits a right-shift with respect to curve 6 by $\Delta V_{GF} \approx$ 20 V. Like the case at room temperature, the right-shift of curve 7 is caused by the negative charges trapped at the T-SiO_2/PI interface with a density of $Q_i = -3.3 \times 10^{11}$e cm^{-2}. The left-shift of curve 5 may be caused by the positive mobile charges with a density of $Q_i = +3.3 \times 10^{11}$e cm^{-2}.

5.4 Al-PI-(P-SiO_2)-Si system

Results for the Al-PI-(P-SiO_2)-Si sample are shown in Fig.5.4, where curves 1 and 2 are those in the first V_G cycle (- 80 V ≤ V_G ≤ + 120 V) for the sample annealed for 2 hours at 120°C with short-circuited electrodes. Curve $\bar{T}$ represents the theoretical result. Following 1 and 2, measurements were done for several V_G cycles (V_G = 180 V → -100 V → 180 V). We find that the difference between the theoretical and experimental curves is initially not too large (see curves 1, 2 and T), however, apparent hysteresis occurs for each subsequent cycle, and the C-V

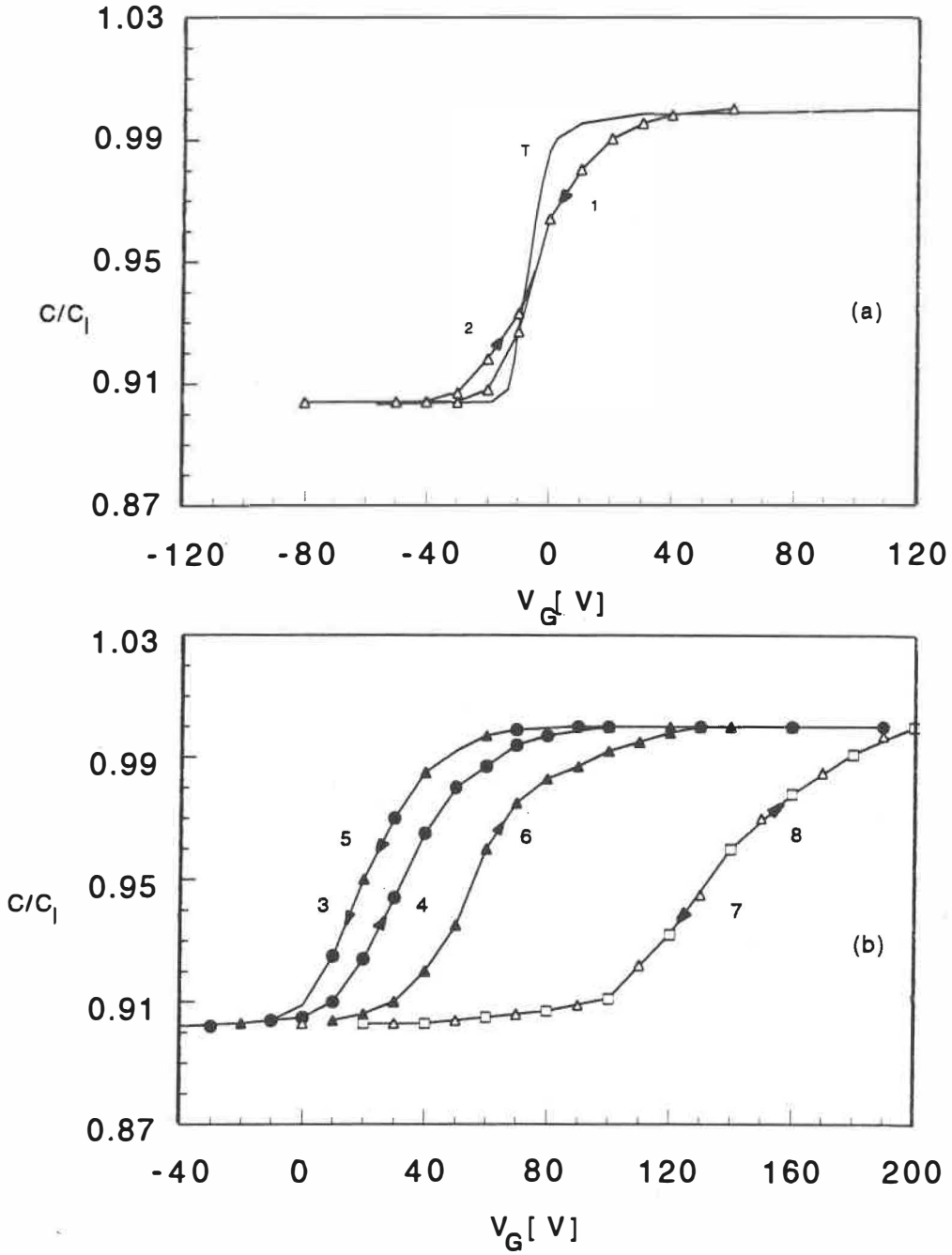

Fig.5.4 C-V curves for Al-PI-(P-SiO_2)-Si system measured at 23°C in vacuum at f=100 kHz. (a): 1, 2 (Δ): sample annealed at 120°C for 2 hours, then cooled down to 23°C (the first cycle); T: ideal sample. (b): 3, 4 (●): following 1 and 2 (the third cycle); 5, 6 (▲): sample applied a bias of +60 V at 120°C for 30 min, then cooled down to 23°C; 7 (Δ): sample applied a bias of -60 V at 120°C for 30 min, then cooled down to 23°C (V_G = +200 V⟶0); 8 (□): following 7, but V_G = 0⟶200 V.

curve shifts systematically to the right. Curves 3 and 4 are the results for the third cycle. B.T. experiment was also carried out. Curves 5 and 6 (V_G = 180 V → -100 V → 180 V) give the results after a V_B of + 60V at 120°C for 30 minutes, and curve 7 (V_G = 200 V → 0) corresponds to the results after a V_B of - 60 V at 120°C for 30 minutes. Following 7, curve 8 was measured using V_G = 0 → 200 V, which repeats curve 7. Curve 5 shifts to the left with respect to curve 4 by ΔV_{GF} = - 10 V, and the positive charges trapped at the P-SiO_2/PI interface is: Q_i = + 1.8×10^{11}e cm^{-2}. The right-shift of curve 7 with respect to curve 6 is ΔV_{GF} = 75 V, the corresponding trapped negative charges is: Q_i = -1.4×10^{12}e cm^{-2}.

Comparing with the results in section 5.3, we find a similar charge transport process both in Al-PI-(T-SiO_2)-Si and in Al-PI-(P-SiO_2)-Si. At room temperature, negative charges (electrons) can be injected from the Al electrode and trapped near the T-SiO_2/PI and P-SiO_2/PI interfaces. At elevated temperatures, both positive and negative charges can be trapped near the T-SiO_2/PI and P-SiO_2/PI interfaces, corresponding to the positive and negative V_B, respectively.

We also measured the Al-PI-(P-SiN)-Si sample. The conclusions are the same as those obtained for the Al-PI-(P-SiO_2)-Si sample.

Chapter 6

Modelling and Discussion

In this chapter, we will first discuss the steady state currents in single layer PI and PET samples, and we will show that their behaviour confirms a hopping conduction mechanism from which we can derive the hopping distance of charge carriers. In the second step, we will describe a model for the transient and steady state currents in double layer P-SiO_2/PI and P-SiO_2/PET structures. First, a potential barrier at the insulator$_1$/insulator$_2$ interface will be discussed, using the observations in Chapter 5. Then, a model, based on this interfacial potential barrier, will be used to interpret the polarity dependence of transient and steady state currents in P-SiO_2/PI, as presented in Chapter 4.

6.1 Bulk conduction in PI and PET

As mentioned in Chapter 2, the charge carriers in PI are mostly protons thermally-ionized from -COOH groups; this applies also to PET at $T > T_g$ as found by Sacher[31]. Figure 6.1 shows the proposed potential energy curves in PI or in PET for protonic hopping conduction, the height of the potential barrier between sites A and B being Δg. Here, Δg is the Gibbs free energy, and it can be written in terms of the corresponding enthalpy Δh and entropy ΔS as[13,15]

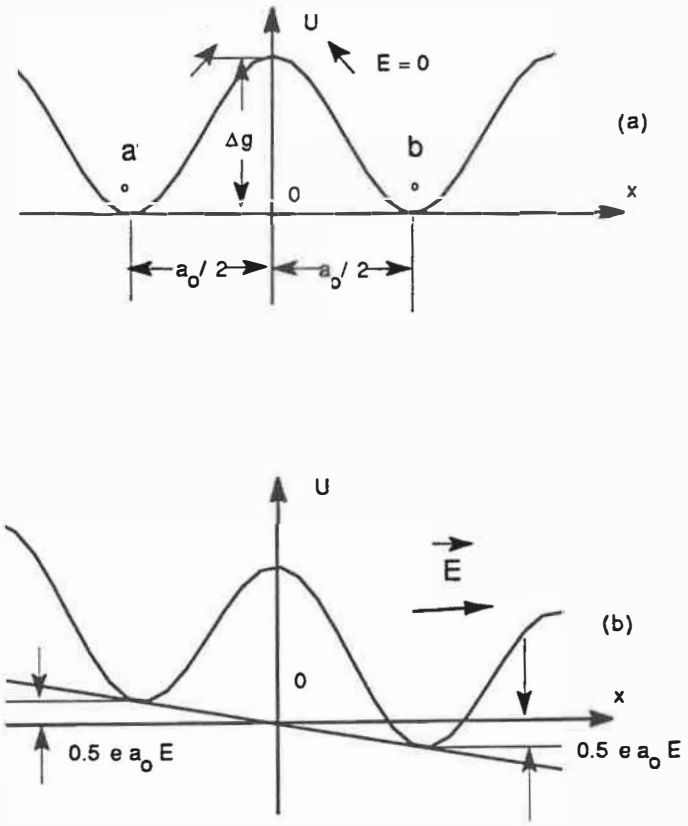

Fig.6.1 Potential energy curves in PI or PET for the protonic hopping conduction: (a) without electric field, (b) with electric field.

$$\Delta g = \Delta h - T\Delta S.$$

The theory of ionic conduction in one-dimensional case allows us to express the mean drift velocity v of the carriers and the steady state current density j as follows[13,14]:

$$v(T, E) = 2 \nu_o a_o \exp\left(-\frac{\Delta g}{kT}\right) \sinh\left(\frac{e a_o}{2kT} E\right) \qquad (6.1a)$$

$$j(T, E) = 2 B(T) a_o \sinh\left(\frac{e a_o}{2kT} E\right) \qquad (6.1b)$$

where, $B = en\nu_o \exp(-\Delta g/kT)$, n is the proton density, a_o is the mean hopping distance, and ν_o is the phonon frequency (10^{12} - 10^{13} Hz)[14]. Here, we have used the average electric field E (= V/L) instead of the local electric field E_L, this is a good approximation for most single layer dielectric materials.

If E is high enough ($> 10^6$ V/cm), equation (6.1b) can be simplified, and j(T,E) becomes:

$$j(T, E) \propto \exp\left(\frac{e a_o}{2kT} E\right) \qquad (6.2)$$

In this case, a_o can be obtained from the slope of the straight line of ln(j) versus E.

At low E, $\exp(\pm ea_oE/2kT) \approx 1 \pm ea_oE/2kT$, and the mobility μ can be obtained from equation (6.1a):

$$\mu = \frac{a_o^2 e \nu_o}{kT} \exp\left(-\frac{\Delta g}{kT}\right) \tag{6.3a}$$

and ohmic conduction is predicted by equation (6.1b) :

$$j(T,E) = \sigma_v(T)\, E \tag{6.3b}$$

where

$$\sigma_v(T) = e\, n\, \mu = \frac{e^2 n \nu_o a_o^2}{kT} \exp\left(-\frac{\Delta g}{kT}\right) \tag{6.3c}$$

Combined with equation (2.13), equation (6.3c) can be rewritten as

$$\sigma_v = \frac{a_o^2 e^2 \nu_o \sqrt{n_o K_o}}{\gamma kT} \exp\left(\frac{\Delta S + 0.5S}{k}\right) \exp\left(-\frac{\Delta h + 0.5h}{kT}\right) \tag{6.4}$$

Here, we have used the relation g = h -TS, similar to the expression for Δg.

We can now compare equation (6.4) with empirical equation (2.2). Following that, the total activation energy E_a for the bulk conduction is expressed as

$$E_a = 0.5h + \Delta h.$$

Equation (6.1b) can be used to calculate the j(T,E) values. The theoretical and experimental results are compared in Fig.6.2. The best agreement between theory and experiment has been found as follows: a) for PI at 24°C, a_o = 110 Å, $B \cdot a_o = 1.3\times10^{-9}$ A/m^2; at 120°C, a_o = 158 Å, $B \cdot a_o = 7.1\times10^{-6}$ A/m^2; b) for PET at 90°C, a_o = 95 Å, $B \cdot a_o = 7.6\times10^{-8}$ A/m^2. The a_o values for PI agree with the literature (see Table 2.1), while the a_o value for PET is somewhat higher than those in Table 2.2. Several reports have confirmed that the hopping distance of ions in polymers is in the range of crystallite dimensions, that is, several tens to several hundreds of angstroms, as mentioned by Barker et al.[40], and by Wintle[14]. The increase in the hopping distance with increasing temperature has been observed in PI and PET by other investigators[23,27,35]. Precise reasons for this are presently unknown, but we feel that thermal expansion may be one of the reasons, since most polymers have high coefficient of thermal expansion. Another possible reason is change of microstructure at elevated temperature.

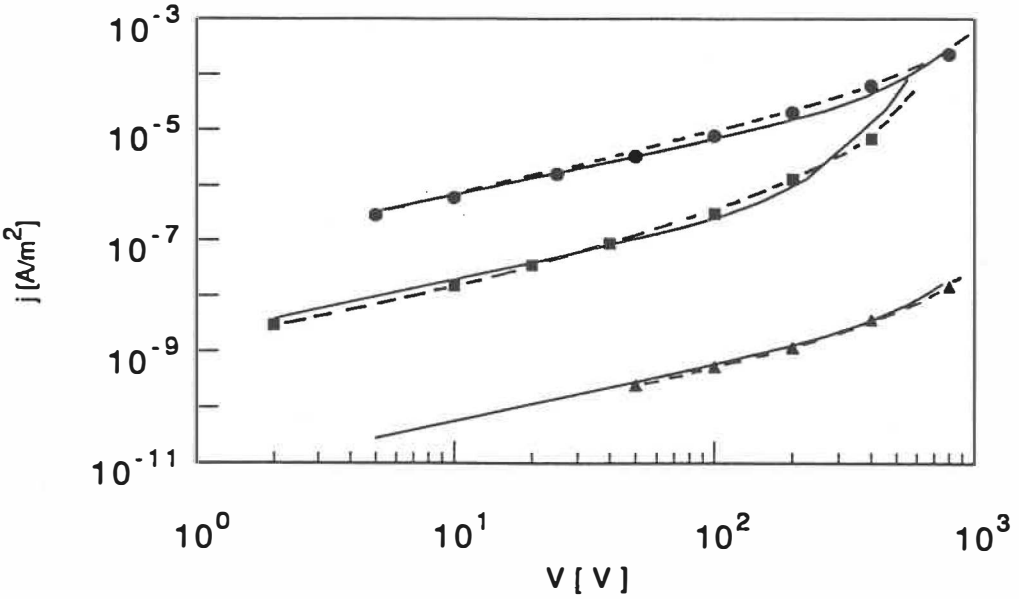

Fig.6.2 Comparison of measured (--: ▲, ■ , ●) and calculated (—) bulk current densities as a function of applied voltage for PI at 24°C (▲) and at 120°C (●),and for PET at 90°C (■).

6.2 Interfacial potential barrier

We have indicated that an interfacial potential barrier is responsible for the polarity dependence of current in double layer structures. The origin of this barrier can be twofold: a) contact potential difference between two insulators, and b) charge accumulation near the interface when a voltage is applied to the sample. A contribution from the latter has been confirmed by C-V measurements in Chapter 5. In the following sections 6.3 and 6.4, we will see that the model based on this assumption can explain d.c. properties very well.

When two insulators are in contact, charge exchange between them can occur near the interface due to a difference in their Fermi levels or work functions. The conductivity in an insulator is usually so low that the charge exchange between two insulators requires a long time. As soon as an equilibrium is established, an interfacial barrier can be formed, depending on the physical parameters of these two insulators in contact. This is qualitatively similar to the contact between two semiconductors or between a semiconductor and a metal. This potential barrier can be present before application of an external electric field.

Charge accumulation near the interface may be a dominating factor causing the potential barrier. We first consider the case for the positive charge accumulation or trapping. Figure 6.3 illustrates the P-SiO_2/PI sample which is subjected to a positive voltage V with respect to the PI layer. From the C–V measurements, we know that positive charges in this case can be accumulated or trapped near the P-SiO_2/PI interface at a high temperature. Under a positive voltage, the positive charge carriers (protons as discussed in Chapter 2) are driven towards the P-SiO_2/PI interface. It is well known (see, for example, Felts et al.[73]) that P-SiO_2 acts as a gas and vapour barrier on various polymers, since P-SiO_2 has much lower permeation towards these molecules than any polymer. In addition, Singh[74] reported that SiO_2 also possesses the ability to block the flow of positive ions. What happens is that the protons (= hydrogen gas ions)

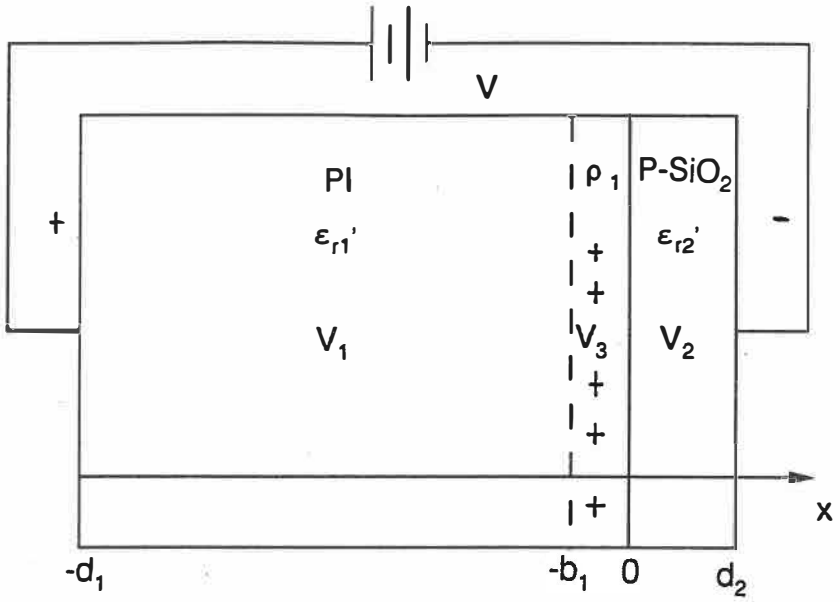

Fig.6.3 Charge distribution in P-SiO_2/PI after a long time of application of a positive voltage.

are partially accumulated near the P-SiO_2/PI interface, on the PI side, as indicated in Fig.6.3. A simplified model is proposed to describe the potential distribution under these conditions. The space charges are assumed to be distributed in a thin layer b_1 ($b_1 << d_1, d_2$) near the interface, with a constant volume density ρ_1. Then, the potential V(x) in three regions can be determined by the following differential equations and boundary conditions:

$$\frac{d^2V_1}{dx^2} = 0 \qquad (-d_1 < x < -b_1) \tag{6.5a}$$

$$\frac{d^2V_2}{dx^2} = 0 \qquad (0 < x < d_2) \tag{6.5b}$$

$$\frac{d^2V_3}{dx^2} = -\frac{\rho_1}{\varepsilon'_{r1}\varepsilon_o} \qquad (-b_1 < x < 0) \tag{6.5c}$$

$$V_1(-d_1) = \frac{V}{d_1 + d_2} d_1 \tag{6.6a}$$

$$V_2(d_2) = -\frac{V}{d_1 + d_2} d_2 \tag{6.6b}$$

$$V_3(0) = V_2(0) \tag{6.6c}$$

$$V_1(-b_1) = V_3(-b_1) \tag{6.6d}$$

$$\varepsilon'_{r1} \frac{dV_3}{dx}(x=0) = \varepsilon'_{r2} \frac{dV_2}{dx}(x=0) \tag{6.6e}$$

$$\frac{dV_1}{dx} = E_1 < 0 \tag{6.6f}$$

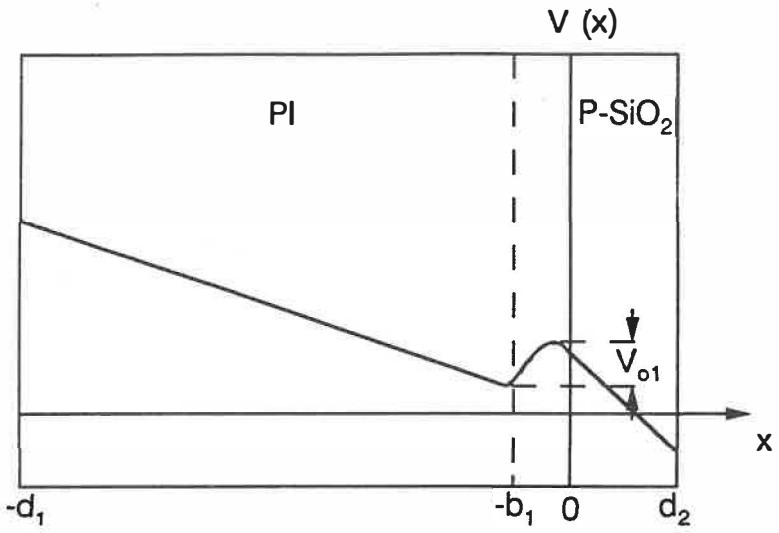

Fig.6.4 Potential distribution in P-SiO_2/PI for the case in Fig.6.3.

Here, E_1 is a constant independent of x, but dependent on the average electric field E [$E = V/(d_1 + d_2)$]. ε_{r1}' and ε_{r2}' are the relative permittivities of PI and P-SiO_2, respectively. The solutions of equations (6.5) and (6.6) are illustrated in Fig.6.4. We can see that a potential barrier for positive charges, from PI to P-SiO_2, is formed at the interface. The height of potential barrier V_{o1} is approximately expressed as

$$V_{o1} \sim \frac{\rho_1 b_1^2}{2\varepsilon'_{r1}\varepsilon_o} \qquad (6.7)$$

The other case is shown in Fig.6.5, in which the sample is subjected to a negative voltage V. C-V measurements have shown that in this case negative charges are accumulated or trapped near the interface. Unlike the case of positive charges, the negative charges (electrons) may be injected from the electrode and trapped near the interface due to the interfacial traps. They may cross the interface to reach the P-SiO_2 layer. Therefore, we here assume that the space charges are distributed on the P-SiO_2 side within a thin layer b_2 ($b_2 << d_1, d_2$), with a constant volume density $-\rho_2$. In the same way, we can solve the above differential equations using the particular boundary conditions. The results are shown in Fig.6.6. A similar interfacial potential barrier as for positive charges, is also noted in this case, and its height V_{o2} is approximately given by:

$$V_{o2} \sim \frac{\rho_2 b_2^2}{2\varepsilon'_{r2}\varepsilon_o} \qquad (6.8)$$

In equations (6.7) and (6.8), $\rho_1 b_1$ and $\rho_2 b_2$ represent the equivalent surface charge densities at the P-SiO_2/PI interface in those two cases. They can roughly be estimated from the B.T. experiment in C-V measurements in section 5.4: $\rho_1 b_1 \sim 2\times10^{11}$e cm^{-2}, and $\rho_2 b_2 \sim 10^{12}$e cm^{-2}. The thicknesses b_1 and b_2 of the space charge layers are unknown; they might conceivably be obtained using other methods such as the pressure-pulse technique and thermal-pulse method[75].

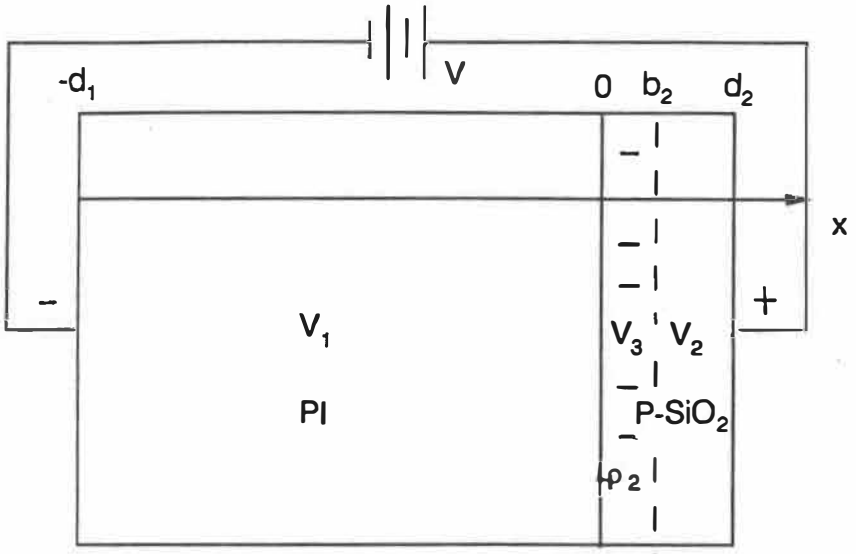

Fig.6.5 Charge distribution in P-SiO_2/PI after a long time of application of a negative voltage.

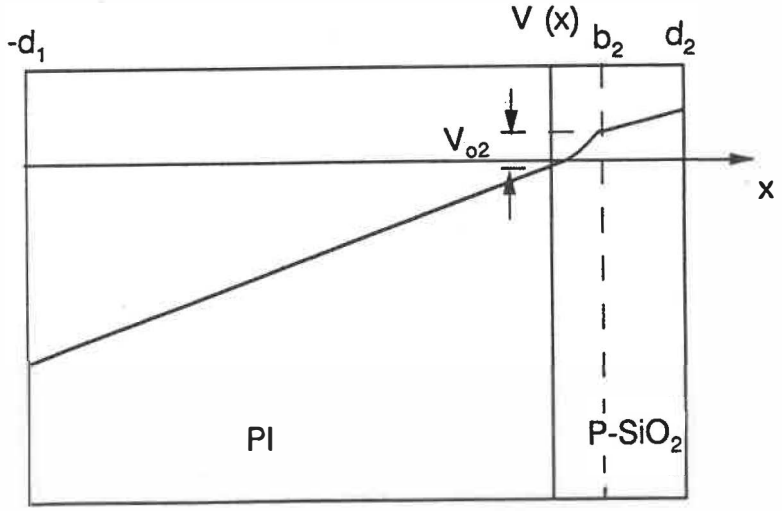

Fig.6.6 Potential distribution in P-SiO_2/PI for the case in Fig.6.5.

Because of the differences between the charge trapping processes for electrons and protons, we have no reason to believe that b_1 and b_2 possess the same value. However, they are estimated to be in the crystallite dimensions in polymers, or in the interphase ranges. Accordingly, we assume, as a first approximation, that b_1, b_2 are about 100 Å, the calculated barrier heights V_{o1} and V_{o2} are 0.07 V and 0.2 V, respectively.

Even if the model used in the above discussion is very simplified, it still provides some important results: 1) the charge accumulated or trapped near the interface can result in an interfacial barrier, and 2) the height of this barrier is about 0.1 V to 0.2 V. Actual distributions of space charges, of potential, and of the electric field are, of course, more complicated, and they will require further investigation.

Now, we consider the difference in charge trapping between the P-SiO_2/PI and P-SiO_2/PET samples. Sacher and Sedor have discussed the concentration of -COOH groups in PI and PET[21,31,76], which can be thermally ionized to produce protons as charge carriers. The -COOH groups in PI are contained in the residual polyamic acid, present in a concentration of 0.05 equiv./g[21], and its repeat unit has two -COOH groups (see Fig.2.1). The -COOH groups in PET are contained in the end groups of the residual terephthalic acid (see Fig.2.2) with a concentration

of $3x10^{-5}$ equiv./g[31]. Therefore, we can conclude that the proton density n in PI is much higher than that in PET, due to the higher concentration of -COOH groups available in PI. At elevated temperatures, when a positive voltage with respect to the PI or PET layer is applied to P-SiO_2/PI or P-SiO_2/PET, the protons can be accumulated near the P–SiO_2/PI interface in a short time, to form the interfacial potential barrier, as discussed above. However, due to the much lower n in PET, it takes a very long time for the same number of protons to accumulate near the P-SiO_2/PET interface, longer than the time (< 2 hours) during which the measurement was carried out. In addition, for the case of a negative voltage with respect to the PET layer applied to P-SiO_2/PET, negative charges (electrons) can not be trapped near the P–SiO_2/PET interface, either. This is felt to be the major reason why no polarity dependence have been observed for the P–SiO_2/PET structure.

In the above discussion, the polarity dependence in P-SiO_2/PI and the difference between P-SiO_2/PI and P-SiO_2/PET have been qualitatively explained.

We will use the results in this section to explain in more detail the results for transient and steady state properties in P-SiO_2/PI. As indicated in equation (3.1b), the charging current I_c flowing through a sample subjected a d. c. voltage is composed of the polarization current I_p, which decreases with time, and the steady

state current $I_{c\infty}$, which does not change with time. In a short charging time, I_p dominates in I_c, while after a long time, I_p drops nearly to zero, and $I_{c\infty}$ dominates. Therefore, the transient behaviour is in fact the property of I_p. I_p is the transient current accompanying the polarization process, and it disappears as soon as the polarization is established.

The charge carriers associated with I_p or $I_{c\infty}$ might be either electrons or ions, depending on different materials and structures. In sections 6.3 and 6.4, we will discuss the polarization and steady state currents in P-SiO_2, respectively. The charge carriers involved in the transient process will be assumed to be electrons, while those involved in the steady state process will be assumed to be protons. The reason for this is that by using this assumption, we have found that the experimental results of both transient and steady state properties of P-SiO_2 or P-SiN/PI at high temperatures, presented in Chapter 4, can be theoretically explained very well. On the other hand, if this assumption is rejected, we have proven that theory can not predict the results which are consistent with experimental results. In fact, the transient and steady state processes are two different processes, we have no reason to believe that the same type of carriers must be involved in them. The assumption of protons as carriers involved in the steady state process for double layer structures is consistent with that for single layer structures (see section 6.1).

6.3 Analysis of transient behaviour for double layer samples

As discussed in Chapter 3, the magnitude of the discharging current I_d is equal to the magnitude of I_p (see eq.3.5c). Therefore, the theoretical results of I_p can be directly compared with the experimental results of I_d.

In amorphous or partially crystalline materials such as certain polymers, or at the interface between two materials, localized electron states can be generated by interruption of natural periodicity of the solid lattice. These localized states in the band gap may be donor-like or acceptor-like according to whether they arise from the valence or conduction band edges, respectively. In addition, the spatial distribution of the localized states is as important as their energy distribution in determining electronic transitions between them, that is, the behaviour of the I_p when a d.c. voltage is applied to the sample.

First, we consider a general case of polarization process in a dielectric material under a d.c. electric field. A set of localized electron states characteristic of this material consists of both D and A sites, where D and A represent the donor – like and acceptor-like sites. A D site is either occupied by an electron or empty, resulting in either neutral or positively charged site; while the occupied and empty A site is negative and neutral, respectively. This can lead to a polarization

P(t), therefore, to a macroscopic polarization current I_p in the direction of the electric field. For the sake of simplicity, we only consider a one-dimensional case. The total polarization P(t) is then

$$P(t) = V_o^{-1}\left(\sum_D e\,(1-f_i)r_i - \sum_A e\,f_i\,r_i \right) \tag{6.9}$$

where f_i is the probability that a state i (D or A) is occupied by an electron, r_i is the distance of this state from a chosen origin, and V_o is the volume of the solid. The polarization current density j_p is expressed as

$$j_p(t) = \frac{dP(t)}{dt} = -\,e\,V_o^{-1} \sum_{A,D} r_i \frac{df_i}{dt} \tag{6.10}$$

df_i/dt can be determined by the Boltzmann equation[77]:

$$\frac{df_i}{dt} = \sum_{j \neq i} (p_{ji}\,f_j - p_{ij}\,f_i) \tag{6.11}$$

where p_{ji} (p_{ij}) is the transition rate from the state j (from the state i) to i (to j). These are determined by the electric field, and by the height and shape of the potential barrier between sites i and j.

Equation (6.11) is difficult to solve. In a simplified case, it is assumed that the electrons hop only between a pair of states which are spatially and energetically favourably aligned[77]. One obtains:

$$\frac{df_i}{dt} = p_{ji} f_j - p_{ij} f_i \qquad (6.12a)$$

$$f_i + f_j = 1 \qquad (6.12b)$$

In this formulation, p_{ij} and p_{ji} depend on local electric field E_L. If redistribution of charges occurs, E_L generally depends on time, except for t very long. As a first approximation, let us assume that the field is independent of time, then the solution of equations (6.12) is:

$$f_i = f_i(\infty) - [f_i(\infty) - f_i(0)] \exp[-(p_{ij}+p_{ji})t] \qquad (6.13a)$$

and

$$f_i(\infty) = \frac{p_{ji}}{p_{ij} + p_{ji}} \qquad (6.13b)$$

where $f_i(0)$ is the initial probability of occupancy at $t = 0$, and $f_i(\infty)$ is the value at $t \to \infty$.

To proceed further, it is necessary to examine the nature of p_{ij} and p_{ji}. First, let us consider a single layer dielectric. The localized states of energies E_i and E_j separated by a potential barrier and at a spacing r_{ij} are represented in Fig.6.7. There are three possible modes of transitions[77]: 1) The first is a single-phonon assisted tunnelling over the distance r_{ij} (absorption or emission of a phonon) to accomplish the energy transition E_j to E_i. 2) The second is a multi-phonon thermal activation over the top of the potential barrier. 3) The third is the general case of multi-phonon activation with tunnelling. The most probable path in this instance depends on the barrier shape and height. In the last two cases an important part of the transition from i to j involves some degree of phonon release and/or local lattice relaxation to complete the process.

Taking into account these various processes, the transition rate may be expressed in the form:

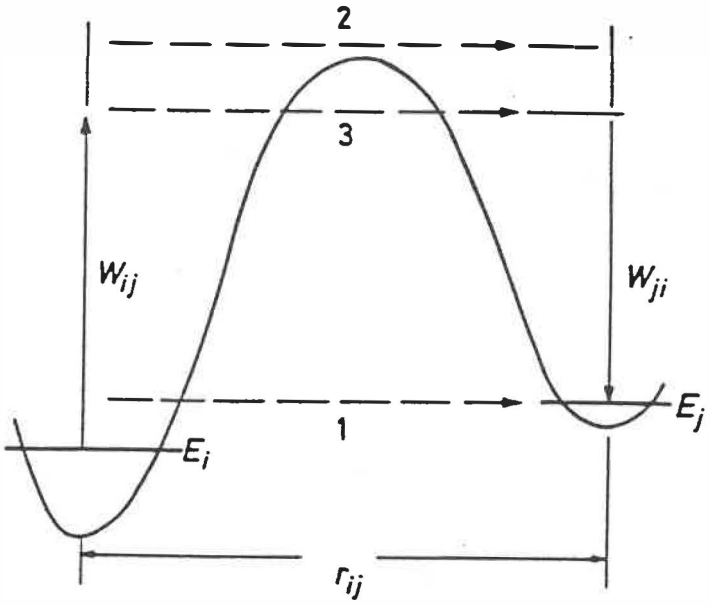

Fig.6.7 Localized pair element showing possible transitions between energy states E_j separated by r_{ij}. (1) Single-phonon assisted tunnelling; (2) multi-phonon activation over potential barrier; (3) the general case of multi-phonon activation with tunnelling. An activation energy W_{ij} is required for the transition i to j and W_{ji} for j to i.

$$p_{ij} = \nu \exp\left(-\phi_{ij} - \frac{W_{ij}}{kT}\right) \tag{6.14}$$

where ν is phonon frequency (typically 10^{12} - 10^{13} Hz)[14,77]. ϕ_{ij} is a tunnelling parameter determined by the wavefunction overlap integral between i and j, and therefore determined by r_{ij} and the shape of the potential barrier. W_{ij} is the energy difference between the equilibrium ground state i and the excited state in which tunnelling occurs (see path 3 in Fig.6.7). A similar expression involving W_{ji} may be written for p_{ji}.

For the single-phonon tunnelling process, one can write[77]

$$\phi_{ij} = 2\alpha r_{ij} \tag{6.15}$$

where α is a measure of the rate at which the wavefunction of site i falls off with distance. In the case of the multi-phonon process, it is reasonable to assume that the tunnelling parameter ϕ_{ij} is small; we can take it to be zero[77]:

$$\phi_{ij} = 0 \tag{6.16}$$

i.e. the tunnelling transmission coefficient is unity.

This approach can now be applied to double layer P – SiO_2/PI dielectric structure (see Fig.6.8). The assumptions can be summarized as follows:

(1) The polarization process occurs near the P-SiO_2/PI interface, and consequently j_p is determined by the localized electron states at the interface.

(2) If the interface is absent, we suppose that $E_i = E_j$, and $W_{ij} = W_{ji} = W$. If the interface is present, we know from section 6.2 that due to the charge accumulation at the interface, an additional energy W_o (interfacial potential barrier) for an electron can be superposed on the PI side, i.e. in this case, the potential barrier for an electron to transit from j to i is $W_{ji} = W_o + W$, while the potential barrier for an electron to transit from i to j is $W_{ij} = W$.

(3) For all pair elements, W_{ij}, W_{ji} and r_{ij} are constant, $r_{ij} = r$, and volume density of pair elements is N.

(4) Electron transition between i and j is multi-phonon activation over potential barrier (see path 2 in Fig.6.7 and eq. 6.16).

Under action of an external field E, the barrier is modified as indicated in Fig.6.8c. Therefore, equation (6.14) can be modified for the transition rates in both directions for the double layer structure as follows:

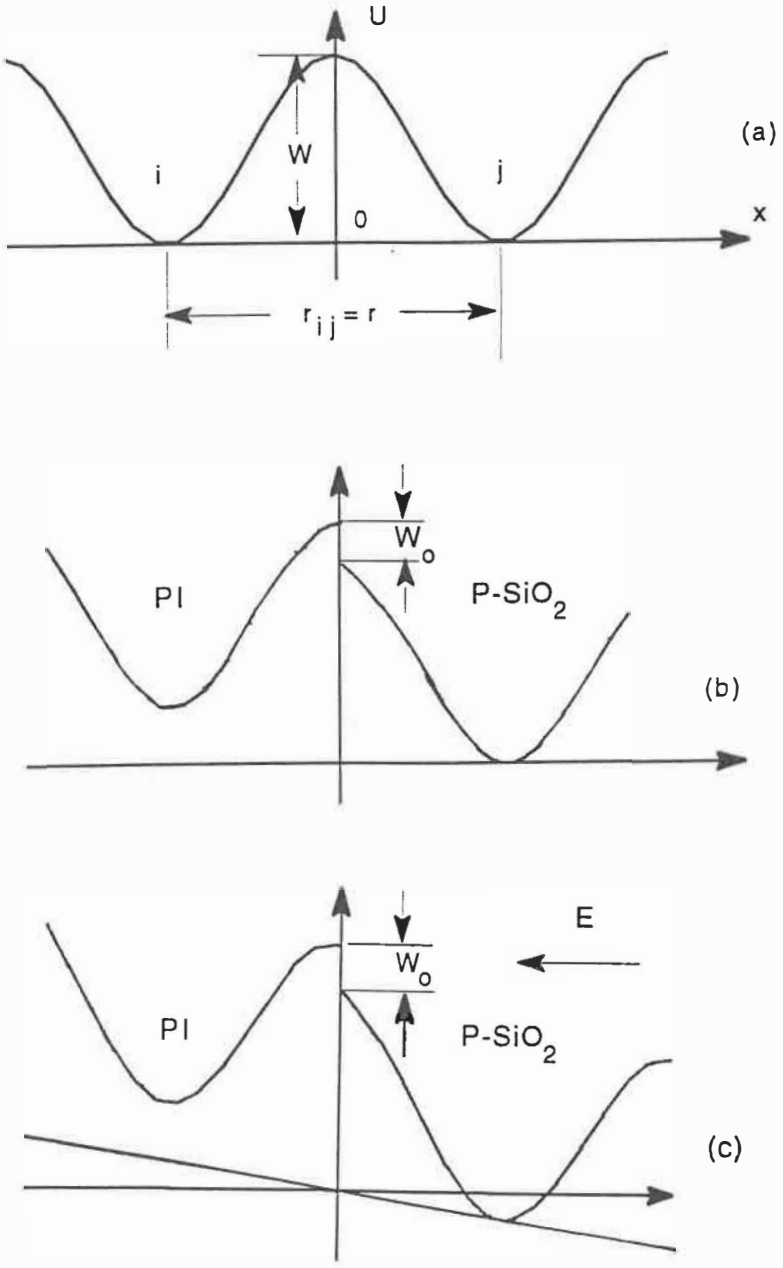

Fig. 6 .8 Potential energy curves for an electron in the polarization process: (a) without interface and without electric field, (b) with interface at x=0 and without electric field, (c) with interface and with electric field.

$$p'_{ji} = \nu_2 \exp\left[-\frac{1}{kT}(W + 0.5erE_L + W_o)\right] \tag{6.17a}$$

and

$$p'_{ij} = \nu_1 \exp\left[-\frac{1}{kT}(W - 0.5erE_L)\right] \tag{6.17b}$$

where ν_1 and ν_2 are the phonon frequencies in PI and in P-SiO_2, respectively. Using equations (6.10), (6.13) and (6.17), and considering the relationship

$$f_i(0) = f_i(\infty)|_{E_L=0} \tag{6.18}$$

we can derive the following expression for j_p:

$$j_p(t, E_L) = 2\,e\,N\,r\,\nu_1 \exp(-\frac{W}{kT})\,H_o \sinh\left(\frac{erE_L}{2kT}\right)\cdot$$
$$\cdot\exp\left[-t\,\nu_1 \exp(-\frac{W}{kT})[\exp(\frac{erE_L}{2kT}) + \frac{\nu_2}{\nu_1}\exp(-\frac{erE_L}{2kT} - \frac{W_o}{kT})]\right] \tag{6.19a}$$

where

$$H_0 = \frac{\frac{\nu_2}{\nu_1}\exp(-\frac{W_o}{kT})}{1 + \frac{\nu_2}{\nu_1}\exp(-\frac{W_0}{kT})} \tag{6.19b}$$

Even though j_p given by equations (6.19) is a complicated function of time, E_L, and of other parameters, we can note the following:

(1) For a reasonably large value of E_L, we find that $|j_p(t,E_L)| \neq |j_p(t,-E_L)|$, i.e j_p depends on the polarity of electric field, due to the non-zero value of W_o. The results in Fig.4.3 have confirmed this.

(2) At low field, one obtains $j_p(t, E_L) \propto E_L$, and the polarity dependence disappears. We have observed this effect at $E < 2\times10^3$ V/cm ($V < 10$ V).

(3) The plot of $\ln(j_p)$ versus t is linear. This is different from the power law (see eq.3.5a) observed in single layer PI (see section 4.1.1).

Theoretical values for j_p ($\approx j_d$) calculated using equations (6.19) and the experimental data for j_d for P-SiO_2/PI at 120°C and at $|E| = 2\times10^4$ V/cm are compared in Fig.6.9. The best agreement between the theory and the experiment has been found for the following set of parameters:

$x_1 = rE_Le = 0.08$ eV,

$x_2 = \nu_1\exp(-W/kT) = 0.012$ Hz,

$x_3 = (\nu_2/\nu_1)\exp(-W_o/kT) = 0.007$,

$x_2 \cdot x_4 = x_2 \cdot eNr = 1.58\times10^{-4}$ A·m^{-2}.

The values of parameters can be compared with other data. If we assume $\nu_1 = \nu_2 = 10^{12}$ Hz (there is usually no large difference in ν for different materials), we

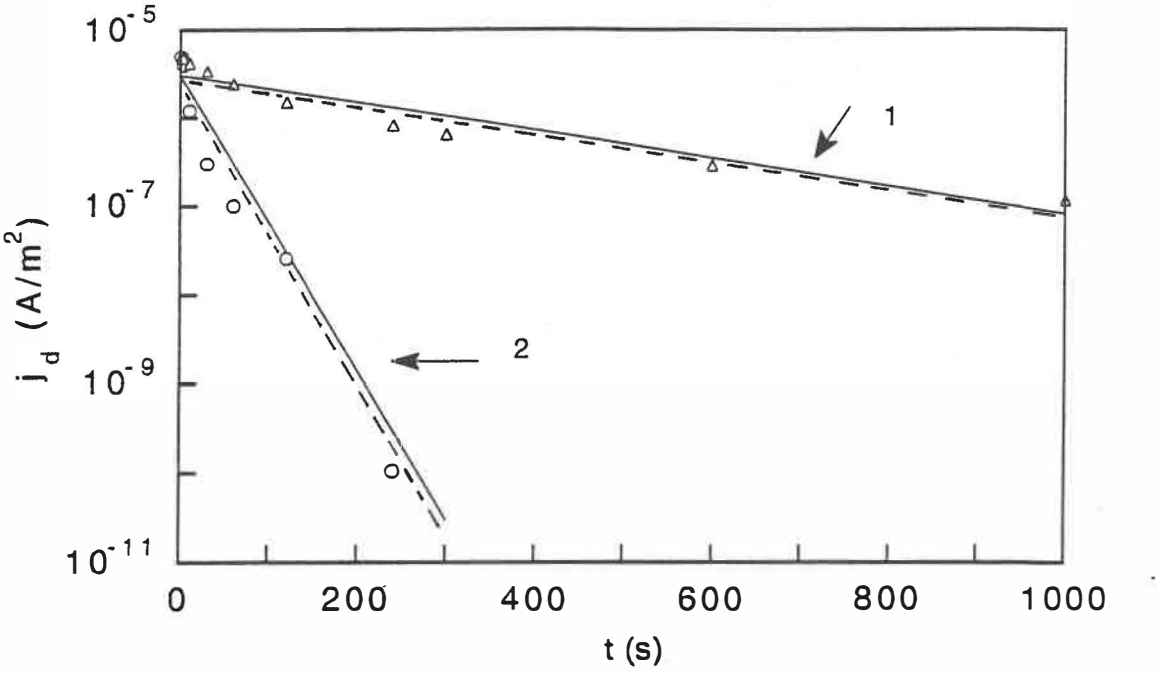

Fig.6.9 Discharging current density j_d for P-SiO_2/PI at 120°C at E = $2x10^4$ V/cm: (1, —) j_{d-}: theory; (2, —) j_{d+}: theory; (Δ, ---) j_{d-}: experiment; (o, ---) j_{d+}: experiment.

can obtain: W = 1.09 eV, W_o = 0.17 eV. In section 6.2, we have estimated that the height of the interfacial potential barrier eV_{o2} is about 0.2 eV, which is basically consistent with W_o. The W value is very close to the E_a value (E_a = 1.0 eV) for PI, and it is also in the range of values for polymers mentioned by Wintle[14], and Ku and Liepins[15]. The local electric field E_L, rather than the average electric field E, has been involved in equation (6.19a). Since, unlike the case of single layer, charges may accumulate near the interface between two insulators in double layer

structure, E_L near the interface may be higher than E. It is difficult to determine an accurate relationship between E_L and E, because we use only the product $x_1 = erE_L = 0.08$ eV, an exact r value is unknown. If we assume for the r value to be in the order between 10^1 and 10^2 Å[40], we obtain that the N value is in the order of 10^{18} cm^{-3}. For comparison, Smith et al.[19] reported $N = 4\times10^{17}$ cm^{-3} for polyimide. The agreement between theory and experiment and the parameter values consistent with literature data confirm that the proposed model is correct.

6.4 Steady state behaviour of double layer samples

We now discuss the polarity dependence of the steady state current in $P-SiO_2/PI$, as shown in Fig.4.4. The charge carriers in polyimide have been assumed to be protons, an assumption we retain for the case of $P\text{-}SiO_2/PI$, and we modify the conduction process due to the presence of the $P\text{-}SiO_2/PI$ interface. Figure 6.10 shows the assumed potential energy curves near the $P-SiO_2/PI$ interface for the one-dimensional case, where an additional potential energy U_o is superposed on the $P\text{-}SiO_2$ side. The conduction is via proton hopping across the potential barrier between sites A and B.

We may compare Fig.6.10 with Fig.6.8. In Fig.6.8, the carriers involved in the transient process are electrons. Therefore, the additional potential barriers are

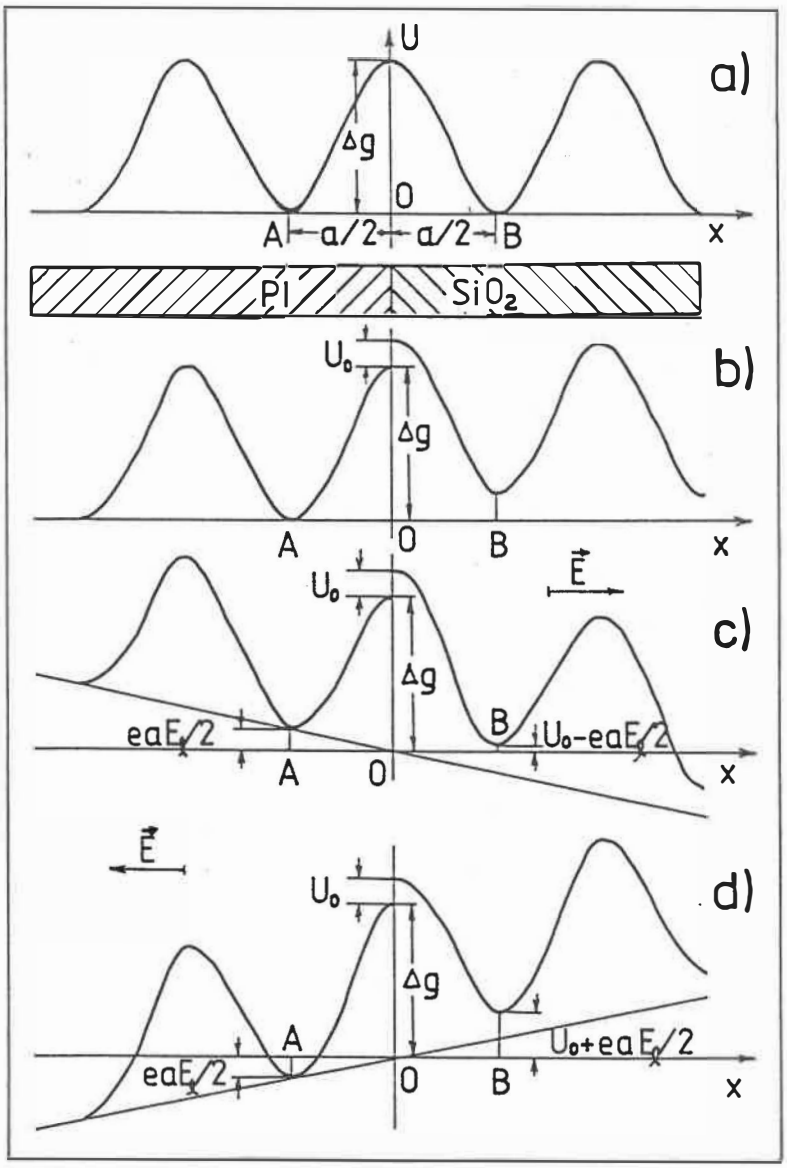

Fig. 6.10 Potential energy curves for a proton in bulk conduction process in double layer structure: (a) without interface, (b) with interface and without electric field, (c) with electric field for P-SiO_2(-)/PI, (d) with electric field for P-SiO_2(+)/PI.

in the different sides in these two cases. In principle, the heights of these two potential barriers should be the same, i.e. $W_o = U_o$, or they are close to each other. In the following, we will find that this really holds.

The applied electric field E modifies the height of the potential barrier. Hopping in the direction of E as shown in Fig.6.10d now takes place with probability P' (the number of attempts per second for a carrier to hop across the potential barrier)[13,14]:

$$P' = \nu_2 \exp\left[-\frac{1}{kT}(\Delta g - 0.5\, e\, E_L\, a)\right] \qquad (6.20a)$$

and hopping against E with a probability P'':

$$P'' = \nu_1 \exp\left[-\frac{1}{kT}(\Delta g + 0.5\, e\, E_L\, a + U_o)\right] \qquad (6.20b)$$

where, a is the mean hopping distance of a proton near the interface. We have assumed that E_L is in the same direction of E. The drift velocity v_+' of a proton caused by E_L is given by

$$v_+' - a(P' - P'') = a\,\nu_2 \exp\left(-\frac{\Delta g}{kT}\right)\left[\exp\left(\frac{e\,a\,E_L}{2\,k\,T}\right) - \frac{\nu_1}{\nu_2}\exp\left(-\frac{U_o}{kT}\right)\exp\left(-\frac{e\,a\,E_L}{2\,k\,T}\right)\right] \tag{6.21}$$

As a first approximation, we assume that E_L is proportional to E, i.e.

$$E_L = \beta_+ E \tag{6.22}$$

β_+ is a constant. Considering for the current density $j_+(E=0) = 0$, the mean drift velocity v_+ at zero field is zero. Therefore, equation (6.21) should be modified to give v_+:

$$v_+(T,E) = a\,\nu_2 \exp\left(-\frac{\Delta g}{kT}\right)\cdot$$
$$\left[\exp\left(\frac{ea\beta_+ E}{2kT}\right) - \frac{\nu_1}{\nu_2}\exp\left(-\frac{U_o}{kT}\right)\exp\left(-\frac{ea\beta_+ E}{2kT}\right) - 1 + \frac{\nu_1}{\nu_2}\exp\left(-\frac{U_o}{kT}\right)\right] \tag{6.23a}$$

In the same way, the mean drift velocity v_- for the case shown in Fig.6.10c is expressed as

$$v_-(T,E) = a\,\nu_2 \exp\left(-\frac{\Delta g}{kT}\right)\cdot$$
$$\cdot\left[\frac{\nu_1}{\nu_2}\exp\left(-\frac{U_o}{kT}\right)\exp\left(\frac{ea\beta_- E}{2kT}\right) - \exp\left(-\frac{ea\beta_- E}{2kT}\right) + 1 - \frac{\nu_1}{\nu_2}\exp\left(-\frac{U_o}{kT}\right)\right] \tag{6.23b}$$

where we have used $E_L = \beta_- E$ to take into account of the possibly different local fields in different polarities.

Using equations (6.23), we can derive the following expressions for the current densities j_+ and j_- in two polarities of E:

$$j_+(T,E) = e\,n(T)\,v_+(T,E)$$
$$= D(T)\left[\exp\left(\frac{ea\beta_+E}{2kT}\right) - \frac{\nu_1}{\nu_2}\exp\left(-\frac{U_o}{kT}\right)\exp\left(-\frac{ea\beta_+E}{2kT}\right) - 1 + \frac{\nu_1}{\nu_2}\exp\left(-\frac{U_o}{kT}\right)\right] \quad (6.24a)$$

as illustrated in Fig.6.10d, and

$$j_-(T,E) = e\,n(T)\,v_-(T,E)$$
$$= D(T)\left[\frac{\nu_1}{\nu_2}\exp\left(-\frac{U_o}{kT}\right)\exp\left(\frac{ea\beta_-E}{2kT}\right) - \exp\left(-\frac{ea\beta_-E}{2kT}\right) + 1 - \frac{\nu_1}{\nu_2}\exp\left(-\frac{U_o}{kT}\right)\right] \quad (6.24b)$$

as illustrated in Fig.6.10c. D(T) is expressed as:

$$D(T) = en(T)\,a\nu_2\exp\left(-\frac{\Delta g}{kT}\right) \quad (6.24c)$$

where n(T) is the density of carriers.

From equations (6.24), one can obtain the following conclusions:

(1) If $\beta_+ \geq \beta_-$, then, j_+ is always larger than j_-, and the difference between

them increases with E. The polarity dependence of current is theoretically predicted. This is consistent with experimental results (see Fig.4.4b).

(2) At low E, both j_+ and j_- show ohmic behaviour:

$$j_+(T,E) \approx D(T)\left[1+\frac{\nu_1}{\nu_2}\exp(-\frac{U_o}{kT})\right]\frac{ea}{2kT}\beta_+ E \qquad (6.25a)$$

$$j_-(T,E) \approx D(T)\left[1+\frac{\nu_1}{\nu_2}\exp(-\frac{U_o}{kT})\right]\frac{ea}{2kT}\beta_- E \qquad (6.25b)$$

If there is no large difference between β_+ and β_-, then the polarity dependence at low field disappears. This conclusion is confirmed by experimental results in Fig.4.4b.

Figure 6.11a gives a comparison between the experimental and theoretical results for P-SiO_2/PI at 120°C. The best agreement with experiment has been found for the following set of parameters: D = 6.4×10^{-6} A/m^2, $(\nu_1/\nu_2)\exp(-U_o/kT)$ = 0.01, and $a\beta_+ = a\beta_-$ = 220 Å. Fig.6.11a confirms a very good agreement between theory and experiment. As mentioned in section 6.3, there is usually no large difference between ν_1 and ν_2. For $\nu_1 = \nu_2$, one obtains U_o = 0.16 eV; this value is comparable with W_o = 0.17 eV for the case of the transient behaviour. The mean hopping distance a_o in PI is 158 Å. If we assume that $a \sim a_o$, we conclude

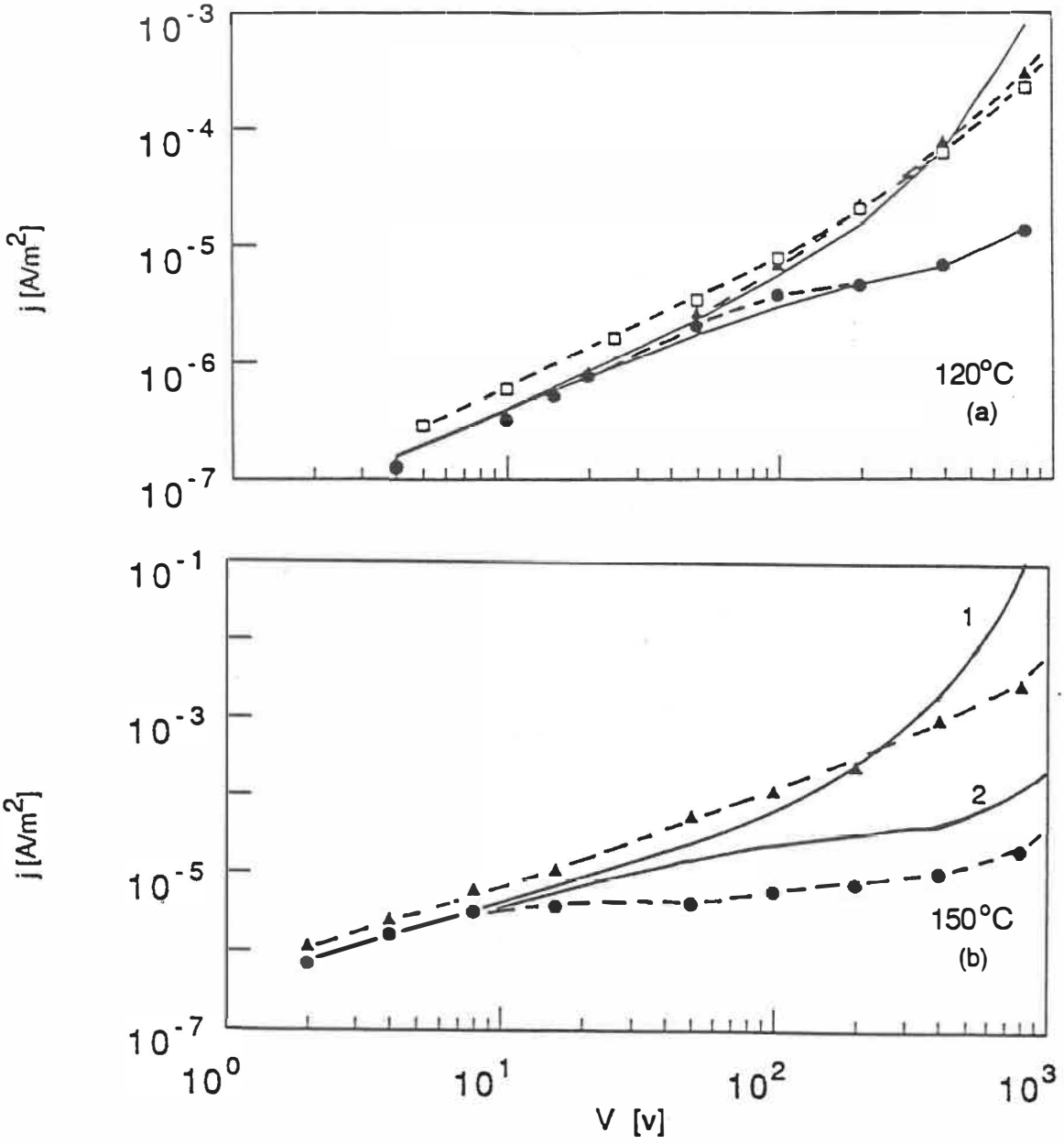

Fig.6.11 Comparison of measured (---:▲, ●, □) and calculated (—) bulk current densities as a function of applied voltage at 120°C (a) and 150°C (b) for PI and P-SiO_2/PI. PI (□), P-SiO_2(+)/PI (j_+: ▲), and P-SiO_2(-)/PI (j_-: ●).

that $\beta_{\pm} > 1$, that is $E_L > E$ near the interface. This is in agreement with the case for the transient process (section 6.3) and the analysis in section 6.2.

Figure 6.11b shows the comparison of theoretical and experimental curves for the same sample at 150°C using the following fitting parameters: $D = 4\times10^{-5}$ A/m^2, $a\beta_+ = a\beta_- = 380$ Å, $(\nu_1/\nu_2)\exp(-U_o/kT) = 0.001$. Qualitative agreement is confirmed, but large deviations between theory and experiment are also found. This model is very simplified, it may describe the experimental results reasonably well at temperatures below 120°C, but above 120°C, we have to consider more complicated situation at the interface.

The parameter $U_o(T)$ can play a key role in determining the behaviour of j_+ and j_-. The larger the $U_o(T)$ value, the greater will be the difference between j_+ and j_-. If $U_o(T) = 0$, $\beta_+ = \beta_- = 1$, equations (6.24a) and (6.24b) become identical to equation (6.1), and the polarity dependence disappears. This can apply to the case of low temperatures: in fact, below 60°C we did not observe any polarity dependence for $P-SiO_2/PI$ (see Fig.4.6a). It follows that U_o, β_+ and β_- vary with temperature.

No polarity dependence was found on $P\text{-}SiO_2/PET$ and P-SiN/PET as presented in Chapter 4. The reason is that the U_o value near the $P-SiO_2/PET$ or

P-SiN/PET interface is too small to cause a difference between j_+ and j_- in the whole ranges of the electric field and temperature. We have discussed this issue in section 6.2.

Finally, we must mention the difference between the Du Pont Kapton, used for d.c. measurements, and the spin-coated polyimide, used for C-V measurements. At a high temperature (120°C), the C-V measurements have confirmed charge accumulation or trapping near the P-SiO_2/PI interface, leading to an interfacial potential barrier. The d.c. measurements have shown that this potential barrier can result in the polarity dependence of bulk current or conductivity. At a low temperature (room temperature), the C-V measurements have also proven the charge accumulation at the interface, however, we did not observe the polarity dependence at room temperature in the d.c. measurements. This means that even at room temperature, this potential barrier can be present at the P-SiO_2/(spin-coated PI) interface but not at the P-SiO_2/(Du Pont PI) interface. Therefore, additional d.c. measurement for the Al-PI-(P-SiO_2)-Si sample were performed, and the results are shown in Fig.6.12, where PI is the spin-coated material. The meanings of I_{c+} and I_{c-} are the same as those used in Fig.4.4b. The polarity dependence of current at both high and low temperatures confirms the above demonstration.

It is not surprising that there is a difference in d.c. property at low temperature between the P-SiO_2/PI and Al-PI-(P-SiO_2)-Si samples. The preparation process of PI is different for these two types of samples: one is Du Pont Kapton-H, while other one is prepared by spin-coating from polyamic acid as mentioned in Chapter 3. The different preparation precesses can significantly affect the electrical properties.

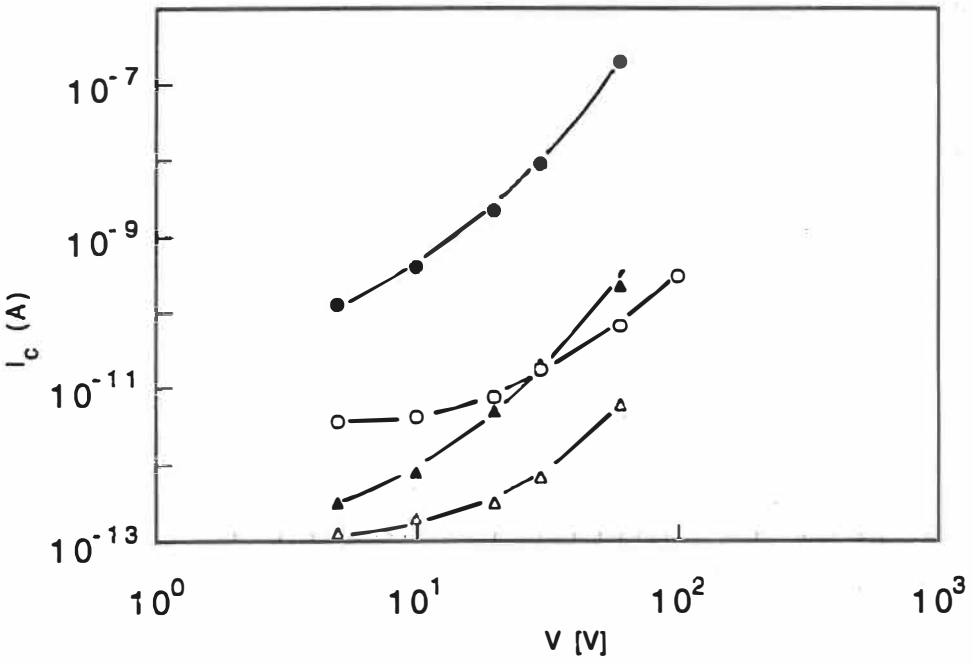

Fig.6.12 Steady state current I_c as a function of applied voltage for Al-PI-(P-SiO_2) - S i system . I_{c+}: (▲, 26°C), (●, 110°C); I_{c-}: (Δ, 26°C), (o, 110°C).

Chapter 7

Conclusions

The coatings of P-SiO_2 and P-SiN, plasma-deposited onto Kapton® (PI) and Mylar® (PET) films used as thermal blankets in space technology, have proven to protect them against the hostile environment of space, for example, attack of atomic oxygen and surface flashovers. In order to understand electrical properties of such double layer dielectric structures, related to the ability to suppress surface flashovers, the double layer P-SiO_2/PI, P-SiN/PI, P-SiO_2/PET and P-SiN/PET samples were prepared and their d.c. bulk and surface electrical conductivities have been investigated.

The research on single layer PI and PET and double layer samples has been based on the measurement of electrical conduction in vacuum, in the temperature range from 19°C to 170°C, using an electric field strength from 2×10^2 to 2×10^5 V/cm. Additional information on the electrical properties has been derived from the C-V measurements on the MIS and MI_1I_2S structures.

The bulk conductivity of PI was found to increase systematically with thermal cycling under vacuum. An initial activation energy of 1.0 eV has been determined. However, after heating for a long time, its value varies within two temperature

regions: E_a = 1.26 eV for T < 90°C, and E_a = 0.86 eV for T ≥ 90°C. The electrical properties of PI have been attributed to the increase of carrier concentration with thermal cycling and to the microstructural rearrangements. Dry PET shows stable bulk conductivity, and exhibits a glass transition temperature at 70°C, resulting in two activation energies: E_a = 1.85 eV at T > 70°C, and E_a = 0.33 eV at T ≤ 70°C.

D.C. bulk conduction measurements for double layer P-SiO_2/PI and P–SiN/PI structures have shown that the transient and steady state properties are very different from those for PI at T ≥ 60°C. The bulk conductivity of these double layer structures depends on the polarity of applied electric field at T ≥ 60°C and E ≥ 2×10^3 V/cm. On the other hand, the bulk conductivity of P-SiO_2/PET and P-SiN/PET does not exhibit any appreciable dependence on the polarity.

An ionic conduction mechanism has been proposed for the bulk conduction in PI and PET. The conduction process is thermally activated-hopping of protons. By comparing experimental and theoretical results, we obtained the hopping distances of 110 Å at 24°C and 158 Å at 120°C for PI, and 95 Å at 90°C for PET.

C-V characteristics of the Al-PI-(P-SiO_2)-Si sample have shown that charges can be trapped at the P-SiO_2/PI or P-SiN/PI interface. These accumulated charges can modify the contact potential difference formed when P-SiO_2 and PI are in

contact with each other, resulting in a potential barrier at the P-SiO_2/PI or P-SiN/PI interface. We have proposed a model, based on this interfacial potential barrier, to interpret the d.c. conducting properties in P-SiO_2/PI or in P-SiN/PI. According to this model, the derived theoretical results can semi-quantitatively explain the properties of the transient and steady state currents in P-SiO_2/PI. Because this potential barrier at the P-SiO_2/PET or P-SiN/PET interface is absent or very small at both low and high temperatures, the bulk conductivity of P-SiO_2/PET and P – SiN/PET does not exhibit any polarity dependence.

The phenomenon of proton trapping at the P-SiO_2/PI or P-SiN/PI interface, observed in this work, can be correlated with the experimental observation by Balmain et al.[11]. They found the reduced surface flashover on the double layer P-SiO_2/PI and P-SiN/PI samples irradiated by a 20 keV electron beam, as mentioned in Chapters 1 and 2. In fact, the protons trapped at the interface can attract back the electrons which have been embedded below the interface, consequently reducing the negative space charge density below the threshold value for discharge. The polarity dependence of bulk current in d. c. conduction for P-SiO_2/PI and P-SiN/PI can also be related to the magnitude of the leakage current, which determines the occurrence or absence of surface flashover, when the bare or coated surface of the similar samples is exposed to the irradiation of an electron beam.

Further experiments should focus on the d. c. measurements at a higher electric field and higher temperature, and on a combination with research of electron-beam charging, to establish the further correlation. Another experimental work, as already mentioned in section 6.2, is the investigation on spatial distribution of charges near the interface between two insulators, in order to understand the detail of the interfacial potential barrier, and to further understand the d.c. properties of double layer dielectric structures. By using experimental results, theoretical work should be engaged in finding the direct relationships between the height of interfacial potential barrier and those parameters such as temperature, electron mobility, the density of surface traps, and electric field. Although many researchers have accepted protons as charge carriers in PI and PET, as indicated in Chapter 2, Senturia et al.[19,61] still considered the role of impurity ion Na^+ in d. c. conduction, and they have found some phenomena in Na^+-doped PI which correlate with Na^+ conduction. Therefore, the confirmation of other ions as possible charge carriers may also be one of the future tasks.

References

1. F. L. BOUQUET and C. R. MAAG, "Ground radiation tests and flight atomic oxygen tests of ITO protectives for Galieo spacecraft", IEEE Trans. on Nuclear Sci., NS33(6), 1408-1412 (1986).

2. C. N. FELLAS, "An arc free thermal blanket for spacecraft use", IEEE Trans. on Nuclear Sci., NS27(6), 1801-1807 (1980).

3. R. D. GOLDSTEIN, E. M. BROWN, and L. C. MALDOON, "Usage of ITO to prevent spacecraft charging", IEEE Trans. on Nuclear Sci., NS29(6), 1621-1628 (1982).

4. F. L. BOUQUET, V. F. HRIBAR, and E. C. METZLER, "Radiation effects measurements on spacecraft electrostatic discharge tapes thermal blankets and thermooptical coatings", IEEE Trans. on Nuclear Sci., NS31(6), 1393-1397 (1984).

5. B. A. BANKS, M. J. MIRTICH, S. K. RUTLEDGE, and D. M. SWEC, "Sputtered coatings for protection of spacecraft polymers", Thin Solid Films, 127, 107-114 (1987).

6. J. E. KLEMBERG-SAPIEHA, M.R. WERTHEIMER, and D. G. ZIMCIK, "Plasma-deposited multipurpose coatings for space applications", ESA Journal, 13, 117-126 (1989).

7. M. F. ROSE, "Electrical insulation and dielectrics in the space environment", IEEE Trans. on Electr. Insul. EI22(5), 555-571 (1987).

8. C. N. FELLAS, "Improved anti-static thermal blankets", IEEE Trans. on

Nuclear Sci., NS28(6), 4571-4574 (1981).

9. C. N. FELLAS, "Spacecraft charging - how to make a large communications satellite immune to arcing", Proc. of an International Sump. on Spacecraft Matter in space Environment, France, 8-12 June 1982 (ESA SP-178), 305-309.

10. C. N. FELLAS and S. RICHARDSON, "Internal charging of indium oxide coated mirrors", IEEE Trans. on Nuclear Sci. NS28(6), 4523-4528 (1981).

11. K.G. BALMAIN and M.R. WERTHEIMER, "Electron-beam charging of plasma-coated spacecraft dielectrics", Proc. IEEE Int. Sump. on Electrets (ISE7), Berlin, FRG (1991), IEEE Doc. 91CH3029-6, pp747-752.

12. P. J. PHILLIPS, "Morphology and molecular structure of polymers and their dielectric behaviour", in "Engineering Dielectrics" Vol.IIA, R. BARTNIKAS/R.M. EICHHORN, Editors, p119-237, ASTM Special Technical Publication 783, 1983.

13. J.J. O'DWYER, "The theory of electrical conduction and breakdown in solid dielectrics", Clarendon Press, Oxford, 1973.

14. H.J. WINTLE, "Conduction processes in polymers", in "Engineering Dielectrics" Vol.IIA, R. BARTNIKAS/R.M. EICHHORN, Editors, p239-354, ASTM Special Technical Publication 783, 1983.

15. Chen C. KU and R. LIEPINS, "Electrical properties of polymers", Hanser Publishers, Munich, 1987.

16. K. L. MITTAL (Editor), "Polyimides", Plenum Press, New York and London, 1982.

17. D. D. DENTON, "Moisture transport in polyimide films in integrated circuits", Ph.D. thesis, MIT, Boston, MA, USA, 1987.

18. A. M. WILSON, "Polyimide insulators for multilevel interconnections", Thin Solid Films, 83(2), 145-163 (1981).

19. F.W. SMITH, H.J. NEUHAUS, S.D. SENTURIA, Z. FEIT, D.R. DAY, and T.J. LEWIS, "Electrical conduction in polyimide between 20 and 350 °C", J. Electronic Mater., 16(1), 93-106 (1987).

20. G.M. SESSLER, B.HAHN, and D.Y. YOON, "Electrical conduction in polyimide films", J. Appl. Phys., 60(1), 318-326 (1986).

21. E. SACHER, "Dielectric properties of polyimide film, II dc properties", IEEE Tans. on Electr. Insul. EI14(2), 85-93 (1979).

22. A. LIAN, L. MARTINU, J.E. KLEMBERG-SAPIEHA, and M.R. WERTHEIMER, "Electrical properties of silicon oxide/polyimide double layer structures", Proc. IEEE CEIDP, IEEE Doc. 90CH2919-9, 159-165 (1990).

23. J. H. NEVIN and G.L. SUMME, "DC conduction mechanisms in thin polyimide films", Microelectronics Reliab. 21(5), 699-705 (1981).

24. H. K. CHANG, W.M. SHEN, and J. YU, "High temperature conductivity of PI films", Proc. IEEE CEIDP, IEEE Doc. 82CH1773-1, 108-113 (1982).

25. G. SAWA, S. NAKAMURA, K. IIDA, and M. IEDA, "Electrical conduction of polypyromellitimide films at temperature of 120-180 °C", Japan. J. Appl. Phys., 19(3), 453-485 (1980).

26. G.A. BROWN, "Reliability implications of polyimide multilevel insulators", Proc. IEEE Intern. Reliability Phys., IEEE Doc. 81CH1619-6, 282-286 (1981).

27. B.L. SHARMA and P.K.C. PILLAI, "Electrical conduction in Kapton polyimide film at high electric fields", Polymer, 23, 17-20 (1982).

28. I. K. VARMA, S. SAXENA, A. TRIPATHI, and D. S. VARMA, "Effect of metal halides on the electrical properties of polyimides", Polymer, 29, 559-565 (1988).

29. M. NAGAO, G. SAWA, M. FUKUI, and M. IEDA, "Dielectric breakdown of polyimide film", Japan. J. Appl. Phys., 15(9), 1813-1814 (1976).

30. T. TANAKA, S. HIRABAYASHI, and K. SHIBAYAMA, "Thermal depolarization current study of polypromellitimide", J. Appl. Phys., 49(2), 784-787 (1978).

31. E. SACHER, "Direct-current conductivity of poly(ethylene terephthalate)", J. Macromol. Sci. - Phys., B4(2), 441-448 (1970).

32. G. CASERTA, B. RISPOLI, and A. SERRA, "Space-charge-limited current and band structure in amorphous organic films", Phys, Stat. Sol., 35, 237-248 (1969).

33. F. S. SMITH and C. SCOTT, "The electrical conductivity of poly(ethylene terephthalate) in the temperature range 180 - 290 °C", Brit. J. Appl. Phys., 17, 1149-1154 (1966).

34. A. C. LILLY, JR. and John R. MCDOWELL, "High-field conduction in films of mylar and teflon", J. Appl. Phys., 39(1), 141-148 (1968).

35. L. E. AMBORSKI, "Structural dependence of the electrical conductivity of polyethylene terephthalate", J. Polymer Sci., 62, 331-346 (1962).

36. D. M. TAYLOR and T. J. LEWIS, "Electrical conduction in polyethylene terephthalate and polyethylene films", J. Phys. D: Appl. Phys., 4, 1346-1357 (1971).

37. K. HAYASHI, K. YOSHINO, and Y. INNISHI, "Carrier mobilities in insulating polymers measured by time of flight method", Japn. J. Appl. Phys., 14(1), 39-45 (1975).

38. E. SACHER, "The d.c. conductivity of poly(ethylene terephthalate) at elevated temperatures", J. Phys. D: Appl. Phys., 15, L17 (1972).

39. J. R. HANSCOMB and Y. KAAHWA, "High-temperature electrical conduction in polyethylene terephthalate", J. Phys. D: Appl. Phys., 12, 579-585 (1979).

40. R. E. BARKER, JR and A. H. SHARBAUGH, "Ionic conduction in polymer films and related systems", J. Polymer Science: Part C, No.10, 139-152 (1965).

41. R. E. BARKER, JR, "Mobility and conductivity of ions in and into

polymeric solid", Pure & Appl. Chem., 46, 157-170 (1976).

42. A. R. FREDERICKSON, "Electric discharge pulses in irradiated solid dielectrics in space", IEEE Trans. on Electr. Insul., 18(3), 337-349 (1983).

43. A. R. FREDERICKSON and A. L. CHESLEY, "Charging/discharging of space shuttle tile material under irradiation", IEEE Trans. on Nuclear Sci., NS30(6), 4296-4301 (1983).

44. A. R. FREDERICKSON and S. WOOLF, "Electric fields in KeV electron irradiated polymers", IEEE Trans. on Nuclear Sci., NS29(6), 2004-2011 (1982).

45. K. G. BALMAIN, "Surface discharge effects", in "Space systems and their interaction with Earth's space environment", edited by H. B. GARRETT and C. P. PIKE, Vol.71 of Progress in Astronautics and Aeronautics, 276-298 (1978).

46. K. G. BALMAIN, "Arc propagation, emission and damage on spacecraft dielectrics: a review", J. Electrostatics, 20, 95-108 (1987).

47. K. G. BALMAIN, A. BATTAGIN, and G. R. DUBOIS, "Thickness scaling for arc discharges on electron-beam-charged dielectrics", IEEE Trans. on Nuclear Sci., NS32(6), 4073-4078 (1985).

48. G. M. SESSLER, "Charge storage in dielectrics", IEEE Trans. on Electr. Insul., EI24(3), 395-402 (1989).

49. D. A. BERKLEY, "Computer simulation of charge dynamics in electron-irradiated polymer foils", J. Appl. Phys., 50(5), 3447-3453 (1979).

50. J. E. WEST, H. J. WINTLE, A. BERRAISSOUL and G. M. SESSLER, "Space-charge distributions in electron-beam charged Mylar and Kapton films", IEEE Trans. on Electr. Insul., EI24(3), 533-536 (1989).

51. L. MARTINU, J. E. KLEMBERG-SAPIEHA, and M. R. WERTHEIMER, "Dual-mode microwave/radio frequency plasma deposition of dielectric thin films", Appl. Phys. Lett. 54(26), 2645-2647 (1989).

52. L. MARTINU, J.E. KLEMBERG-SAPIEHA, O. M. KUTTEL, and M.R. WERTHEIMER, "Electrical properties of dual-frequency plasma deposited silicon-compound films", Proc. IEEE CEIDP, IEEE Doc.90CH2919-9, 178-183 (1990).

53. J. MORT and F. JANSEN, "Plasma deposited thin films", CRS Press, Inc., Bock Raton, Florida, 1986.

54. M. R. WERTHEIMER, J. E. KLEMBERG-SAPIEHA, and H. P. SCHREIBER, "Advances in basic and applied aspects of microwave plasma polymerization", Thin Solid Films, 115, 109-124 (1984).

55. P. RABILLER, "Propriétés électriques de couches minces d'oxynitrure de silicium obtenues par dépôt en phase vapeur assisté par plasma micro-onde", M. Sc.A. Thesis, Department of Engineering Physics, Ecole Polytechnique, Montreal, Quebec, Canada (1988).

56. P. RABILLER, J.E. KLEMBERG-SAPIEHA, M.R. WERTHEIMER, and A. YELON, "Electrical properties of a-SiO_xN_y:H films prepared by microwave PECVD", ICSD3, Trondheim, Norway, July 3-6 (1989), IEEE Doc. 89CH2726-8, pp299-303.

57. J. E. KLEMBERG-SAPIEHA, O. M. KUTTEL, L. MARTINU and M. R. WERTHEIMER, "Dual microwave-r.f. plasma deposition of functional coatings", Thin Solid Films, 193/194, 965-972 (1990).

58. ASTM (American Society for Testing and Materials), "Standard test method for d-c resistance or conductance of insulating materials", in "1991 Annual Book of ASTM Standards Vol.10.01 Electrical Insulation (I) Designation D257-91", pp111-126.

59. S. M. SZE, "Physics of semiconductor devices", John Wiley & Sons,1981.

60. L. MARTINU and A. CASTELLI, "Electrical measurement on polymers, III electrical conductivity", Internal Report, Instituto Guido Donegoni, Novara, Italy (1988).

61. H. J. NEUHAUS and S. D. SENTURIA, "Space-charge modified transient current in polyimide", Proc. IEEE CEIDP, IEEE Doc. 88CH2668-2, 454-459 (1988).

62. E. H. NICOLLIAN, J. R. BREWS, "MOS (metal oxide semiconductor) physics and technology", John Wiley & Sons, New York, 1982.

63. H. KLIEM, B. SCHUMACHER, and G. ARLT, "Transient current measurements in polyimide", Proc. IEEE CEIDP, IEEE Doc. 86CH2315-0, 168-173 (1986).

64. F. Y. AWAKUNI and J. H. CALDERWOOD, "Water vapour adsorption and surface conductivity in solids", J. Phys. D: Appl. Phys., 5, 1038-1045 (1972).

65. G. SAWA and J.H. CALDERWOOD, "Dependence of surface conduction current in oxidized polyethylene on electric field at various humidities", J. Phys., 4, 2313-2318 (1971).

66. A.S. GROVE, B.E. DEAL, E.H. SNOW and C.T. SAH, "Investigation of thermally oxidised silicon surfaces using metal-oxide-semiconductor structures", Solid-State Electronics, 8, 145-163 (1965).

67. Robert F. PIERRET, "Field effect devices", Vol.IV, in "Modular Series on Solid State Devices", Addison-Weslley, Reading, MA, 1983.

68. M. MAISONNEUVE, Y. SEGUI and Bui AI, "Charge transport in thin polymer films as shown by C-V measurements", Thin Solid Films, 44, 209-216 (1977).

69. M. MAISONNEUVE, Y. SEGUI and A. BUI, "Electrical properties of metal-polymer(polysiloxane)-silicon structures and application of polysiloxane to the passivation of semiconductor devices", Thin Solid Films, 33, 35-41 (1976).

70. B. R. HAHN and D. Y. YOON, "Electrical and interfacial properties of metal-polyimide-silicon structures", J. Appl. Phys., 65(7), 2766-71 (1989).

71. T. A. BROOKS and D. W. HESS, "Plasma-enhanced chemical vapour deposition of silicon nitride from 1,1,3,3,5,5,-hexamethylcyclotrisilazane and ammonia", Thin Solid Films, 153, 521-529 (1987).

72. D. H. TOTTERDELL, "Electron injection effects in polymer dielectrics", J. Phys. D: Appl. Phys., 19, L111-L114 (1986).

73. J. T. FELTS and A. D. GRUBB, "Commercial-scale application of plasma processing for polymeric substances: from laboratory to production", J. Vac. Sci. & Tech. A, 10(4), 1675-1681 (1992).

74. B. R. SINGH, "A study of the polarization phenomenon in lead silicate glass using the MGOS structure", J. Phys. D: Appl. Phys., 7, 443-450 (1974).

75. G. M. SESSLER, "Physics principles of electrets", in "Electrets", G. M. Sessler, Editor, p13-80, Springer-Verlag Berlin Heidelberg, 1980.

76. E. SACHER and D. G. SEDOR, "The possibility of further imidization in polyimide film", J. Polym. Sci.: Polym. Phys. Ed., 12, 629-632 (1974).

77. T.J. LEWIS, "The dielectric behaviour of non-crystalline solids", in "Dielectric and related molecular processes - volume 3", A specialist periodical report, The Chemical Society, Burlington House, London W1V 0BN, 1977.

LI

19